

INFORMATION TO USERS

This manuscript has been reproduced from the microfilm master. UMI films the text directly from the original or copy submitted. Thus, some thesis and dissertation copies are in typewriter face, while others may be from any type of computer printer.

The quality of this reproduction is dependent upon the quality of the copy submitted. Broken or indistinct print, colored or poor quality illustrations and photographs, print bleedthrough, substandard margins, and improper alignment can adversely affect reproduction.

In the unlikely event that the author did not send UMI a complete manuscript and there are missing pages, these will be noted. Also, if unauthorized copyright material had to be removed, a note will indicate the deletion.

Oversize materials (e.g., maps, drawings, charts) are reproduced by sectioning the original, beginning at the upper left-hand corner and continuing from left to right in equal sections with small overlaps. Each original is also photographed in one exposure and is included in reduced form at the back of the book.

Photographs included in the original manuscript have been reproduced xerographically in this copy. Higher quality 6" x 9" black and white photographic prints are available for any photographs or illustrations appearing in this copy for an additional charge. Contact UMI directly to order.

UMI

A Bell & Howell Information Company
300 North Zeeb Road, Ann Arbor MI 48106-1346 USA
313/761-4700 800/521-0600

**Two- and Three-Dimensional Study of the Kelvin-Helmholtz
Instability, Magnetic Reconnection and their Mutual Interaction at
the Magnetospheric Boundary**

A
THESIS

Presented to the Faculty
of the University of Alaska Fairbanks
in Partial Fulfillment of the Requirements
for the Degree of

DOCTOR OF PHILOSOPHY

By
Qinxue Chen, B.S., M.S.

Fairbanks, Alaska

August 1997

UMI Number: 9804765

UMI Microform 9804765
Copyright 1997, by UMI Company. All rights reserved.
This microform edition is protected against unauthorized
copying under Title 17, United States Code.

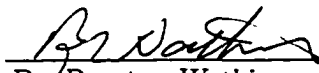
UMI
300 North Zeeb Road
Ann Arbor, MI 48103


Two- and Three-Dimensional Study of the Kelvin-Helmholtz
Instability, Magnetic Reconnection and their Mutual Interaction at
the Magnetospheric Boundary

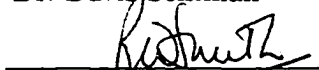
by

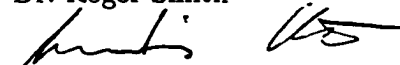
Qinxue Chen


RECOMMENDED:


Dr. Brenton Watkins



Dr. Davis Sentman



Dr. Roger Smith

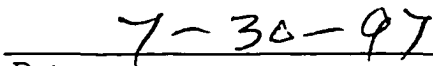

Dr. Antonius Otto, Chairman, Advisory Committee


Dr. Brenton Watkins, Head, Physics Department

APPROVED:


Dr. Paul Reichardt, Dean, College of Natural Sciences


Dr. Joseph Kan, Dean of the Graduate School


Date

Abstract

Magnetic reconnection and the Kelvin-Helmholtz (KH) instability regulate the transport of magnetic flux, plasma, momentum and energy from the solar wind into the magnetosphere. In this thesis, I use two-dimensional and three-dimensional MHD simulations to investigate the KH instability, magnetic reconnection, and their relationship. The major emphasis of this thesis is on the interaction processes in the presence of magnetic shear and flow shear, the mechanism of vortex-induced reconnection, the interaction of the tearing and KH instabilities, and the KH-related magnetopause processes. Two basic flow and magnetic field configurations are distinguished at the Earth's magnetopause: (1) configurations where the difference in plasma velocity between the two sides of the boundary $\Delta\mathbf{v}$ (velocity shear) is parallel to the difference of the magnetic field $\Delta\mathbf{b}$ (magnetic shear), and (2) configurations where the velocity shear is perpendicular to the magnetic shear. For configuration (1), either magnetic reconnection is modified by the shear flow, or the KH instability is modified by the magnetic shear and resistivity. The evolution of the basic configuration (2) requires three dimensions. In this case, both processes can operate simultaneously in different planes. If the KH instability grows faster initially, it can wrap up the current layer and thereby initiate a very fast and turbulent reconnection process. The resulting magnetic turbulence can provide the first explanation of often very turbulent structures of the magnetopause current layer. For the first time, it is quantitatively confirmed that the KH instability operates at the magnetospheric boundary at low latitudes.

Contents

Abstract	iii
List of Figures	viii
List of Tables	xv
Acknowledgments	xvi
1 Introduction	1
1.1 The Tearing Mode and Kelvin-Helmholtz Instabilities	4
1.1.1 The Tearing Mode Instability	4
1.1.2 The Kelvin-Helmholtz Instability	7
1.2 Magnetopause Processes	11
1.2.1 Magnetic Reconnection	11
1.2.2 Viscous Transport Due to the Kelvin-Helmholtz Instability .	13
1.3 Motivation of the Thesis	16
1.4 Outline of the Thesis	19
2 Numerical methodology	21

2.0.1	Basic Equations	21
2.0.2	Boundary Conditions and Numerical Method	22
3	The interaction of parallel flow shear and magnetic shear	24
3.1	Introduction	24
3.2	Equilibrium and Initial Perturbation	28
3.3	Simulation Results	32
3.3.1	Sub-Alfvénic Shear Flow: The Tearing Mode	33
3.3.2	Super-Alfvénic Velocity Shear Effects on the Kelvin-Helmholtz Mode	39
3.4	Summary and Discussion	49
4	Linear properties of the Kelvin-Helmholtz and tearing instabilities in three dimensions	56
4.1	Introduction	56
4.2	Equilibrium, Initial Perturbation, and Simulation Setup	60
4.3	Simulation Results	65
4.3.1	Properties of the Tearing Instability	66
4.3.2	Properties of the Kelvin-Helmholtz Instability	69
4.3.3	Simultaneous Growth of the Kelvin-Helmholtz and Tearing Modes	70
4.4	Discussion and Conclusion	77
5	Nonlinear dynamics of the interaction of KH and tearing insta- bilities in three dimensions	82

5.1	Introduction	82
5.2	Simulation Model	85
5.3	Simulation Results	86
5.3.1	The KH instability Induces the Tearing Instability	86
5.3.2	Coupling of the Kelvin-Helmholtz and Tearing Instabilities	105
5.4	Discussion and Conclusion	120
6	The Kelvin-Helmholtz instability: Comparison with observation	122
6.1	Introduction	122
6.2	Structure of the Magnetopause	123
6.2.1	Simulation Comparison	125
6.3	The Kelvin-Helmholtz Instability at the Magnetotail Boundary	131
6.3.1	Simulation Model	136
6.3.2	Results and Comparison	139
6.4	Conclusion and Discussion	149
7	Summary and discussion	152
7.1	Main Results	152
7.1.1	Configuration (1): A Tearing-Mode-Dominated Regime for Sub-Alfvénic Flows and the KH-unstable Regime for Super-Alfvénic Flows	153
7.1.2	Configuration (2): The 3-D KH-Induced Reconnection and the Interaction of the Tearing and KH Modes.	155
7.1.3	Comparison with Observations	157
7.2	Summary and Open Problems	158

References

List of Figures

1.1	Sketch of the Earth's magnetopause [<i>Kennel et al.</i> , 1979]	2
1.2	The development of the tearing mode instability	6
1.3	The KH instability	8
1.4	The coordinate system used in Miura's simulations	10
1.5	Magnetic field and flow field configuration at the dayside magnetopause [<i>Kennel et al.</i> , 1979]	18
3.1	Sketch of the initial configuration of magnetic field and shear flow, where the shaded region is the current sheet. Arrows labeled v and b indicate the directions of the velocity and the magnetic field, respectively	30
3.2	Magnetic field lines (solid lines) and velocity vectors of cases 1, 3, and 4 (constant resistivity) are shown at time $t = 600$, with a shear velocity of $V_0 = 0$, $V_0 = 0.3$, and $V_0 = 0.5$ (from left to right). Note velocities are in units of the Alfvén speed, time is measured in Alfvén transit times, and length is measured in units of the half width of the initial current sheet	35

- 3.3 (a) Linear growth rate q of the tearing mode as a function of the wavenumber k , where the solid line is the dispersion relation for a resistivity of $\eta = 0.001$ [Otto et al., 1990] and symbols represent simulation results for cases 1 to 8. (b) The variation of the reconnection rate R as a function of time for different shear flow cases 36
- 3.4 From left to right, magnetic field lines and velocity vectors for cases 5, 7, and 8 at the time $t = 200$, with shear velocities of $V_0 = 0$, $V_0 = 0.3$, and $V_0 = 0.5$, respectively 38
- 3.5 For a current sheet with current dependent resistivity (a) the linear growth rate q of the tearing mode is presented as a function of the wavenumber k , where the solid line is for the effective resistivity $\eta = 0.011$, the dotted line is for constant resistivity $\eta = 0.001$, and other straight lines with different symbols are from simulation results of cases 9 to 12, and (b) the evolution of the reconnection rate for different shear flow cases is shown 40
- 3.6 From left to right, magnetic field lines and velocity vectors for cases 13 to 15 at time $t = 100$, where the values of the resistivity are $\eta = 0.001$, $\eta = 0.005$, and $\eta = 0.01$, respectively 42
- 3.7 For a current sheet with constant resistivity, (a) the perturbation $\ln(\max(v_x) - \min(v_x))$ along the y axis as a function of time for different resistivity cases 13 to 15. For the same cases (b) the maximum current density amplitude as a function of time and (c) the reconnection rate R 43

3.8	(a) A plot of the magnetic field lines and velocity vectors in a small subdomain of the system at $t = 19$, and (b) b_y and v_x along a cut at $x = 0$ for times $t = 19, t = 39$, and $t = 59$ to illustrate the mode structure for case 13	46
3.9	From left to right, magnetic field lines and velocity vectors for cases 16 to 18 for current dependent resistivity at time $t = 80$	48
3.10	For a current sheet with current dependent resistivity, (a) the perturbation $\ln(\max(v_x) - \min(v_x))$ along the y axis as a function of time for different resistivity cases 16 to 18. For the same cases (b) the maximum current density and (c) the reconnection rate amplitude as a function of time	50
3.11	(a) Magnetic field lines and plasma velocity vectors for a large resistivity of $\eta = 0.3$. (b) The profiles of b_y (solid) and v_y (dotted) for times $t = 0, t = 24$, and $t = 49$	52
4.1	Sketch of the tearing and KH modes in configuration (2)	59
4.2	Sketch of equilibrium magnetic field and flow field	61
4.3	A sketch of the hodogram for the b_y and b_z components for a trajectory through the current layer	63
4.4	(a) A typical tearing mode, (b) tearing growth rate as a function of resistivity ($k = 0.2$). The solid line is from the normalized unit current width, the dashed line is from analytical results, and the dotted line is from the $\frac{d\ln(\max(b_x) - \min(b_x))}{dt}$	68

4.5	(a) A typical KH mode, and the KH growth rate as a function of (b) b_{yc} (for $k = 0.31$, $\kappa = 0$) and (c) κ (for $k = 0.31$, $b_{yc} = 0$)	71
4.6	The KH growth rate as a function of (a) V_0 (for $b_y = 0$ and $\beta = 3$) and (b) β (for $V_0 = 0.3$ and $b_y = 0$)	72
4.7	Parse the KH and tearing modes from the coupled mode for (a) case 1, (b) case 2, (c) case 3, and (d) case 4	75
4.8	The possible tearing modes and KH modes in the yz plane for (a) only the magnetic shear, (b) only the flow shear, (c) both the mag- netic and flow shears, (d) both the magnetic and flow shears where the shear velocity is larger than the fast mode speed	79
4.9	The tearing mode for northward IMF	80
5.1	time evolution of normal velocity, magnetic field components, and maximum current density of case 1	88
5.2	(a) The change of flux tube cross-section from t_1 to t_2 . (b) The length of the contour line for $b_z = 0$ as a function of time	90
5.3	Winding-up processes of the current sheet and formation of multiple current layers due to Kelvin-Helmholtz vortices, where isosurfaces of $b_z = 0$ at (a) $t = 0$, (b) $t = 75$, (c) $t = 100$, and (d) $t = 125$ are shown	91
5.4	The mechanism of the formation of multiple current layers	93
5.5	When multiple current layer reconnection is triggered, the current sheet is modified, where isosurfaces of $b_z = 0$ at (a) $t = 155$, (b) $t = 160$, (c) $t = 165$, and (d) $t = 170$ are shown	94

5.6	Snap shots of the magnetic field vectors across the surface $y = -7$ at times $t = 160$, $t = 165$, and $t = 170$, where part of x range is shown	96
5.7	Snap shots of the contour lines of resistivity across the surface $y = -7$ at times $t = 160$, $t = 165$, and $t = 170$, where part of x range is shown. The solid and dashed contour lines denote high and low resistivity regions respectively	97
5.8	Snap shots of the contour lines of velocity component v_z across the surface $y = -7$ at times $t = 160$, $t = 165$, and $t = 170$, where part of x range is shown. The solid and dashed contour lines denote regions with positive and negative v_z respectively	98
5.9	At $t=165$, three magnetic field filaments pass through $(-4.5, -7, 3.5)$, $(-4.5, -7, 1.5)$, and $(-4.5, -7, 0)$ in a flux tube viewed from (a) origin (b) top (c) the position turned -40° along the z axis	100
5.10	At $t=165$, a magnetic field filament pass through $(-3, -7, -2)$ viewed from (a) origin (b) top (c) the position turned -40° along the z axis (d) the position turned -90° along the z axis	102
5.11	A magnetic field filament pass through $(-3, -7, -5)$ viewed at (a) $t=165$ (b) $t=170$ (c) $t=175$	103
5.12	At $t=165$, five current field filaments viewed from (a) origin (b) top; five velocity field filaments viewed from (c) top; and reconnection patchies viewed from (d) top	104
5.13	At $t=165$, three density distribution cuts along (a) the z direction, (b) y direction, and three pressure distribution cuts along (c) the z direction, (d) the y direction	106

5.14	At $t=165$, three pressure distribution cuts along (a) the z direction, (b) y direction, and three pressure distribution cuts along (c) the z direction, (d) the y direction	107
5.15	Time evolution of normal velocity, magnetic field components and maximum current density of case 2	109
5.16	Magnetic field vectors, contour lines of magnetic field component b_y and velocity component v_y in the xz plane are shown at $t = 210$ in a two-dimensional simulation	111
5.17	Velocity vectors, contour lines of resistivity and magnetic field b_z in the xy plane are shown at $t = 210$ in a two-dimensional simulation .	112
5.18	At $t = 210$, three cuts of magnetic field vectors along $y = -8$, $y = -4$, and $y = 1$ in the three-dimensional simulation	114
5.19	Magnetic field vectors comparison cut along $y = -4$ at $t = 150$, $t = 180$, and $t = 210$ in the three-dimensional simulation	116
5.20	At $t = 210$, three cuts of flow field vectors along $z = -13$, $z = -7$, and $z = 11$ in the three-dimensional simulation	117
5.21	The topology of magnetic flux tube at $t = 210$ viewd from (a) the original place (b) top (c) left (d) the low bottom	119
6.1	Plasma and magnetic field simulation data presentation through a cut $z = -8$, $y = -5.3$ at $t = 180$	126
6.2	Magnetic field hodogram	128
6.3	Walén relation presentation	130

6.4	Observational plasma data near the duskside magnetotail boundary on March 24, 1995 (from Fairfield)	134
6.5	Observational magnetic field data near the duskside magnetotail boundary on March 24, 1995 (from Fairfield)	135
6.6	The simulation coordinate system	138
6.7	The contour lines of plasma velocity v_z in the MSP coordinate system and velocity vectors and streamlines in the simulation plane at $t = 70$	140
6.8	B_{z-msp} contour lines, Magnetic field lines, and velocity vectors in the simulation plane at (a) $t = 45$, (b) $t = 70$, and (c) $t = 86$	142
6.9	(a) B_{x-sim} , which is generated by the vortex motion, deducts the northward IMF B_z . (b) The mechanism of component reconnection and magnetic flux transfer process	143
6.10	Contour lines of plasma density and temperature at (a) $t = 45$, (b) $t = 70$, and (c) $t = 86$	145
6.11	Plasma and magnetic field signatures for a probe rested at (3152,900,2501) in the MSP frame	146
6.12	Plasma and magnetic field data representation through a cut $y = 6.0$ at $t = 403$	148

List of Tables

3.1	Properties of the Tearing and KH modes	25
3.2	Summary of Cases	29
4.1	Summary of 3-D Simulation Cases	73

Acknowledgments

I would like to thank Dr. Antonius Otto, my thesis advisor, for his constant encouragement, advice, and help during my thesis study. I have been extremely fortunate to have this opportunity to study space physics under his guidance.

My sincere appreciation also goes to the other committee members-Drs. Brenton Watkins, Davis Sentman, and Roger Smith. I appreciate their invaluable time spent reading the document. Their concerns and helpful suggestions improved the quality of my thesis.

I also thank the people in the Writing Center of UAF for the help in the preparation of the thesis. I also express my gratitude to my friends, Mr. Knut, Ms. Twurtz, and their little daughter, Flora, for the wonderful summer time together with them. Many of my fellow Chinese students in Fairbanks provide me transportation and any other help they can give in this summer. I am grateful for their friendship.

I am greatly indebted to my parents, my wife Ms. Y. Zheng, and other family members for their love, continuous support, and encouragement. Without them, the thesis would not have been completed.

This work was supported by grants from the Department of Energy, the National Aeronautics and Space Administration, the National Science Foundation, and Alaska Space Grant Program to the University of Alaska. The Computing work was supported by the Arctic Region Supercomputing Center.

Chapter 1

Introduction

The transport of plasma, momentum, and energy across the magnetopause is of central importance for the dynamics of the entire magnetosphere. The solar wind interaction with the magnetosphere controls the intrinsic, microscopic structure of the magnetospheric boundary, and regulates the motion and energy dissipation of magnetosheath plasma during the process of its entry into the magnetosphere proper. According to the magnetic field, flow field, and plasma structure, the Earth's magnetopause is made up of the magnetopause current layer, the low-latitude boundary layer (LLBL), the entry layer, the cusp, the mantle, and the magnetotail boundary layer, sketched in Figure 1.1 [*Kennel et al.*, 1979].

The magnetopause current layer can be defined as the region where the currents flow that cause a more or less abrupt change in the magnetic field and plasma configuration, separating magnetosheath from magnetosphere [*Willis*, 1975; *Sonnerup*, 1976]. The low latitude boundary layer forms a broad belt from the subsolar region past the flanks toward the magnetotail. The observed LLBL flow has a strong

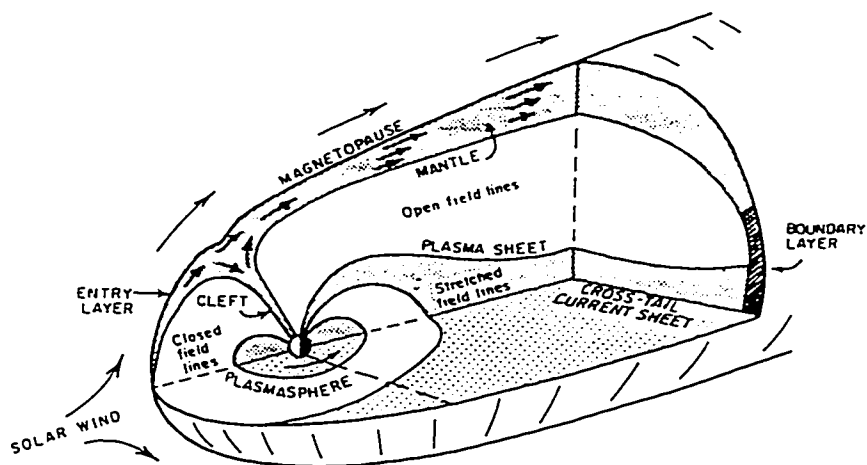


Figure 1.1 Sketch of the Earth's magnetopause [Kennel *et al.*, 1979].

cross-field component [Akasofu *et al.*, 1973]. The entry layer is thought to be a consequence of the entry of magnetosheath plasma through the dayside magnetopause [Paschmann *et al.*, 1976]. The field lines in this layer seem to be closed. The entry layer consists of field-aligned streaming of plasma of density and temperature nearly the same as in the magnetosheath, but with reduced flow speed [Sckopke *et al.*, 1976]. The cusp or cleft is a longitudinally elongated region of intense low-energy charged particle fluxes with field-aligned streaming, composed of entry layer plasma that is approaching the earth's ionosphere [Heikkila *et al.*, 1971]. The plasma mantle is a persistent layer of field-aligned tailward flow of magnetosheath-like plasma inside and adjacent to the magnetopause, tailward of the cusp. The flow speed in the mantle is less than the concurrent flow speed in the magnetosheath. The particle density, temperature and bulk speed decrease gradually with depth from the magnetopause to the inner boundary of the mantle [Rosenbauer *et al.*, 1975].

A study of these boundary layers is of particular importance because it involves dynamical phenomena that are unique to plasma flow interfaces and do not occur in the more uniform portions of the solar wind flow and inside the magnetosphere. A study of the transport and of the main processes of this transport at the magnetopause is central to the state and dynamics of the entire magnetopause which is controlled by the magnetopause boundary layer processes.

There are various instabilities that occur at the magnetopause. The two most prominent models for macroscopic transport at the magnetopause are viscous interaction and magnetic reconnection. Sources of free energy for the corresponding instabilities at the magnetopause are the different magnetic fields, the different

velocities, or the different densities of the solar wind and magnetospheric plasma. The free energies can cause a variety of instabilities. The most important instabilities on macroscopic scales are the tearing mode instability, which can operate in the presence of a magnetic shear, and the Kelvin-Helmholtz (KH) instability, which is an interchange instability driven by the presence of a velocity shear. Although the individual instabilities are well understood in two dimensions, the three dimensional nonlinear dynamics, the interaction of the two instabilities and applications to the magnetopause are poorly understood. These are the topics of this thesis.

1.1 The Tearing Mode and Kelvin-Helmholtz Instabilities

Before I introduce the physical processes at the magnetopause related to the two instabilities, it is worthwhile to review the basic properties of the two instabilities.

1.1.1 The Tearing Mode Instability

The resistive tearing mode instability takes place on a characteristic time scale that is much larger than the Alfvén transit time and is much smaller than the diffusion time. It develops in a limited region where $\mathbf{k} \cdot \mathbf{b}$ is 0 (\mathbf{k} is the wave vector and \mathbf{b} is the magnetic field), and where finite resistivity plays an important role. The free energy of the instability is magnetic energy. The basic theory of the tearing mode is included in the fundamental paper of *Furth et al.* [1963]. Analytical and

numerical studies of the linear tearing mode instability have been used in many different fields [e.g., *Coppi et al.*, 1966; *Killeen and Shestakov*, 1978; *Steinolfson and Van Hoven*, 1983; *Terasawa*, 1983; *Chen and Morrison*, 1990; *Otto and Birk*, 1992].

The sketch in Figure 1.2 presents the required magnetic geometry and the evolution of the tearing instability. The tearing mode requires an initial configuration with antiparallel magnetic field components \mathbf{b}_1 and \mathbf{b}_2 separated by a current sheet (Figure 1.2a). The tearing mode leads to the formation of magnetic islands which grow during the linear phase with an exponential growth rate (Figure 1.2b). For a hyperbolic magnetic field profile $b_y = B_0 \tanh(x/L)$, the relation between the growth rate q and the wavenumber k under certain η is written as [*Otto*, 1990]:

$$Q^2 = \frac{\lambda_0^{1/2}}{\pi} (1 - \lambda_0^2) (1 - A^2) \frac{\Gamma(\frac{\lambda_0+1}{4})}{\Gamma(\frac{\lambda_0+3}{4})} \quad (1.1)$$

where $Q = q\eta^{-1/2}$, $A = k\eta^{-1/4}$, $\eta = 1/S$, and $\lambda_0 = \frac{Q^{3/2}}{A}$. Here S is the Magnetic Reynolds number, k is the wave vector normalized to the inverse current sheet half width L , and q is the growth rate measured in units of the inverse Alfvén transit time $\tau_A = L/V_A$ with $V_A = B_0/\sqrt{\mu_0\rho}$ and ρ being the plasma density. The growth rate q is mainly dependent on normalized resistivity η and wave number k . Two branches of tearing modes have been identified: the constant- ψ tearing mode, whose growth rate scales as $\eta^{3/5}k^{-2/5}$ and a wave number close to 1, and the nonconstant- ψ tearing mode, whose growth rate scales as $\eta^{1/3}k^{2/3}$ and wave number close to 0. Constant and nonconstant- ψ refer to the x dependence of the eigenmode in the vicinity of $x = 0$. The maximum growth rate scales as $\eta^{1/2}$.

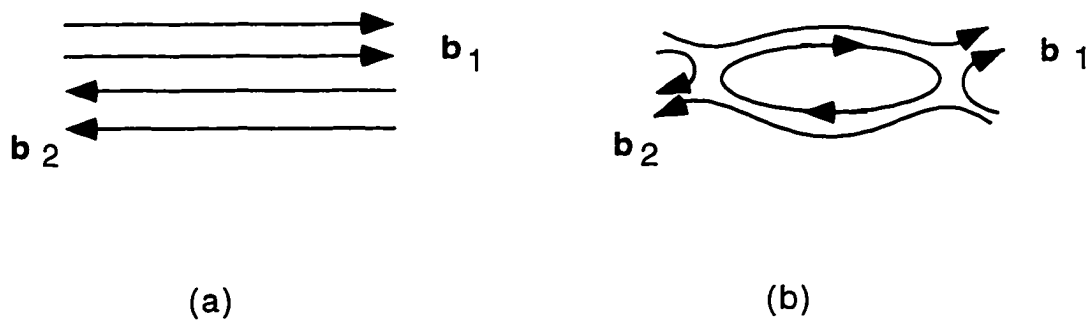


Figure 1.2 The development of the tearing mode instability.

1.1.2 The Kelvin-Helmholtz Instability

Figure 1.3 shows a sketch of the process of the Kelvin-Helmholtz (KH) instability. The presence of a velocity shear makes an unmagnetized fluid susceptible to the KH instability without a velocity threshold. The free energy source of the KH instability lies in the kinetic energy of the differential motion across a plane boundary. The growth rate of the KH mode for a basic case with uniform density and a discontinuous velocity with $v_y = \begin{cases} V_0 & x > 0 \\ -V_0 & x < 0 \end{cases}$ is $q = kV_0$, where k is the wavenumber of the KH mode.

The KH instability is stabilized by magnetic fields with a direction aligned with the shear flow [Chandrasekhar, 1961]. Consider two uniform magnetized fluids of plasma density ρ_1 and ρ_2 separated by a plane boundary, where the velocities and magnetic fields of the two incompressible fluids are $\mathbf{v}_1, \mathbf{v}_2$ and $\mathbf{b}_1, \mathbf{b}_2$ respectively. The dispersion relation for the KH mode is [Chandrasekhar, 1961]:

$$\omega = \frac{\rho_1 \mathbf{v}_1 + \rho_2 \mathbf{v}_2}{\rho_1 + \rho_2} \cdot \mathbf{k} \pm \sqrt{\rho_1 (\mathbf{V}_{A1} \cdot \mathbf{k})^2 + \rho_2 (\mathbf{V}_{A2} \cdot \mathbf{k})^2 - \frac{\rho_1 \rho_2}{\rho_1 + \rho_2} [(\mathbf{v}_1 - \mathbf{v}_2) \cdot \mathbf{k}]^2}$$

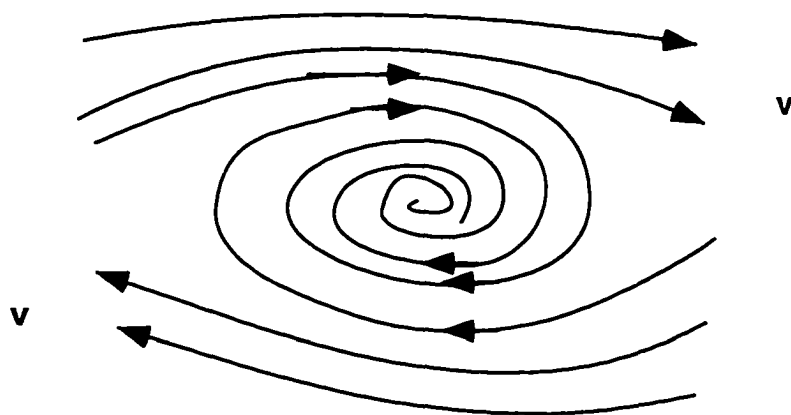
where ω is the frequency and $\mathbf{V}_{A1} = \mathbf{b}_1 / (\mu_0 \rho_1)^{1/2}$, $\mathbf{V}_{A2} = \mathbf{b}_2 / (\mu_0 \rho_2)^{1/2}$.

The development of the KH instability means ω has an imaginary part. The wave is growing in a frame moving with the velocity $\frac{\rho_1 \mathbf{v}_1 + \rho_2 \mathbf{v}_2}{\rho_1 + \rho_2}$ and yields a growth rate of

$$q = \sqrt{-\rho_1 (\mathbf{V}_{A1} \cdot \mathbf{k})^2 - \rho_2 (\mathbf{V}_{A2} \cdot \mathbf{k})^2 + \frac{\rho_1 \rho_2}{\rho_1 + \rho_2} [(\mathbf{v}_1 - \mathbf{v}_2) \cdot \mathbf{k}]^2} \quad (1.2)$$

provided that

$$\rho_1 \rho_2 [\Delta \mathbf{v} \cdot \mathbf{k}]^2 > \frac{1}{\mu_0} (\rho_1 + \rho_2) [(\mathbf{b}_1 \cdot \mathbf{k})^2 + (\mathbf{b}_2 \cdot \mathbf{k})^2] \quad (1.3)$$



Kelvin-Helmholtz Instability

Figure 1.3 The KH instability.

Here the velocity shear $\Delta \mathbf{v}$ equals $\mathbf{v}_1 - \mathbf{v}_2$, and $|\Delta \mathbf{v}| = 2V_0$. In the thesis, $\rho_1 = \rho_2 = \rho$ are used most of time. If $\mathbf{b}_1 = \mathbf{b}_2$, the onset condition of the KH instability is very simple:

$$V_0 > V_A \quad (1.4)$$

In a compressible plasma for a configuration as shown in Figure 1.4, *Miura et al.* [1982] found that for the sheared velocity perpendicular to the uniform magnetic field \mathbf{b}_0 (along the z direction) when

$$(V_0/V_f)^2 < \frac{k_y^2 + k_z^2}{k_y^2} \quad (1.5)$$

the KH instability operates, where $V_f = \sqrt{V_A^2 + V_s^2} [1 + \sqrt{\frac{1-4V_s^2 V_A^2 \cos^2 \theta}{(V_A^2 + V_s^2)^2}}]$. V_f , V_s , and V_A are respectively the fast mode speed, sound speed, and Alfvén speed, and θ is the angle between the magnetic field and the wave vector. If the sheared velocity (along the y direction) is parallel to the uniform magnetic field \mathbf{b}_0 when

$$(V_0/V_s)^2 < \frac{k_y^2 + k_z^2}{k_y^2} < (V_0/V_A)^2 \quad (1.6)$$

the KH instability operates, where V_s , and V_A are sound speed and Alfvén speed, k_y and k_z are the y and z components of the wave vector.

In addition, the KH instability also has two other properties: (1) A finite thickness of the shear layer stabilizes the KH mode for large wavenumbers [*Ong and Roderick, 1972*]. (2) Both compressibility and a magnetic field component parallel to the flow stabilize KH modes [*Miura and Pritchett, 1982*].

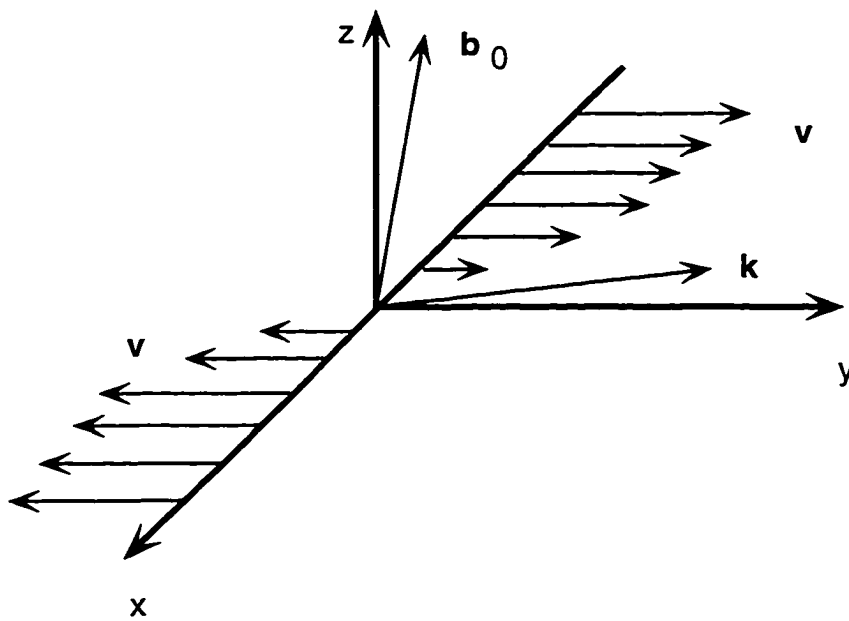


Figure 1.4 The coordinate system used in Miura's simulations.

1.2 Magnetopause Processes

The two basic processes for transport at the magnetopause are magnetic reconnection and viscous interaction [*Axford and Hines, 1961*]. The magnetospheric plasma convection is mainly controlled by a north-south component of the interplanetary magnetic field lines. This is assumed to be caused by an interconnection of interplanetary magnetic field lines to terrestrial magnetic field lines by day-side reconnection process. An important and quite interesting the observation of the plasma convection is observed residual plasma convection caused by some viscous-like interaction between the flowing magnetosheath plasma and the stationary magnetospheric plasma. Although such a viscous-like contribution to the magnetospheric convection appears to be small, it is important for complete understanding of the solar wind-magnetosphere interaction.

1.2.1 Magnetic Reconnection

The state of the terrestrial magnetosphere is firmly linked to conditions in the solar wind. The magnetopause is almost constantly moving because the magnetopause location is determined both by the solar wind dynamic pressure or momentum flux and also by the southward component of the IMF. A southward IMF orientation leads to a greater energy input into the magnetosphere and increased geomagnetic activity than a northward IMF orientation. *Dungey [1961]* suggested magnetic reconnection, which is favorable for southward IMFs, to explain this observation. Plasma and magnetic field observations from ISEE 1 and 2, launched in 1977 [*Paschmann et al., 1979; Sonnerup et al., 1981*], demonstrated strong evidence for

magnetic reconnection.

Russell and Elphic [1978] noted isolated disturbances in the magnetic field and plasma and particle environment of the low-latitude magnetosheath. They appeared to be encounters with reconnected flux tubes (FTEs). In addition to magnetosheath FTEs, magnetospheric FTEs have also been observed [*Daly and Keppler*, 1982]. The magnetosheath FTEs and magnetospheric FTEs are part of the same physical phenomenon at the magnetopause [*Rijnbeek et al.*, 1984]. The major character of FTEs is a bipolar signature in the magnetic B_N component in the nominal plane of the magnetopause. *Paschmann et al.* [1982] also noted the tendency for accelerated flow in the magnetosheath. *Berchem and Russell* [1984] and *Rijnbeek et al.* [1984] both found that FTE occurrence is greatest for southward IMF orientations. Magnetic field strength typically is enhanced during FTEs. For large FTEs, the area of the flux tube cross-section is typically $1 R_E^2$ and elongated in the L-direction of a boundary normal coordinate system [*Papamastorakis et al.*, 1989]. Twisted magnetic field lines are observed [*Goertz et al.*, 1985; *McHenry and Clauer*, 1987; *Wei and Lee*, 1990].

To explain the intermittent nature of the dayside magnetic reconnection process associated with FTEs, a number of theoretical models have been proposed. These include: (1) the elbow-shaped flux tube model [*Russell and Elphic*, 1978, 1979], (2) the multiple X line reconnection model (MXR) [*Lee and Fu*, 1985], (3) the bursty single X line reconnection model [*Scholer*, 1988; *Southwood et al.*, 1988], (4) the random turbulent reconnection model [*Kan*, 1988; *Nishida* 1989], (5) the vortex-induced tearing model [*Hu and Liu*, 1986], (6) the three-dimensional generation of bursty single X line model [*Otto*, 1990, 1991], and (7) the three-dimensional

linkage reconnection model [*Otto*, 1995].

The elbow-shaped flux tube model proposes that the relaxation of the bent, elbow-shaped flux tubes intermittently formed during the patchy reconnection at the dayside magnetopause results in the observed features of FTEs. The MXR model indicates that the interplanetary magnetic fields reconnect with the geomagnetic fields along several reconnection lines (X lines). The FTE signatures are generated by the convection of the magnetic flux tubes that are intermittently formed during the MXR process. The bursty single X reconnection model presents that the FTE signatures are due to an enhancement and a subsequent reduction of the reconnection rate at the reconnection region. A magnetic bulge formed at the low-latitude region propagating to high-latitude region produces magnetic perturbations and energetic particle features similar to that of FTEs. Model (5) relates the KH instability to the tearing mode instability to explain FTEs, but it confines its explanation to an incomplete two-dimensional picture. I will show it should be a fundamental process in three dimensions. Chapters 3, 4, 5, and 6 will discuss this in detail.

1.2.2 Viscous Transport Due to the Kelvin-Helmholtz Instability

The viscous interaction model was originally proposed by *Axford and Hines* [1961]. The viscous interaction between the solar wind and the Earth's magnetosphere can allow the momentum and energy of solar wind to diffuse or penetrate into closed magnetospheric magnetic field lines. A classic viscosity by ion-ion Coulomb colli-

sion is negligibly small to explain the tangential stress necessary for the observed residual plasma convection. Therefore the viscosity at the magnetopause boundary must be essentially anomalous. Anomalous transport may be caused by micro-turbulence like lower hybrid waves [*Huba et al.*, 1980; *Tsurutani and Stone*, 1985]. It also can be caused by macro-turbulence like the Kelvin-Helmholtz instability [e.g., *Southwood*, 1968; *Scopke et al.*, 1981; *Lee et al.*, 1981; *Miura*, 1984; *Pu and Kivelson*, 1983; *Wu*, 1986]. The KH instability can account for the momentum transport.

Surface waves have long been observed at the magnetopause as multiple boundary crossings with oscillatory variations in the boundary normal which are characteristic of a tailward moving surface perturbation [*Fairfield*, 1979]. The KH instability is a candidate for generating the waves, because the plasma bulk flow in both the magnetosheath and boundary is tailward and forms a shear layer capable of driving the instability. The growth of KH modes along the flow direction is most easily excited by shear flow perpendicular to the magnetic field, a condition which can be met at both the magnetopause and especially at the inner edge of the boundary layer where the magnetic field is northward at low latitudes.

If the KH instability is excited at the magnetopause, solar wind flow energy is converted into vortex motion and magnetic tension which lead to a viscous interaction at the magnetospheric boundary. *Chen et al.* [1993] found that an extended interval of quasi-periodic plasma and magnetic field variations (periods 5 min) at the pre-dawn flank of the magnetopause lasted for about four hours from the event occurred from 1400 to 1800 UT on February 15, 1978 when ISEE 1 and 2 hovered near apogee on the dawn flank of the magnetotail. The fluctuations in

the magnetic field appeared consistent with magnetopause crossings indicating a motion of the magnetospheric boundary. They compiled several reported surface wave observations at various locations at the magnetospheric boundary, which suggest a characteristic wave period for surface waves at the magnetopause of the order of 5 minutes.

Several studies have been done involving computer simulations of the KH instability at the magnetopause [MHD simulation: *Miura*, 1982, 1984, 1985, 1987, 1990, 1992; *Wang and Robertson*, 1984; *Wu*, 1986; *La Belle-Hamer et al.*, 1988; *Belmont and Chanteur*, 1989; *Manuel and Samson*, 1993. Hall MHD simulations: *Huba*, 1994; Hybrid MHD simulations: *Thomas and Winske*, 1991, 1993; *Terasawa et al.*, 1992; *Fujimoto and Terasawa*, 1994]. Their prime objective has been to understand the nonlinear evolution of the KH instability at the magnetopause and the nature of the transport of momentum and energy (and mass when the frozen-in condition is violated) into the magnetosphere by the instability. The direct evidence of the transport of momentum, energy, and mass across the magnetopause is the presence on the magnetospheric side of the magnetopause of the low latitude boundary layer (LLBL) [*Eastman et al.*, 1976]. In the LLBL a magnetosheath-like plasma is present and the plasma is flowing tailward.

Miura [1995] found that the observed rotation of the unperturbed magnetic field across the magnetopause leads to significant dependence of the magnetopause KH instability on the orientation of the magnetosheath magnetic field.

The above evidence shows that the KH instability is a very important process at the magnetopause and magnetotail boundary layer.

1.3 Motivation of the Thesis

The Earth's magnetopause, a boundary between the magnetosheath and the magnetosphere, is neither quiescent nor impenetrable, and this accounts for the interest in understanding its properties. The entire dynamics depends on the transport through the magnetopause. There are four basic macroscopic processes at the magnetopause: (1) magnetic reconnection, (2) Kelvin-Helmholtz instability, (3) pressure pulses, and (4) impulsive penetration. They are believed to relate to several very important magnetopause events: FTE's, boundary motion, local accelerated plasma flow [Otto *et al.*, 1995]. For about 20 years, those process were discussed as individual separate processes. However, they may not be mutually exclusive at the magnetopause. In particular, the KH instability was studied only in two dimensions. Such studies appear incomplete in order to understand the magnetopause structure and dynamics. Observations strongly indicates the existing of magnetic reconnection and the KH instability at the magnetopause. It is to be expected that under certain conditions (to be determined) the processes interact with each other.

I choose to focus on the relation between magnetic reconnection and the KH instability as the two most important processes for the magnetospheric boundary. *Hu and Liu* [1986] presented a theory of vortex-induced reconnection, which suggested the developed flow vortices may induce magnetic field lines to reconnect. This assumes a coupling of the two instabilities, but the mechanism and dynamics of the physical processes are still debatable. They argued that above and below the subsolar point the flow is not perpendicular but rather parallel to

the magnetopause so that the concept of driven reconnection does not apply. In these regions the magnetopause should be susceptible to the KH instability. The resulting large-scale vortices twist the magnetic field. In the case of antiparallel magnetic field reconnection sets in above and below the fluid vortices, leading to magnetic field islands. But around the subsolar point, the shear flow is very weak. It is unlikely that the KH instability, which is expected to cause wave growth with increasing distance from the subsolar point, operates at the subsolar magnetopause. There are possibly other regions where vortex induced reconnection might operate. However, it requires to be investigated.

At the magnetopause or LLBL there are many regions where velocity flow shear $\Delta\mathbf{v}$ (see section 1.1.2) and magnetic shear $\Delta\mathbf{b}$ (see section 1.1.1) co-exist, which implies that magnetic reconnection and the KH instability can operate simultaneously and play equally important roles at the magnetopause. This is a strong motivation to study the relation between magnetic reconnection and the KH instability. Figure 1.5 a sketch of the magnetopause in relation to magnetosheath flow v and confined magnetic field direction b . There are two very important configurations: (1) configurations where the velocity shear is parallel to the magnetic shear ($\Delta\mathbf{v}\parallel\Delta\mathbf{b}$) and (2) configurations where the velocity shear is perpendicular to the magnetic shear ($\Delta\mathbf{v}\perp\Delta\mathbf{b}$). For configuration (1), the role of the tearing and KH instabilities and the relation between magnetic reconnection and the KH instability need to be identified and resolved. For configuration (2), if both instabilities operate, the question of the identity of the corresponding process arises. This configuration poses a 3-D problem which can not be resolved in two dimensions.

In addition, the KH instability itself is a very powerful process at the magne-

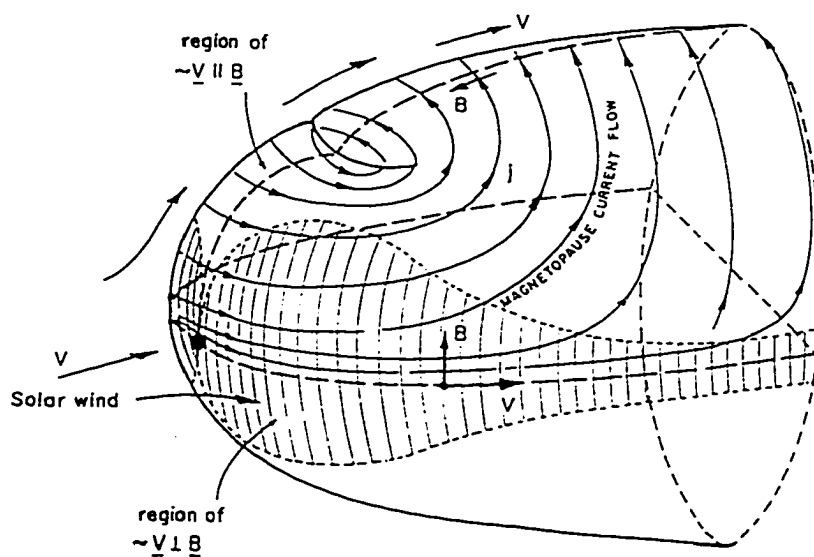


Figure 1.5 Magnetic field and flow field configuration at the dayside magnetopause [Kennel *et al.*, 1979].

topause and the magnetotail boundary layer. The KH instability and the interaction of the tearing and KH modes have not been studied in the literature.

1.4 Outline of the Thesis

In this thesis, I use two-dimensional and three-dimensional MHD simulations to investigate the KH instability, magnetic reconnection, and their relationship. The major emphasis of this thesis is on the interaction processes in the presence of magnetic shear and flow shear, the mechanism of vortex-induced reconnection, the interaction of the tearing and KH instabilities, and the KH-related magnetopause processes. Some of the results are compared with the observations at the magnetopause or lower latitude boundary layer.

Chapter 2 introduces basic numerical methods for this work.

In Chapter 3, I reconsider the interaction between reversed magnetic fields and shear flows antiparallel to the magnetic fields. This interaction is studied in the framework of two-dimensional compressible simulations. The influence of shear flow on the tearing mode is investigated using different shear velocities. I also look at the KH instability in the presence of different resistivities and discuss the possibility of vortex induced reconnection.

In Chapter 4, I investigate the linear properties of the tearing and KH instabilities. This study requires 2-D and 3-D compressible simulations and analytical theory. The possible tearing and KH modes at the magnetopause are also analyzed.

In Chapter 5, I extend this study to the nonlinear interaction between reversed magnetic fields and shear flows perpendicular to the magnetic fields. This nonlinear

interaction is investigated in three-dimensional, compressible simulations. The thinning of current sheets by the nonlinear KH vortices, the formation of multiple current layers, and induced multiple current layer reconnection are analyzed. The interaction of the KH and tearing instabilities is also investigated.

In Chapter 6, I compare two-dimensional simulations with observations at the tailward magnetospheric boundary and investigate structures of the magnetopause.

In the last chapter, I briefly summarize the results and suggest possible topics for future studies.

Chapter 2

Numerical methodology

Numerical simulation is a very powerful tool to solve nonlinear dynamic problems. To study the KH instability, magnetic reconnection, and their mutual interaction at the magnetospheric boundary, 2-D and 3-D numerical simulations are used to solve the nonlinear MHD equations.

2.0.1 Basic Equations

In this thesis, I solve the full set of resistive MHD equations [e.g., *Otto et al.*, 1990].

$$\frac{\partial \rho}{\partial t} = -\nabla \cdot \rho \mathbf{v} \quad (2.1)$$

$$\frac{\partial \rho \mathbf{v}}{\partial t} = -\nabla \cdot (\rho \mathbf{v} \mathbf{v} + \frac{1}{2}(p + \mathbf{b}^2)\mathbf{I} - \mathbf{b} \mathbf{b}) \quad (2.2)$$

$$\frac{\partial \mathbf{b}}{\partial t} = \nabla \times (\mathbf{v} \times \mathbf{b} - \eta \nabla \times \mathbf{b}) \quad (2.3)$$

$$\frac{\partial h}{\partial t} = -\nabla \cdot (h \mathbf{v}) + \frac{\gamma - 1}{\gamma} h^{1-\gamma} \eta \mathbf{j}^2 \quad (2.4)$$

with $h = (p/2)^{1/\gamma}$ and $\mathbf{j} = \nabla \times \mathbf{b}$. Here ρ is the plasma mass density, \mathbf{v} is the plasma velocity, p is the plasma pressure, \mathbf{b} is the magnetic field, \mathbf{j} is the current

density, η is the resistivity, \mathbf{I} is the unit tensor, and γ is the ratio of specific heats ($\gamma = 1.667$). Here all quantities are normalized to characteristic values for the system, that is, length scales l to a typical length a , density ρ to $\rho_0 = n_0 m_0$ with the number density n_0 and the ion mass m_0 , magnetic field \mathbf{b} to B_0 , velocity \mathbf{v} to the typical Alfvén velocity $V_A = B_0(\mu_0 \rho_0)^{-1/2}$, pressure to $P_0 = B_0^2/(2\mu_0)$, and time t to a characteristic Alfvén transit time $t_A = a/V_A$. The growth rate q , the reconnection rate R , the reconnected flux Φ , and the current density \mathbf{j} are measured in units of t_A^{-1} , $V_A B_0$, $a B_0$, and $B_0/(\mu_0 a)$, respectively. The normalized resistivity is $\eta = H_0/(\mu_0 a V_A)$ with H_0 being the resistivity in MKS units. For a constant resistivity, $S = \eta^{-1}$ is the magnetic Reynolds number for the current sheet in the initial configuration.

2.0.2 Boundary Conditions and Numerical Method

The numerical method I used is a leapfrog scheme [Potter, 1973]. Free boundary conditions are applied to the two boundaries in the x direction. Periodic boundary conditions are used at the two boundaries along the y and z directions. The Courant Freidrichs Levy condition is satisfied in all of the 2-D and 3-D simulations.

The grid is chosen to be uniform along the y and z directions and nonuniform along the x direction with a minimum grid separation of ϵ_x in the center of the system to resolve the evolution of thin current layers during the dynamical evolution. The number of grid points and the maximum resolution is varied for different simulations. This very high resolution is necessary to resolve the non-linear KH mode for a sufficiently long time during the simulation. Without this

resolution the nonlinear evolution would be dominated by numerical dissipation (the numerical roundoff error is $O(\Delta x^2, \Delta t^2)$).

In addition to the growth rate I evaluate the reconnected magnetic flux and reconnection rate. These parameters are important to distinguish ideal instabilities from the resistive tearing mode. In two dimensions,

$$\mathbf{b} = \nabla A \times \mathbf{e}_z \quad (2.5)$$

where A is the z component of the vector potential. The reconnected flux is the magnetic flux between the X line and the O line:

$$\Phi = \int_{y_o}^{y_x} b_x dy \quad (2.6)$$

and the electrical field along z direction is given by

$$E_z = -\frac{\partial A}{\partial t} \quad (2.7)$$

From equation 2.5 I can get $A_x - A_o = \int_{y_o}^{y_x} b_x dy$. So $\Phi = A_x - A_o$, and the reconnection rate is $R = E_{z_x} - E_{z_o}$. As a consistency test the reconnected flux can be calculated also from

$$\Phi = \int_0^t E_{z_x} - E_{z_o} dt = \int_0^t \eta_x j_x - \eta_o j_o dt \quad (2.8)$$

In my particular cases the X and the O lines are static points.

In three dimensions, I do 2-D and 3-D comparisons for the same configurations.

Chapter 3

The interaction of parallel flow shear and magnetic shear

This chapter has been published in the Journal of Geophysics Research, 102, 151, 1997.

3.1 Introduction

The Kelvin-Helmholtz (KH) instability and the tearing instability are two important instabilities in magnetospheric physics. Both of them are believed to play crucial roles for many phenomena at the magnetopause.

The basic properties of the tearing and KH modes are summarized in Table 3.1. The development of the KH instability is affected by the presence of magnetic fields. The KH instability is stabilized by magnetic fields with a direction aligned with the shear flow [*Chandrasekhar, 1961*]. *Miura and Pritchett [1982]* found the

Table 3.1 Properties of the Tearing and KH modes.

item	tearing mode	KH mode
free energy	magnetic shear	shear velocity
stabilization	shear flow	magnetic field

KH mode completely stabilized for a velocity jump $2V_0 < 2V_A(\hat{k} \cdot \hat{b}_0)/(\hat{k} \cdot \hat{v}_0)$ in a plasma with a uniform magnetic field, where \hat{b}_0 and \hat{v}_0 are the unit vectors of magnetic field and velocity, respectively, and V_A is Alfvén velocity. Only modes with $k\Delta < 2$ are unstable, and the fastest growing modes occur for $k\Delta \sim 0.5 - 1.0$, where Δ is the width of the shear flow layer. Both compressibility and a magnetic field component parallel to the flow stabilize KH modes. *Wu* [1986] compared the convective KH instability with the periodic KH instability. In the linear stage there was no difference.

The resistive tearing mode instability takes place on a characteristic timescale that is much larger than the Alfvén transit time and is much smaller than the diffusion time. The basic theory of the tearing mode is included in the fundamental paper of *Furth, et al.* [1963]. Analytical and numerical studies of the linear tearing mode instability have been used in many different fields [e.g., *Coppi et al.*, 1966; *Killeen and Shestakov*, 1978; *Steinolfson and Van Hoven*, 1983; *Terasawa*, 1983; *Chen and Morrison*, 1990; *Otto and Birk*, 1992].

At the Earth's magnetopause both velocity and magnetic shear coexist. *Hu and Liu* [1986] suggested that the development of the KH instability near the magnetopause may twist the magnetic field lines and lead to the formation of

magnetic islands. They called this type of reconnection vortex-induced magnetic reconnection (VIR). *Einaudi and Rubini* [1986] first investigated the modification of the tearing mode by shear flows parallel to the magnetic field. For fast velocity shear ($V_0 > V_A$) they found a transition to the ideal KH mode, provided the flow profile has a maximum in the current sheet.

Subsequently, many studies have focused on the modulation of the tearing mode by velocity shear and on magnetic reconnection caused by the formation of flow vortices. For various flow and magnetic field orientations, *La Belle-Hamer et al.* [1988] found a coupling of tearing and KH modes which can enhance the tearing mode growth rate. *Pu et al.* [1990a] found an enhanced tearing growth rate for flow velocities larger than $0.4V_A$ with a steep increase for $V_0 = V_A$ which they described as a vortex-induced tearing mode. This mode has been suggested to explain magnetic flux transfer events at the dayside magnetopause [*Pu et al.*, 1990b]. When shear flow is parallel to a reversed magnetic field, *Pu et al.* concluded that the Alfvén Mach number (the ratio of shear velocity to local Alfvén speed) plays an essential role in determining the evolution of the coupled instability. Recently, *Fu et al.* [1995] claimed a transition to VIR for Alfvén mach numbers above 0.3 to 0.6. These studies [e.g., *Pu et al.*, 1990a, b; *Fu et al.*, 1995] on VIR assume an incompressible plasma and relatively low magnetic Reynolds numbers.

In contrast to these results, various analytic and computational studies have found a stabilization of the tearing mode by velocity shear. *Einaudi and Rubini* [1986] demonstrated a total stabilization of the tearing mode for super-Alfvénic flows with a tanh profile. *Chen and Morrison* [1990] and *Ofman et al.* [1991] found the fastest growing nonconstant- ψ solutions stabilized by shear flow. MHD

simulations with constant resistivity by *Ofman et al.* [1993] demonstrated a stabilization and an earlier saturation of the tearing mode due to shear flow. All of these studies were carried out in the limit of incompressible MHD. In the framework of compressible MHD, *La Belle-Hamer et al.* [1995] found that nonlinear magnetic reconnection is switched off when the plasma velocity relative to the X line is super-Alfvénic. These results seem to contradict a coupling of tearing and KH modes with an enhanced growth of the tearing mode for sub-Alfvénic shear flow.

In this chapter I attempt to resolve the problem of the interaction of tearing and KH for a basic two-dimensional configuration using the nonlinear compressible MHD equations. A particularly important aspect appears to be the choice of a sufficiently small resistivity. This condition applies for the following reasons. First, the evolution of the tearing mode requires a large magnetic Reynolds number S or small resistivity such that the diffusion timescale and the growth time are well separated. Otherwise, the lack of an approximate equilibrium or steady state invalidates the concept of an instability. Second, fast diffusion caused by a large resistivity reduces the magnetic tension force and may lower the threshold velocity for the onset of KH. Third, the magnetopause is a rather thin magnetic boundary layer [*Berchem and Russell*, 1982] which cannot exist in the presence of too much resistive diffusion. Thus an application to the magnetopause requires a natural limit to the diffusion. In this respect the assumption of a current dependent resistivity is attractive because it can switch off resistive diffusion if the current layer becomes too wide. In this study I will use both a constant and a current dependent resistivity to clarify influences of the dissipation on the instability processes.

The chapter is organized as follows. Section 2 presents initial and boundary conditions, Section 3 shows my simulation results. In section 4 I discuss and summarize my results.

3.2 Equilibrium and Initial Perturbation

I consider the idealized interaction between reversed magnetic fields and shear flows antiparallel to the magnetic fields. For all simulations I consider a one-dimensional initial equilibrium configuration which separates two regions of different magnetic field orientation as illustrated in Figure 3.1. Here x is the direction normal to the current layer, and y is along the direction with maximum antiparallel fields. The k vector of the considered instability is along the y direction. The simulation domain is a rectangular box with $|x| \leq L_x$ and $|y| \leq L_y$. For all simulations, L_x is chosen to be 15 (to minimize the influence of the boundary conditions) in units of the equilibrium shear width, and L_y is listed in Table 3.2 for the cases considered. As illustrated in Figure 3.1, the initial magnetic field and the plasma flow are along the y direction. The plasma is initially uniform in total pressure (including dynamical and magnetic pressure). The equilibrium is determined by

$$b_{x0}(x) = 0 \quad (3.1)$$

$$b_{y0}(x) = \tanh x \quad (3.2)$$

$$v_{x0}(x) = 0 \quad (3.3)$$

$$v_{y0}(x) = -V_0 \tanh x \quad (3.4)$$

$$p_0(x) = \beta_0 + \cosh^{-2} x \quad (3.5)$$

Table 3.2 Summary of Cases.

Case	L_y	η_0	α	j_c^2	V_0	P Type
1	15	0.001	0	0	0.0	T
2	15	0.001	0	0	0.1	T
3	15	0.001	0	0	0.3	T
4	15	0.001	0	0	0.5	T
5	10	0.001	0	0	0.0	T
6	10	0.001	0	0	0.1	T
7	10	0.001	0	0	0.3	T
8	10	0.001	0	0	0.5	T
9	15	0	0.005	0.8	0.0	T
10	15	0	0.005	0.8	0.1	T
11	15	0	0.005	0.8	0.3	T
12	15	0	0.005	0.8	0.5	T
13	5	0.001	0	0	1.5	KH
14	5	0.005	0	0	1.5	KH
15	5	0.010	0	0	1.5	KH
16	5	0	0.001	0.95	1.5	KH
17	5	0	0.01	0.95	1.5	KH
18	5	0	0.01	0.9	1.5	KH

$$\rho_0(x) = 1 \quad (3.6)$$

where β_0 is the ratio of dynamical to magnetic pressure at the boundaries $|x| = L_x$. For all cases, β_0 is chosen to be 4 which is consistent with typical values in the magnetosheath and in the dayside low-latitude boundary layer [*Phan and Paschmann, 1996*].

A small amplitude perturbation is given in terms of the velocity profile:

$$v_x(x, y) = v_{x0}(x) + \delta v_x \quad (3.7)$$

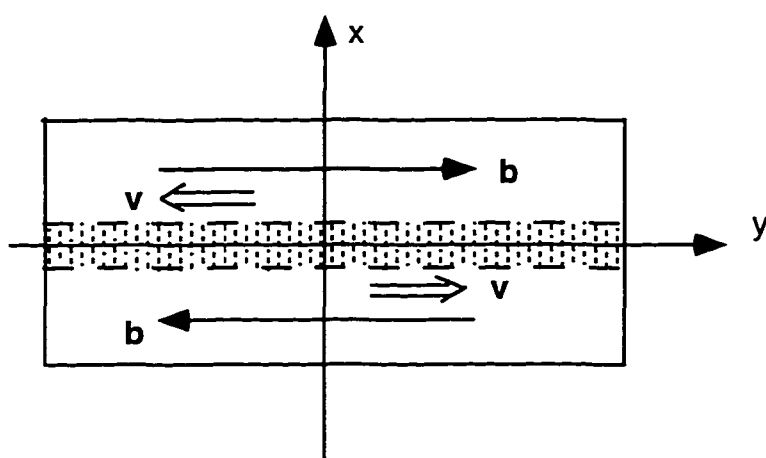


Figure 3.1 Sketch of the initial configuration of magnetic field and shear flow, where the shaded region is the current sheet. Arrows labeled v and b indicate the directions of the velocity and the magnetic field, respectively.

$$v_y(x, y) = v_{y0}(x) + \delta v_y \quad (3.8)$$

For the tearing mode related problem the following tearing-like perturbation is given:

$$\delta v_x = v_1 x (\pi/L_y) \cos(y\pi/L_y) \cosh^{-2} x \quad (3.9)$$

$$\delta v_y = -v_1 \cosh^{-2} x [1 - 2x \sin(y\pi/L_y) \tanh x] \quad (3.10)$$

where $v_1 = 0.001$. For the KH mode related problem the following vortex-like perturbation is given:

$$\delta v_x = v_1 (\pi/L_y) \sin(\pi y/L_y) \cosh^{-2} x \quad (3.11)$$

$$\delta v_y = -2v_1 \cos(\pi y/L_y) \tanh x \cosh^{-2} x \quad (3.12)$$

where $v_1 = 0.0001$. These perturbations have the same symmetry as the related eigenmodes, and they are chosen such that $\nabla \cdot \mathbf{v} = 0$.

In this study I consider cases with constant resistivity and current dependent resistivity where the current dependent resistivity is determined by

$$\eta = \eta_0 + \begin{cases} \alpha(j^2 - j_c^2) & j \geq j_c \\ 0 & j < j_c \end{cases} \quad (3.13)$$

where $j = |\mathbf{j}|$ and j_c is a critical current density. This form can be interpreted as the result of current-driven enhanced resistivity. For the considered cases the current dependent resistivity serves two purposes. First, it clarifies the influence of different resistivity models on the dynamics, in particular, of the KH instability. Second, a current dependent resistivity appears more realistic for applications to the magnetopause, (1) because it implies a negligible resistivity almost everywhere

in the system, as expected for a highly collisionless plasma, and (2) because it prohibits the evolution of singular current sheets with an arbitrarily small thickness. A current dependent resistivity can be expected as a result of microturbulence [e.g., *Papadopoulos, 1980, Brackbill et al., 1984*].

In the simulations addressing the tearing mode I use 63×43 grid points with a resolution of $\epsilon_x = 0.05$ and $\epsilon_y = 0.75$. In the simulations related to the development of the KH mode I use 203×83 grid points with a resolution of $\epsilon_x = 0.008$ and $\epsilon_y = 0.125$.

3.3 Simulation Results

A summary of the cases discussed in this section is provided in Table 3.2. Here the first two columns present the case number and the half wavelength of the discussed modes. The next three columns identify the properties of the resistivity model. The sixth column presents the magnitude of the shear flow, and the last column shows perturbation type. I have used in addition other perturbations to verify the results. Typically, the tearing mode is also obtained with the KH type perturbation; however, the evolution takes longer because the corresponding normal mode has a smaller amplitude in the spectrum of the perturbation.

Cases 1 to 8 use a constant resistivity and sub-Alfvénic shear velocity to study the influence of shear flow on the tearing mode. Here cases 1 to 4 consider long wavelengths and cases 5 to 8 consider short wavelengths. Cases 9 to 12 study the tearing mode for current dependent resistivity and sub-Alfvénic shear velocity. The instability of the shear velocity layer for super-Alfvénic plasma flow (KH type)

is studied with cases 13 to 18. These also consider various resistivity models.

3.3.1 Sub-Alfvénic Shear Flow: The Tearing Mode

The influence of shear flow on the tearing mode is investigated using different shear velocities but otherwise the same parameters. An evaluation of the growth rates of the tearing mode and reconnection rates is used to identify the influence of the shear flow. Note that a proper evaluation can not only rely on the growth rate of the modes because the coupling of the tearing mode with another instability can result in significant growth rates but may show a decrease in the reconnection rate. For instance, the transition of the tearing mode to the radiative tearing instability yields large growth rates even for $\eta = 0$, but in the limit of vanishing resistivity the reconnection rate also tends to zero [e.g., *Birk and Otto*, 1991].

Figure 3.2 shows the magnetic field lines and velocity vectors of three cases with the same constant resistivity $\eta = 0.001$ and different shear flow velocities at $t = 600$. Magnetic field lines are plotted with a uniform spacing in magnetic flux. The plot in Figure 3.2 shows only a subdomain of the entire simulation to enhance the relevant features. The biggest magnetic island appears in case 1 in which there is no shear flow. Shear flow has an obvious tendency to reduce the size of the magnetic island. This earlier saturation of the tearing mode is consistent with an investigation by *Ofman et al.* [1993] for the case of incompressible dynamics and smaller wavelengths. Note that the results shown in Figure 3.2 also include the effects of diffusion which are important on the considered timescales. Consistent with theoretical expectations [*Chen and Morrison*, 1990], the results

do not indicate any coupling to a KH instability.

Figure 3.3a shows growth rates of the instability [Furth *et al.*, 1963] for different shear velocity as a function of the wavenumber. Growth rates are obtained from $\delta b_x|_{x=0} = 0$ and are corrected for effects from diffusion. The solid line is the dispersion relation for the tearing mode without shear flow in an incompressible plasma. In my compressible simulations the growth rates of case 1 and case 5 are still close to the theoretical case without shear flow. For the same wavenumbers, the growth rate decreases when the shear velocity V_0 increases from 0 to 0.5. This indicates that shear flow stabilizes the tearing instability. Figure 3.3b shows the reconnection rate as a function of time for the different cases. It shows a significant decrease of the reconnection rate with increasing shear velocity. Close to $t = 600$ the reconnection rate levels off indicating the start of the saturation of the cases with $V_0 = 0.0$ and $V_0 = 0.1$ shown in Figure 3.2, while larger shear velocity cases saturate earlier.

Often, current dependent resistivity models are used to simulate physical problems at the magnetopause. In the following I consider cases (9 to 12) with the same parameters as in cases 1 to 4, however, with the current dependent resistivity model.

From left to right, Figure 3.4 presents magnetic field lines and velocity vectors of three cases with the same resistivity model parameters, $\eta_0 = 0$, $\alpha = 0.005$, and $j_c^2 = 0.8$, but different shear flow velocities $V_0 = 0$, $V_0 = 0.3$, and $V_0 = 0.5$, respectively. All plots show the same time, $t = 200$. Similar to the constant resistivity cases the largest magnetic island appears for case 9, in which there is no shear flow. Again, increasing shear flow has the obvious tendency to reduce the

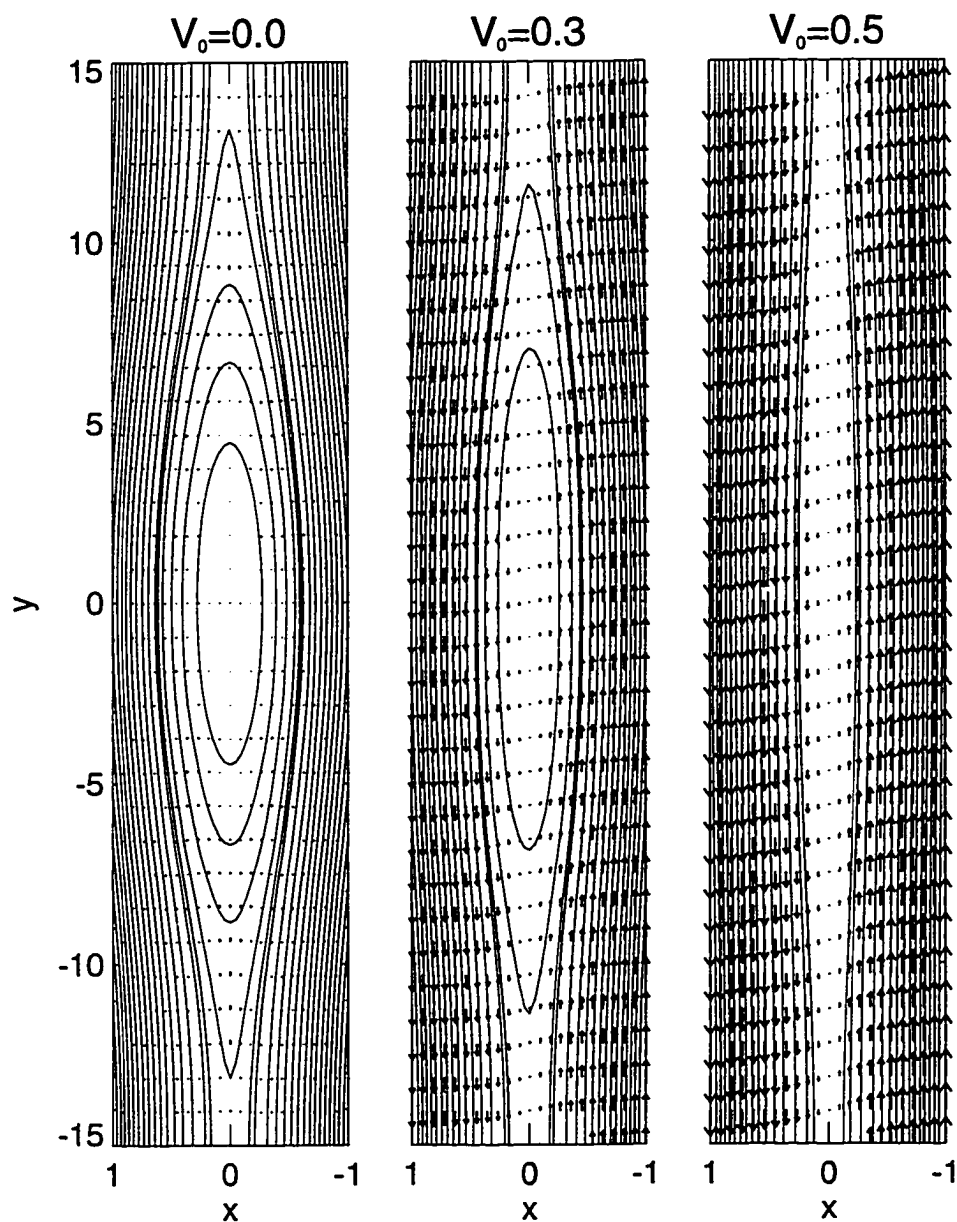


Figure 3.2 Magnetic field lines (solid lines) and velocity vectors of cases 1, 3, and 4 (constant resistivity) are shown at time $t = 600$, with a shear velocity of $V_0 = 0$, $V_0 = 0.3$, and $V_0 = 0.5$ (from left to right). Note velocities are in units of the Alfvén speed, time is measured in Alfvén transit times, and length is measured in units of the half width of the initial current sheet.

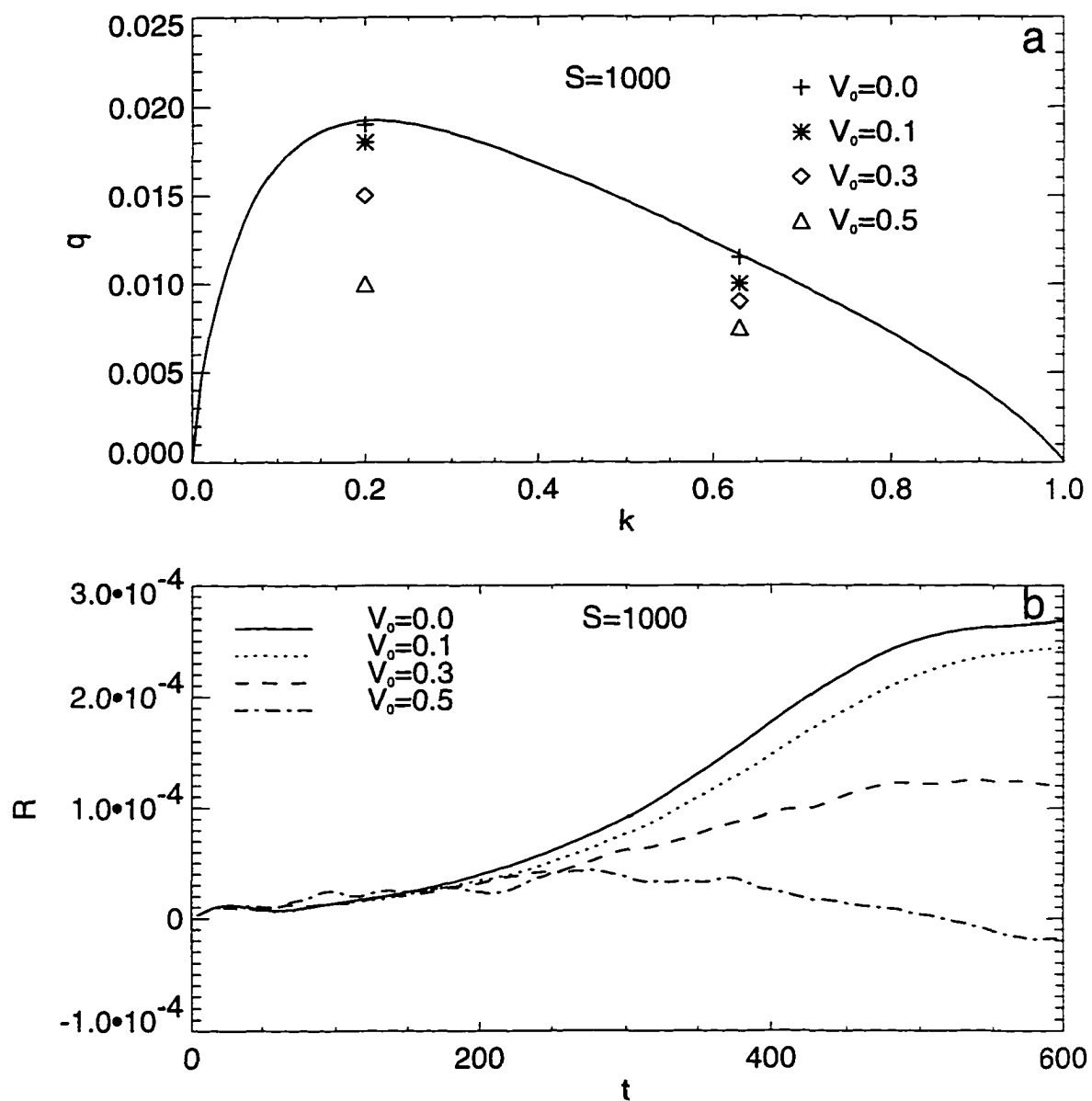


Figure 3.3 (a) Linear growth rate q of the tearing mode as a function of the wavenumber k , where the solid line is the dispersion relation for a resistivity of $\eta = 0.001$ [Otto *et al.*, 1990] and symbols represent simulation results for cases 1 to 8. (b) The variation of the reconnection rate R as a function of time for different shear flow cases.

width of the resulting magnetic islands. I remark that for these current dependent resistivity cases I did not find well saturated final configurations. During the later evolution the cases with $V_0 = 0$, $V_0 = 0.1$, and $V_0 = 0.3$ exhibit more complex configurations which include a splitting of the X line. The final island width before it decays into more complex structures appears to be only slightly reduced by the shear flow up to $V_0 = 0.3$. The case with $V_0 = 0.5$ saturates much earlier. Consistent with theoretical expectations, Figure 3.4 shows no indication of a KH instability.

For the cases with current dependent resistivity the dispersion relation of the tearing mode can be obtained by using an effective resistivity. The maximum growth rate of the tearing mode without shear flow scales as $\sqrt{\eta_{\text{eff}}}$ [Otto, 1991]. This effective resistivity is obtained from the linearized form of (17):

$$\begin{aligned} \eta_{\text{eff}} &= \eta_{t=0} + \frac{\partial \eta}{\partial j} j_0 \\ &= \begin{cases} \alpha(j_0^2 - j_c^2) + 2\alpha j_0^2 & j_0 \geq j_c \\ 0 & j_0 < j_c \end{cases} \end{aligned} \quad (3.14)$$

where j_0 indicates the equilibrium current density. Note that the resistivity $\eta_{t=0}$ for the model parameters is 0.001, that is, the same as for the constant resistivity cases such that diffusion is rather slow. However, the effective resistivity, which determines the growth rate of the tearing mode, is $\eta_{\text{eff}} = 0.011$ for the equilibrium which implies much faster growth for the cases considered here.

Figure 3.5a shows the comparison of growth rates between theoretical and simulation values. Without shear flow the solid line and the dashed line theoretically present the growth rate as a function of wavenumber for the effective resistivity $\eta_{\text{eff}} = 0.011$ and the zero-order resistivity $\eta_{t=0} = 0.001$, respectively. The other

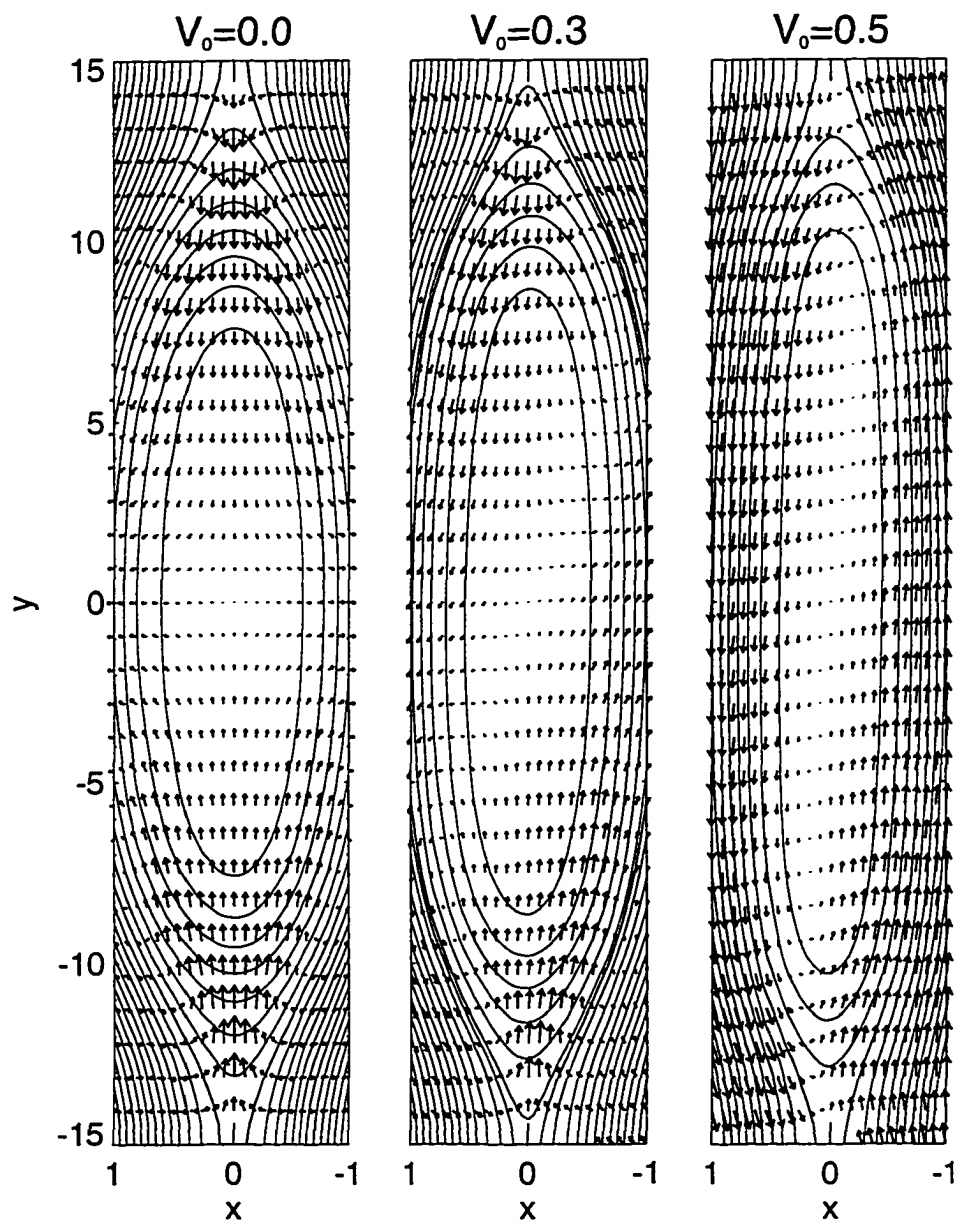


Figure 3.4 From left to right, magnetic field lines and velocity vectors for cases 5, 7, and 8 at the time $t = 200$, with shear velocities of $V_0 = 0$, $V_0 = 0.3$, and $V_0 = 0.5$, respectively.

lines marked with different labels are from simulation results of cases 9 through 12. Because of magnetic field diffusion, the current sheet width increases from 1 to 1.5 in the simulation for all four cases, and thus the wavenumber shifts from 0.2 to about 0.3 (there are only very limited shifts in the cases with constant small resistivity). The growth rate for small shear flow is close to the solid line and for all cases is above the dashed line. For the same wavenumbers the growth rate decreases with increasing shear velocity. This indicates that shear flow stabilizes the tearing instability in a manner similar to the constant resistivity cases. Figure 3.5b shows the variation of the reconnection rate as a function of time in different shear velocity cases. The reconnection rate also shows a decrease with increasing shear velocity.

For shear flow with $0.5 < V_0 < 1.0$ and small resistivity, strong fluctuations made it difficult to identify the growth rate of the tearing mode for either constant or current dependent resistivity models. However, the overall growth rate is smaller than that in the cases with $V_0 < 0.5$, and there is also no indication of a KH instability.

3.3.2 Super-Alfvénic Velocity Shear Effects on the Kelvin-Helmholtz Mode

For super-Alfvénic shear flows (for example, I set $V_0 = 1.5$) the primary instability is expected to be the KH. There are various unresolved basic problems: Is there a coupling of the tearing and the KH instabilities? Does the choice of the resistivity have an influence on the KH instability? What is the relation between the KH

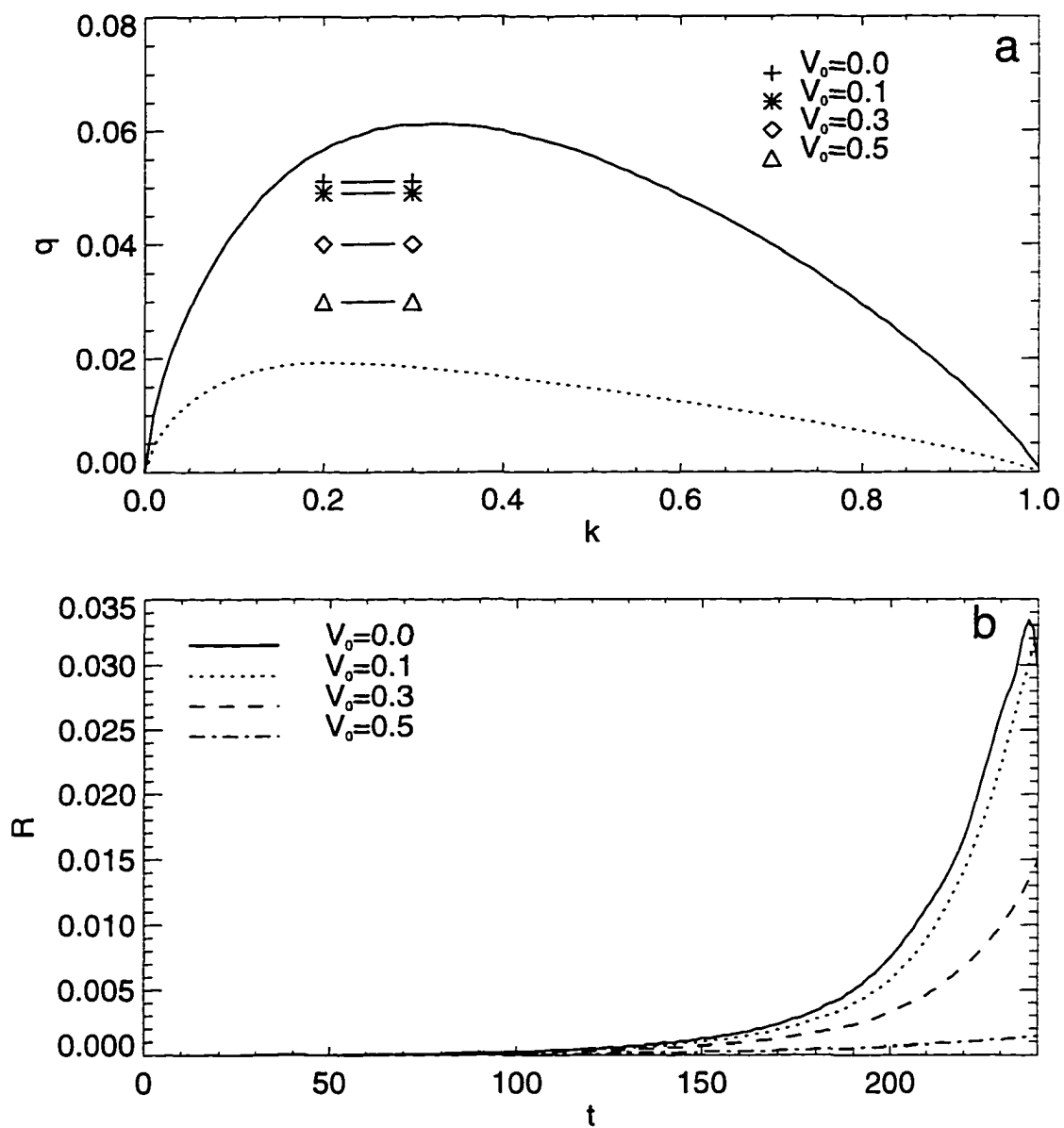


Figure 3.5 For a current sheet with current dependent resistivity (a) the linear growth rate q of the tearing mode is presented as a function of the wavenumber k , where the solid line is for the effective resistivity $\eta = 0.011$, the dotted line is for constant resistivity $\eta = 0.001$, and other straight lines with different symbols are from simulation results of cases 9 to 12, and (b) the evolution of the reconnection rate for different shear flow cases is shown.

instability and magnetic reconnection?

First, I present some results for constant resistivity cases. Figure 3.6 shows magnetic field lines and velocity vectors of cases 13 to 15 at the time $t = 100$, where the values of resistivity are $\eta = 0.001$, $\eta = 0.005$, and $\eta = 0.01$, respectively. Velocity vectors indicate the evolution of the KH instability. In addition, I see different size magnetic islands which demonstrates that magnetic reconnection is operating. The largest magnetic island and flow vortex is formed at $\eta = 0.01$, and the smallest is formed at $\eta = 0.001$. However, does this imply a tearing instability or a mode coupling of KH and tearing modes?

Figure 3.7a shows $\ln(\max(v_x) - \min(v_x))$ along the y axis as a function of time for three different cases with $\eta = 0.001$, $\eta = 0.005$, and $\eta = 0.01$. Here the regions of approximately constant slope measure the growth rate. Figure 3.7a shows a very rapid increase of the perturbation around $t = 10$. I will come back to this feature a little later. The large-scale KH mode dominates the growth between $t = 65$ and $t = 90$. The slope during this interval and the growth time appear to be very similar for the three cases. For the wavelength of $\lambda = 10$ these slopes give a growth rate of $q \approx 0.11$ such that the growth of the KH mode does not appear to be affected much by the choice of the resistivity.

In Figures 3.7b and 3.7c, the maximum absolute current density and the reconnection rate, respectively, are presented as a function of time. From $t = 65$ to $t = 90$ the values of both the reconnection rate and the maximum current density magnitude clearly increase for different cases. The increase of the maximum current density is a result of the pinching of the current layer by the KH instability. In the resistive system the increase of the current density generates an increase in

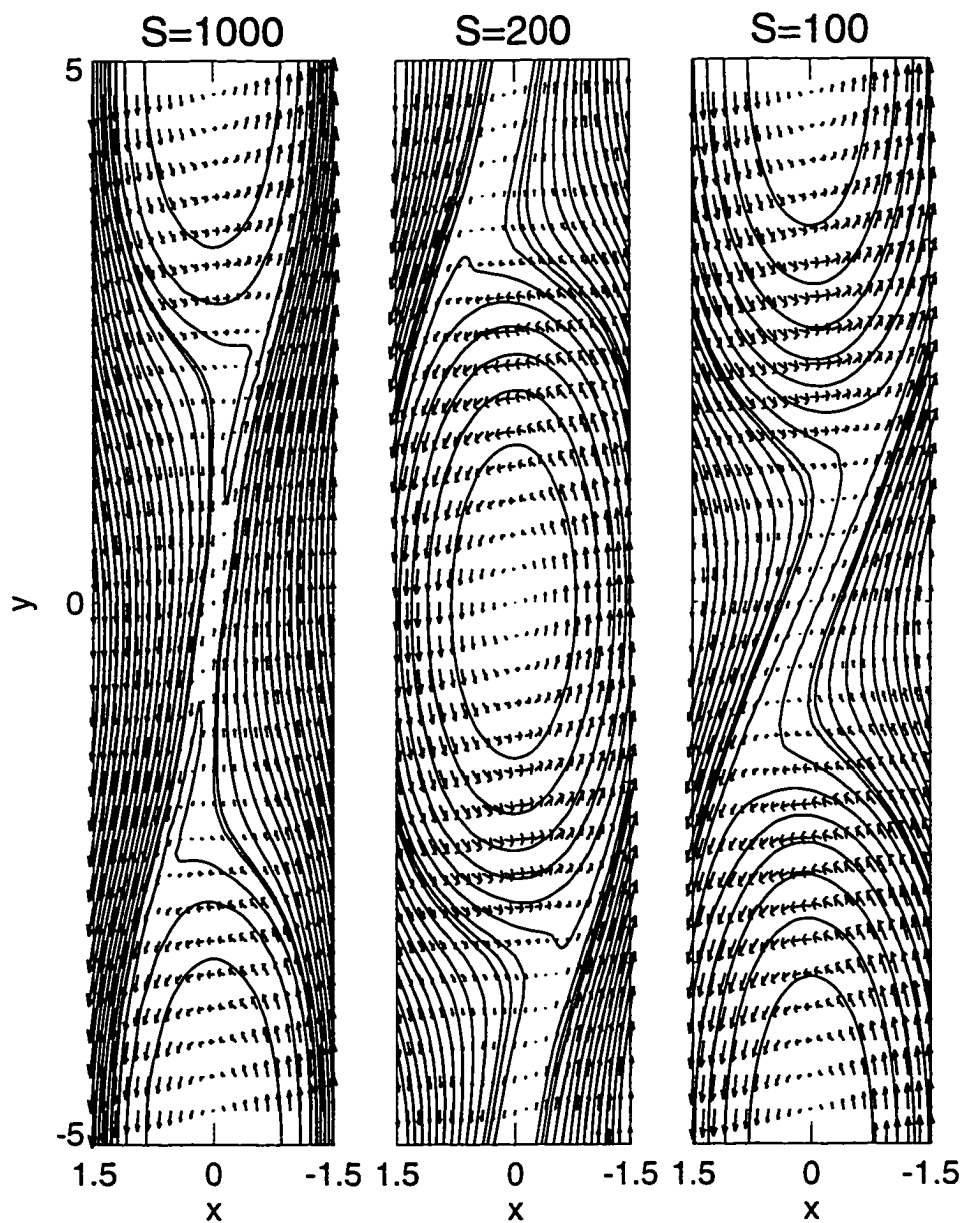


Figure 3.6 From left to right, magnetic field lines and velocity vectors for cases 13 to 15 at time $t = 100$, where the values of the resistivity are $\eta = 0.001$, $\eta = 0.005$, and $\eta = 0.01$, respectively.

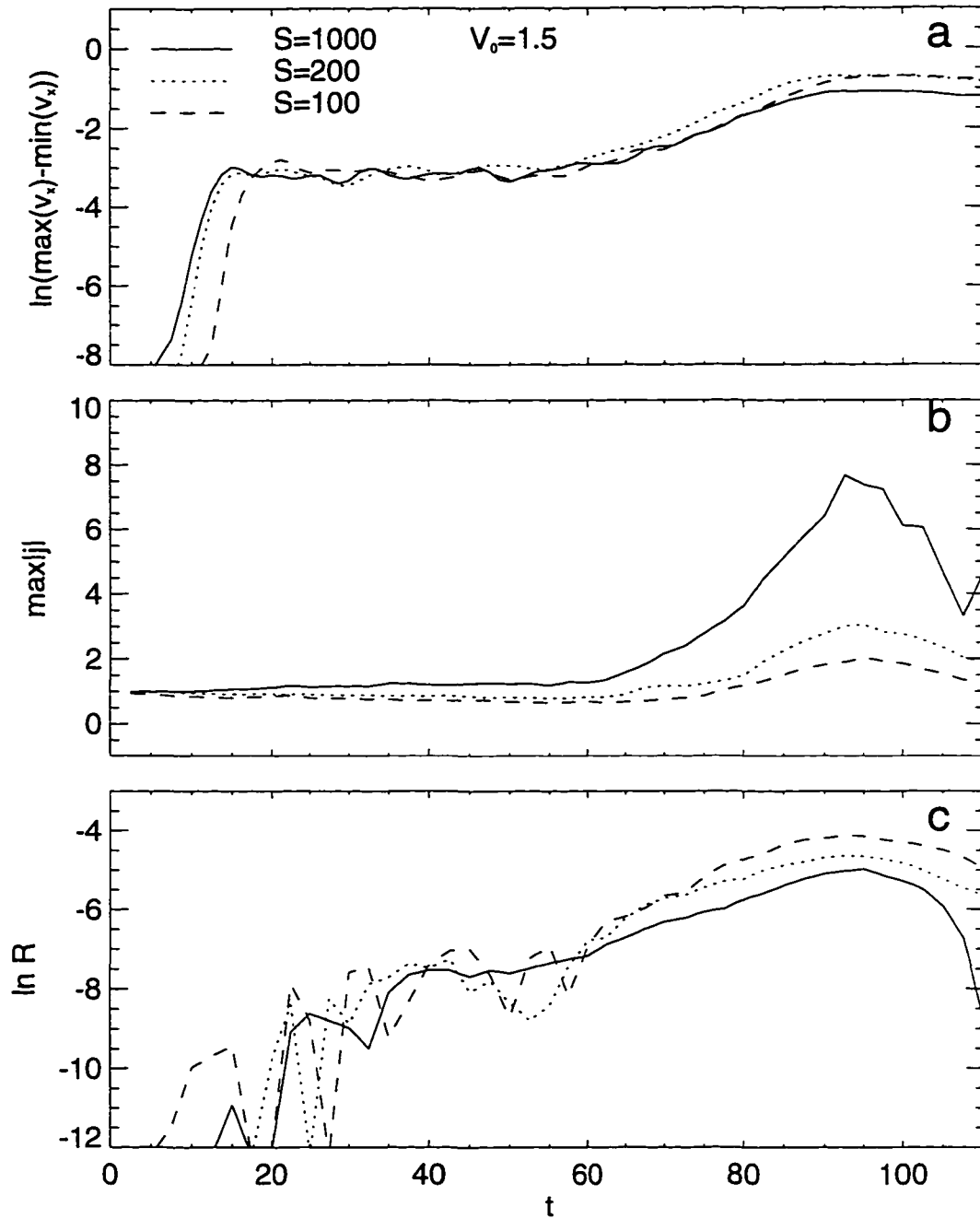


Figure 3.7 For a current sheet with constant resistivity, (a) the perturbation $\ln(\max(v_x) - \min(v_x))$ along the y axis as a function of time for different resistivity cases 13 to 15. For the same cases (b) the maximum current density amplitude as a function of time and (c) the reconnection rate R .

the electric field and thus forces magnetic reconnection.

The separation of linear and nonlinear evolution is not straightforward. At about $t = 70$ the current density for the case $S = 1000$ has doubled which is clearly a nonlinear perturbation. At this time the amplitude of the KH mode has reached $\delta v_x \approx 0.1$. Nevertheless, the growth of the KH mode continues largely unaffected until about $t = 90$ where it saturates with an amplitude of $\delta v_x = 0.3$ to 0.4. Despite the larger fluctuations at earlier times, Figure 3.7c indicates an increase of the reconnection rate with approximately the same slope as the growth rate of the KH instability. Before $t = 60$ the reconnection rate is less than 0.001 and not significant for the total reconnected flux.

Although resistivity has some influence on the reconnection rate, I was not able to identify a resistive mode in the current sheet, partially because the system is evolving rapidly after about $t = 60$. Note also that the growth rate of a tearing mode in the current layer would be far too small to affect the system in any significant way. Attempting a scaling of the reconnection rate of the form $R \propto S^{-r} \delta$, where δ is some typical perturbation, indicates a value of $r < 0.5$, that is, a relatively weak dependence on the magnetic Reynolds number.

In summary, these results indicate that the reconnection process is very much driven by the formation of the KH vortices rather than being a result of nonlinear mode coupling. In the later case one would expect a stronger feedback to the KH instability which would be observable, for instance, in a modification of the growth rate and stronger dependences of the overall structure on the value of the resistivity. Locally, I do not observe fast reconnection flows. This may indicate that the reconnection process in the current layer is a rather diffusive process which

is consistent with the strong increase in the current density for $S = 1000$.

Before $t = 20$, Figure 3.7 shows a very rapid growth of the perturbation with a growth rate of $q = 3$. The rapid growth indicates an ideal instability with rather small wavelengths. This is confirmed by a strong magnification of the central shear flow layer which demonstrates the evolution of very small KH vortices in this layer. Figure 3.8a shows the very small KH vortex at $t = 19$ for case 13 in a tiny subdomain of the entire system. The wavelength of the vortex is 0.5, and the shear layer width is $\delta = 0.08$. I remark that this result can be predicted from $q = kV_0$. On these small scales the growth rates for the small wavelength KH modes are much larger and the magnetic Reynolds number is much smaller: that is, the plasma is not as well frozen to the magnetic field. Note that although the initial perturbation has a wavelength of $\lambda = 10$, this is not an exact normal mode such that perturbations with other (smaller) wavelength are also contained in the spectrum of the initial perturbation.

Figure 3.8b shows the velocity component v_x and the magnetic field component b_y at $x = 0$ for different times. Obviously, the velocity shows the form which one would expect from the small-scale KH turbulence. For the particular equilibrium, b_y actually provides a somewhat better measure of the growth of the large-scale mode because it increases with distance from the neutral sheet and thus amplifies larger displacements. Note that the small-scale velocity perturbations indicate that modes with varying wavelengths are present in the system. It is only after the amplitude of the larger-scale KH mode surpasses those of the already saturated small-scale KH vortices that the larger-scale mode becomes visible in the plot in Figure 3.7a. Although the small-scale modes are saturated early, the larger mode

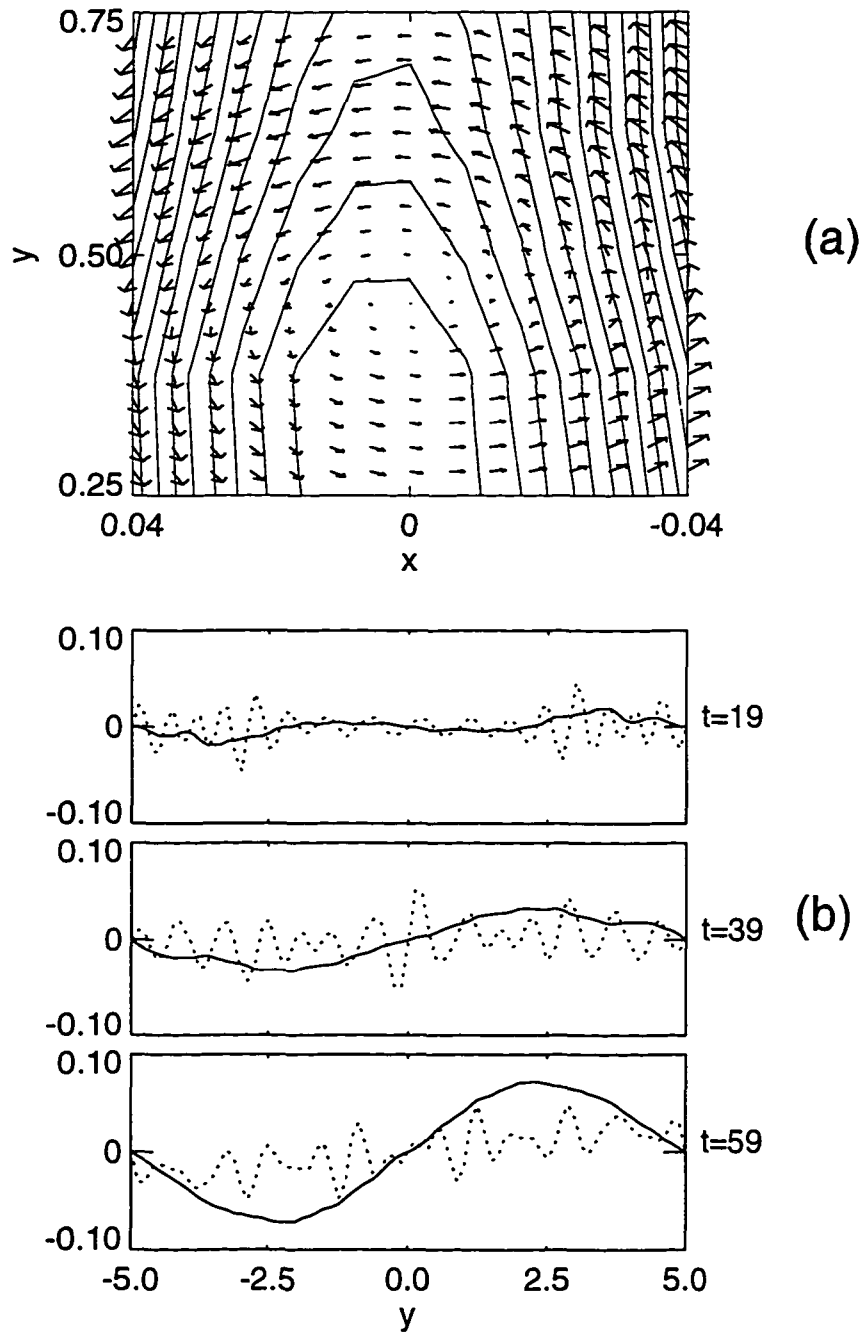


Figure 3.8 (a) A plot of the magnetic field lines and velocity vectors in a small subdomain of the system at $t = 19$, and (b) b_y and v_x along a cut at $x = 0$ for times $t = 19, t = 39$, and $t = 59$ to illustrate the mode structure for case 13.

appears to grow independent of this turbulence with the growth rate which is expected theoretically until about $t = 80$ or $t = 90$ when the large-scale mode starts to saturate.

Finally, it is interesting to look at the KH instability in the presence of a current dependent resistivity. For cases 16 to 18, Figure 3.9 shows magnetic field lines and velocity vectors at the same time $t = 80$. The evolution of the KH vortices is quite evident for all cases, as is the magnetic reconnection which generates the magnetic islands. The parameters of the models are such that lowest initial resistivity occurs for case 16 with $\eta_{t=0} = 0.00005$ and the largest for case 18 with $\eta_{t=0} = 0.001$. The islands for all cases again demonstrate magnetic reconnection. The island in case 18 appears to contain slightly more magnetic flux than the others.

Figure 3.10a shows the evolution of the perturbation $\ln(\max(v_x) - \min(v_x))$ along the y axis as a function of time. It is evident that these cases again show very similar growth for the large-scale KH mode as the constant resistivity cases shown in Figure 3.7a. This confirms that the resistivity and resistive modes have a rather minor influence on the growth even in the nonlinear stage. Figures 3.10b and 3.10c show the maximum current density and the reconnection rate, respectively, again. Here the larger current density (i.e., smaller current sheet width) and the slightly smaller reconnection rate for case 18 are remarkable. Resistive processes in the system require a significant increase in the current density. Since the threshold current density is very similar for the three cases, this increase depends very much on the coefficient α in (17). This coefficient is a factor of 10 smaller for case 16 ($\alpha = 0.001$) than for cases 17 and 18. Obviously, this implies less diffusion at the same current density in case 16. In other words, the current sheet needs to be

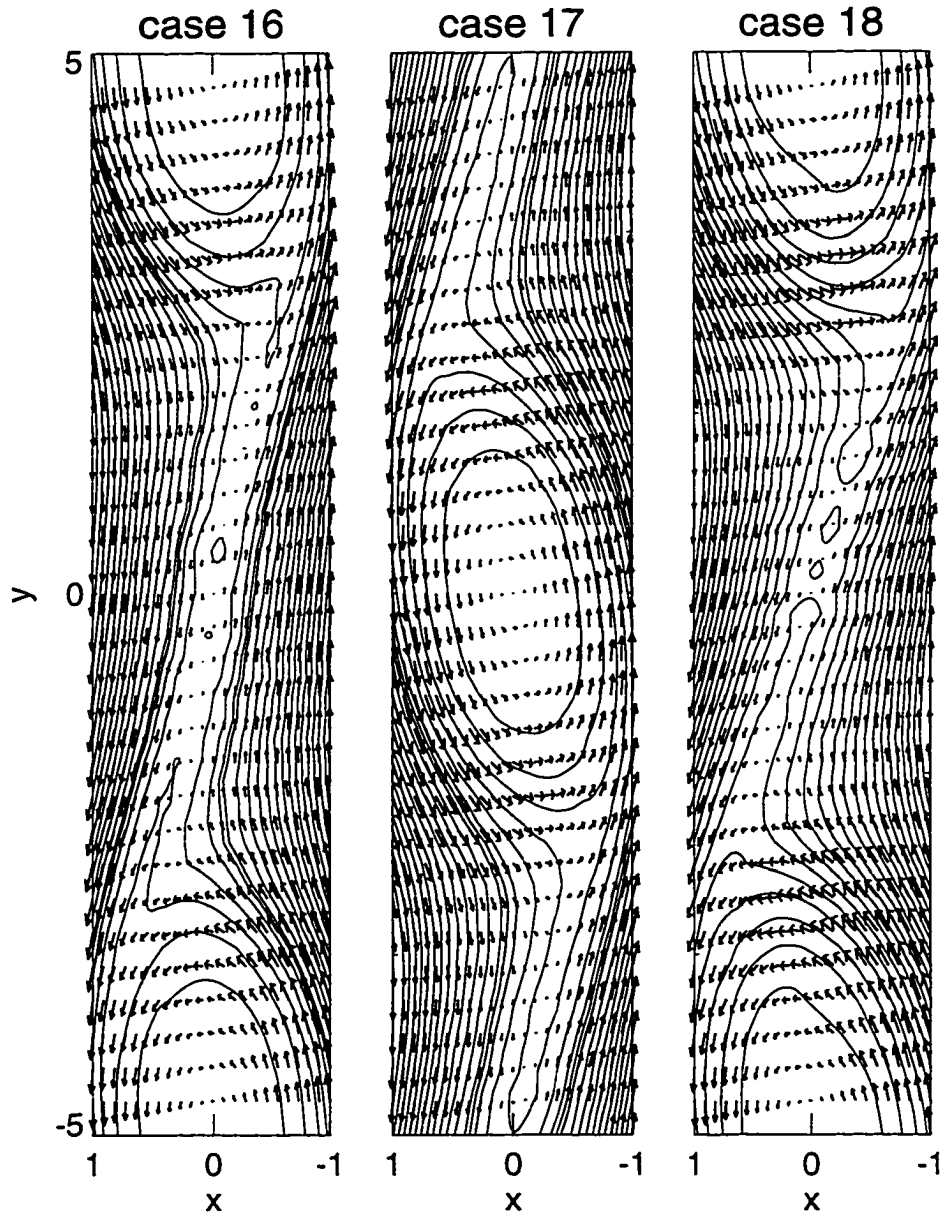


Figure 3.9 From left to right, magnetic field lines and velocity vectors for cases 16 to 18 for current dependent resistivity at time $t = 80$.

more pinched in this case in order to develop the same diffusion as in the other cases. This explains the larger current density and the slightly smaller reconnection rate. The reconnection rate is somewhat higher in these cases as compared to the constant resistivity cases.

3.4 Summary and Discussion

Our results on the dynamics of shear-flow and magnetic-shear layers indicate two different regimes, that is, a tearing-mode-dominated regime for sub-Alfvénic flows and the KH-unstable regime for significantly super-Alfvénic flows. Such regimes had been identified previously by *Miura and Pritchett* [1982] for the KH instability and in a linear analysis by *Einaudi and Rubini* [1986].

1. For sub-Alfvénic flow the reconnection rate decreases with increasing velocity shear. I was unable to identify a KH unstable behavior for shear flow with less than the Alfvén velocity unless η is very large. This conclusion is opposite to what the models and simulations on VIR predict [e.g., *Pu et al.*, 1990a, b; *Fu et al.*, 1995]. The question is, why do I obtain a different result for this parameter regime?

As mentioned in the introduction, a sufficiently small resistivity is required to study reconnection and is more realistic for applications to the Earth's magnetopause. In my simulations I have used typically a value of $\eta = 0.001$ for the initial resistivity (except cases 14 and 15). This implies that the frozen-in condition is not strongly violated. Typically, numerical studies on VIR use a rather large resistivity. A large resistivity generates immediately a strong diffusion process which

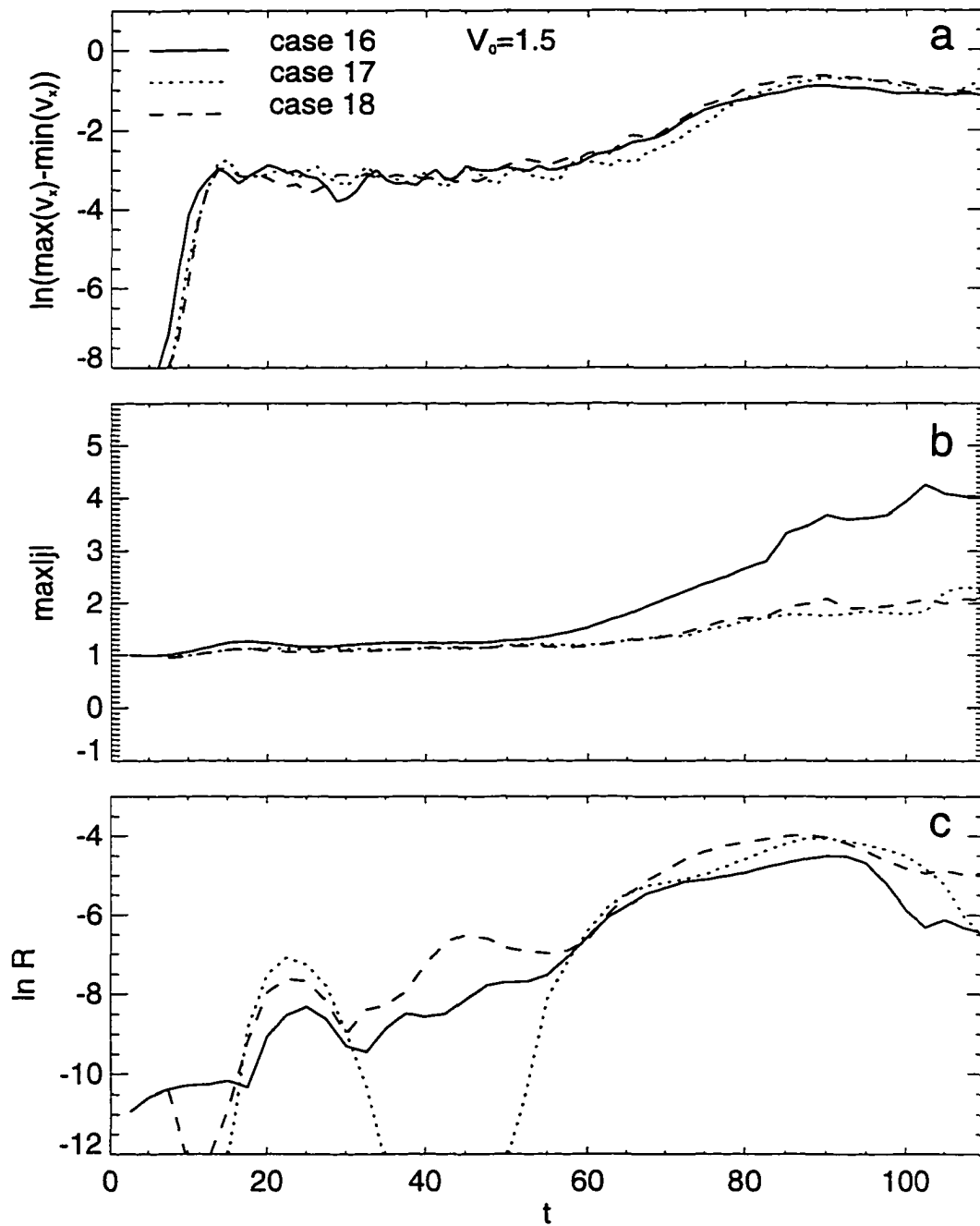


Figure 3.10 For a current sheet with current dependent resistivity, (a) the perturbation $\ln(\max(v_z) - \min(v_z))$ along the y axis as a function of time for different resistivity cases 16 to 18. For the same cases (b) the maximum current density and (c) the reconnection rate amplitude as a function of time.

widens the current sheet and thus reduces the magnetic tension which stabilizes the KH instability. In addition, the violation of the frozen-in condition allows plasma transport across the magnetic field and should also lower the threshold for the onset of a KH instability.

I have tested this hypothesis with a resistivity $\eta = 0.3$ and a shear flow velocity $V_0 = 0.5$. Figure 3.11a shows magnetic field lines and velocity vectors at $t = 100$. The velocity vectors clearly present the typical vortex for the KH instability. During its evolution the magnetic field is very gently pinched giving rise to the magnetic island which is seen in the magnetic field plot. Note that the magnetic field strength is strongly reduced compared to the initial field.

To demonstrate the mechanism for the KH instability, Figure 3.11b shows the evolution of the profile of the velocity v_y , and the magnetic field b_y which is approximately the Alfvén speed. As long as the gradient in b_y is larger than the gradient in v_y the KH mode is stabilized. However, at about $t = 24$ the diffusion has widened the current sheet so much that it becomes KH unstable. At $t = 49$ there is a large region of the current layer which is now KH unstable. Thus modes with a very small wavelength start to grow initially, and relatively soon a large-scale KH mode can develop. Thus VIR requires a large resistivity or a super-Alfvénic shear velocity to destabilize a configuration which has been initially KH stable.

Within the accuracy of my results there is no difference between short wavelength modes and long wavelength modes. In an analytical study, *Chen and Morrison* [1990] observed a slight destabilization of the constant- ψ tearing mode for rather small shear flow.

2. If the shear flow is super Alfvénic, I could not identify a tearing mode.

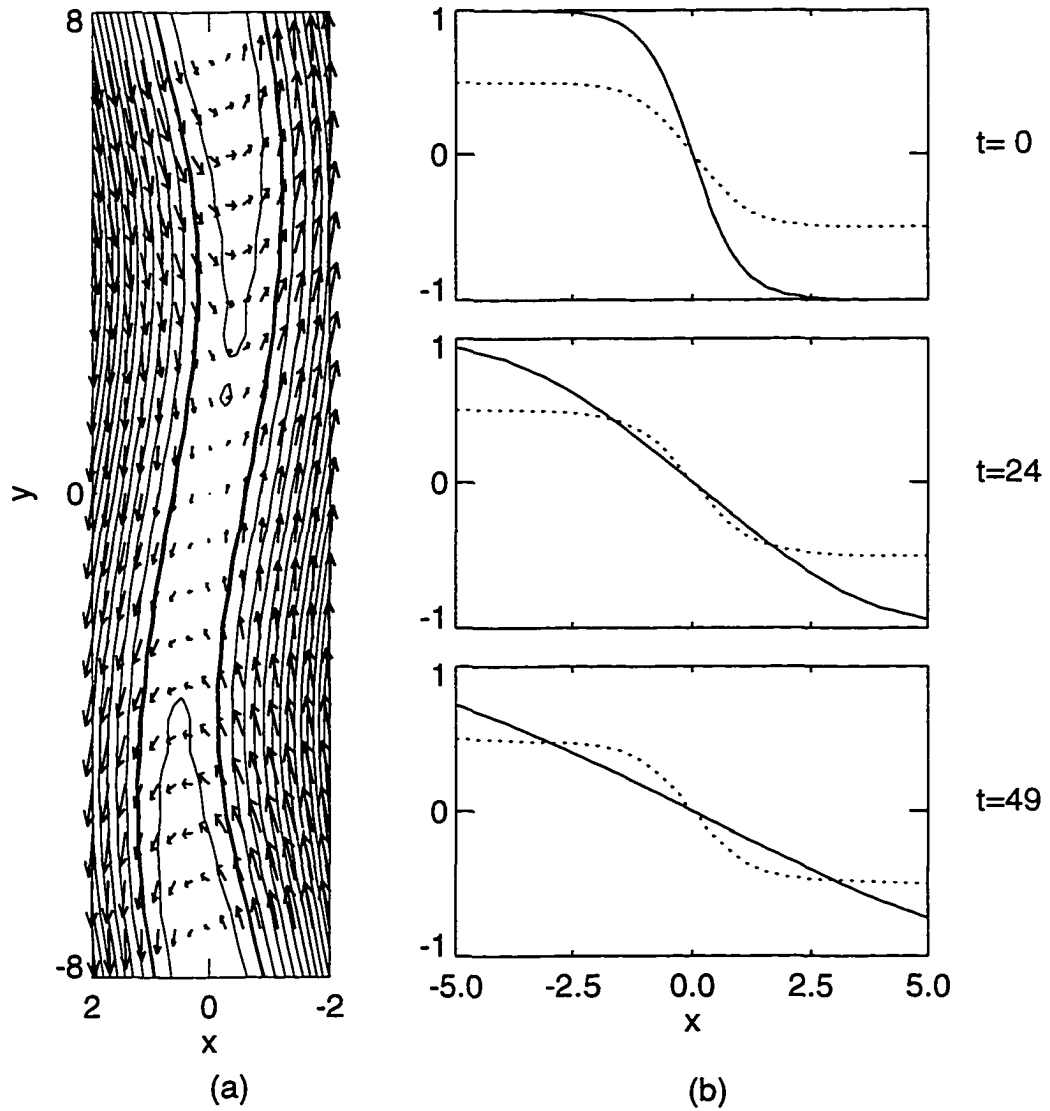


Figure 3.11 (a) Magnetic field lines and plasma velocity vectors for a large resistivity of $\eta = 0.3$. (b) The profiles of b_y (solid) and v_y (dotted) for times $t = 0$, $t = 24$, and $t = 49$.

The KH instability evolves largely independently of a sufficiently small resistivity, even if this model is changed to a current dependent form which can generate a locally enhanced resistivity.

In its nonlinear evolution the KH instability leads to a significant pinching of the current sheet. The increase in the current density generates a corresponding increase in the resistive electric field. This mechanism generates magnetic reconnection and magnetic islands of the size of the KH vortices. The corresponding reconnection process is obviously strongly driven by the pinching of the current layer. The reconnection process is expected to occur also if the system is initially fully collisionless because the KH vortices would generate arbitrarily thin current sheets if no dissipation is available and thus force the generation of a dissipation process.

The evolution of the KH mode even with large nonlinear amplitudes appears largely unaffected by the reconnection process. Because of the fast pinching of the current sheet, I could not identify a tearing mode structure or tearing mode growth during the later times of the KH evolution. Thus the question whether the local (compared to the large-scale KH mode) reconnection process is caused by a resistive tearing mode or just a process driven by the current sheet pinching remains unresolved. A more accurate evaluation of the local reconnection processes in the long current layer requires further studies which are beyond the scope of this study. The plasma outflow occurs in regions which are created by the KH vortices and do not show the typical reconnection layer structure.

3. The current dependent resistivity model generates larger reconnection rates than the constant resistivity model. Remarkably, the current dependent resistivity

can be very small for an initial system with a current density close to or below the threshold. However, the growth and reconnection rate can be very large depending on the particular choices for the model. A current dependent resistivity appears to be a more realistic choice, particularly for many magnetospheric processes, because the dissipation is negligible almost everywhere and is strongly localized only where the current sheet is driven very thin either by external forces or by the internal dynamics of an instability process.

4. Kelvin-Helmholtz vortices can induce magnetic reconnection which is a viable process at the Earth's magnetopause. However, the location for the occurrence of these structures is disputable. First, the formation requires a magnetosheath flow velocity which is larger than the threshold velocity of the KH instability. This condition largely excludes the subsolar magnetopause if the flow is strongly aligned with the field (which is necessary to obtain a significant reconnection process). Second, the vortices should be almost fully developed otherwise the reconnected flux is small. During their formation the flow vortices move downstream at a speed close to the magnetosheath plasma velocity. The actual growth time t_g is much longer than the KH growth time in an unmagnetized plasma, that is, $t_g = n\lambda/(\pi v_{\text{msh}})$, where v_{msh} is the magnetosheath plasma velocity and n is typically a factor between 5 and 10 (I obtained $n \approx 8$). Thus the vortex moves a distance of $l = 1.5\lambda$ to $l = 3\lambda$ during one growth time. For a wavelength of $2 R_E$ (which yields a vortex size of about $1 R_E$ consistent with typical flux transfer event observations) this implies a motion of about 3 to $6 R_E$ during one growth time. Since the formation requires a time of at least several times the KH growth time, a vortex has at least moved $6 R_E$ and probably more than twice this value. This excludes the major

portion of the dayside magnetopause as a possible location to observe the resulting structures.

I finally remark that this study has like almost all other studies considered fairly specific magnetic field and flow configurations and is subject to the constraint of two dimensionality. An extension, in particular, into the three-dimensional dynamics of magnetic and velocity shear processes may yield important further insight.

Chapter 4

Linear properties of the Kelvin-Helmholtz and tearing instabilities in three dimensions

4.1 Introduction

Understanding the linear dynamics of the tearing and KH instabilities will provide important insights into the dynamics and properties of the nonlinear evolution and interaction of the two instabilities. In particular, the linear analysis yields the onset condition and the growth rates of the two instabilities. It thus also provides the conditions for which a nonlinear interaction of the two instabilities can be expected and under which for given plasma and magnetic fluid conditions only one of the instabilities may operate.

Many studies have analyzed only the tearing or the KH mode [*Fu et al.*, 1986; *Scholer et al.*, 1988; *Fu et al.*, 1990; *Otto et al.*, 1990; *Miura et al.*, 1982, 1984, 1987; *La Belle-Hamer et al.*, 1988, etc]. Studies which consider both modes have focused mostly on two-dimensional dynamics. Studies which consider three spatial dimensions have investigated either the tearing or the KH mode, but not both. Those studies are incomplete for a full understanding of magnetopause processes. In this section, I will review some of these results and consider both tearing and KH modes in one simulation domain.

The KH and tearing instabilities at the magnetopause are mainly dependent on the velocity shear $\Delta\mathbf{v}$ and magnetic shear $\Delta\mathbf{b}$ on the two sides of the magnetopause respectively. The two basic configurations in this study are: (1) $\Delta\mathbf{v}\parallel\Delta\mathbf{b}$ and (2) $\Delta\mathbf{v}\perp\Delta\mathbf{b}$. In Chapter 3, I discussed the development of the tearing mode or the KH mode in a configuration with shear flow parallel to the magnetic shear (configuration (1)). Here I focus on the linear properties of configuration (2).

Major background results are mainly from two dimensional simulations, which are very helpful to my study. *Miura and Pritchett* [1982] found, for $\Delta\mathbf{v}\perp\mathbf{b}_0$, that the KH mode is destabilized only if the velocity difference is smaller than twice the fast magnetosonic mode speed. The growth rate for the incompressible case reaches a maximum for wave vector $k = 0.45$ and then decreases to zero for $k = 1$. For an increasing Alfvén Mach number (the ratio of the velocity difference to difference in Alfvén speed), the growth rate is reduced considerably and the wavenumber of the fast growing mode is shifted toward smaller values. *La Belle-Hamer et al.* [1988] investigated configuration (2) in an incompressible plasma. They found that the KH and tearing instabilities are decoupled in the linear stage

if the wave vector moves in a plane from the direction of the shear flow to that of the magnetic field. *La Belle-Hamer* [1994] found that flow perpendicular to the magnetic field will generate a magnetic field component along the direction of shear flow when the tearing instability operates. The magnitude of the component is proportional to the shear flow velocity. Even though they consider shear flow and magnetic shear in their study, there is not a true interaction of modes because of the limitation of 2-D approximation. Both of their simulations are simple mode cases, i.e., a tearing mode modified by velocity shear or KH mode modified by magnetic shear. 2-D analysis always assumes the third direction extends infinitely. In other words, there is no variation of physical parameters in this direction. At the magnetopause boundary layer, the tearing and KH modes are always confined to planes perpendicular to the magnetopause or lower latitude boundary layer (LLBL), and can only propagate in the plane defined by the boundary normal and the mode wave vector.

Those difficulties in 2-D simulations and analysis are resolved in 3-D simulations. At the magnetopause or LLBL the geometry configuration is such that shear flow and magnetic shear intersect at a nonzero angle. Figure 4.1 shows a sketch to present the configuration (2). The tearing mode and the KH mode are respectively related to the region where magnetic shear exists and where flow velocity exists, and their wave vectors are perpendicular to each other. If both instabilities operate, only 3-D simulations can be carried out to solve the problem.

This chapter will contribute to understanding linear properties of the KH and tearing instabilities in three dimensions. Configuration (2) in a 3-D simulation domain is my most important target. Section 4.2 introduces the equilibrium, initial

Illustration of basic configuration

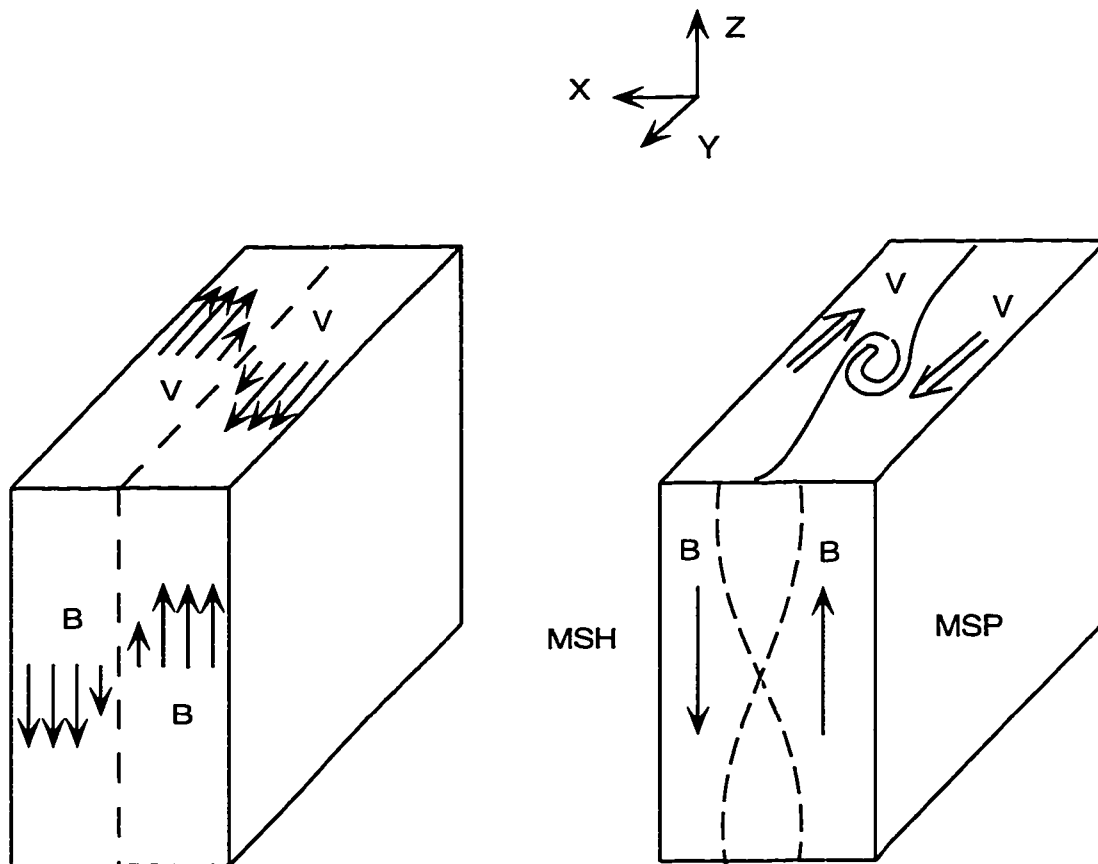


Figure 4.1 Sketch of the tearing and KH modes in configuration (2).

perturbation, and simulation setup. Section 4.3 presents 2-D and 3-D simulation results. The 2-D analysis deals with the linear properties of each single instability, which will be compared with related analytical results. In my 3-D simulations, the linear superposed effects of two modes are presented to deal with the relation of the tearing mode and the KH mode. Section 4.4 summarizes the results.

4.2 Equilibrium, Initial Perturbation, and Simulation Setup

In the simulation, the magnetic current sheet and the flow shear layer initially coincide. The normal component of the current sheet is along the x direction, and flow shear is along the y direction. The magnetic field is assumed in the z direction. Throughout this and other later chapters, I use this coordinate system.

Figure 4.2 shows a sketch of the equilibrium magnetic field and the flow field. Generally, there is some background b_y component in addition to the antiparallel magnetic field component in the z direction. The magnetic field component b_y , which is the westward magnetic field component, is often observed to be enhanced in the current layer of the dayside magnetopause and the nightside magnetotail. In that way, the magnetic field has some shear angle between the magnetospheric field and the interplanetary magnetic field. For convenience, I use an angle α to present the magnetic shear angle across the current layer. Thus the initial equilibrium is

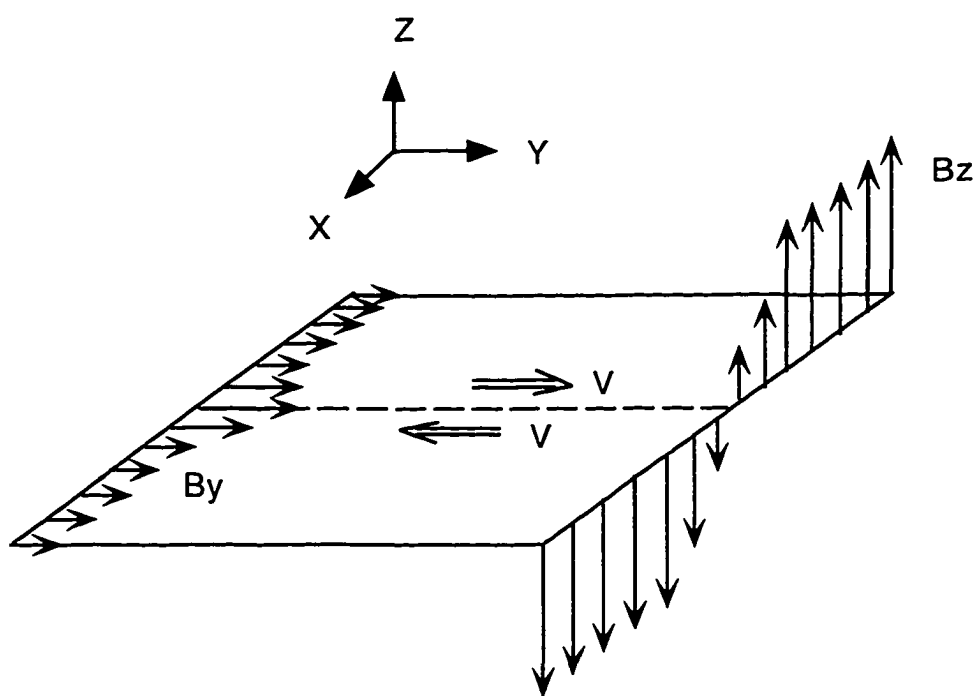


Figure 4.2 Sketch of equilibrium magnetic field and flow field.

given by

$$b_{x0}(x) = 0 \quad (4.1)$$

$$b_{y0}(x) = \sqrt{b_{yc}^2 + \kappa b_{\Delta}^2 \cosh^{-2} x} \quad (4.2)$$

$$b_{z0}(x) = -b_{\Delta} \tanh x \quad (4.3)$$

$$v_{x0}(x) = 0 \quad (4.4)$$

$$v_{y0}(x) = -V_0 \tanh x \quad (4.5)$$

$$v_{z0}(x) = 0 \quad (4.6)$$

$$p_0(x) = \beta_0 + (1 - \kappa) b_{\Delta}^2 \cosh^{-2} x \quad (4.7)$$

$$\rho_0(x) = 1 \quad (4.8)$$

where β_0 is the ratio of thermal pressure to magnetic pressure $b_{\Delta} = \sin(\alpha/2)$, $b_{yc} = \cos(\alpha/2)$, and κ is a parameter which determines the variation of b_y across the initial current sheet. A sketch of the hodogram for the b_y and b_z components, which presents a trajectory through the current layer, is presented in Figure 4.3. $\kappa = 0$ implies that initial state has a constant y component of the magnetic field across the current layer (see (a)), and $\kappa = 1$ represents a force-free initial configuration (see (b)).

For the 3-D simulations, small amplitude perturbations are given in terms of the velocity profile:

$$v_x(x, y) = v_{x0}(x) + \delta v_{xT} + \delta v_{xKH} \quad (4.9)$$

$$v_y(x, y) = v_{y0}(x) + \delta v_{yKH} \quad (4.10)$$

$$v_z(x, y) = v_{z0}(x) + \delta v_{zT} \quad (4.11)$$

where T and KH denote tearing and KH type perturbation. In the 2-D simulations,

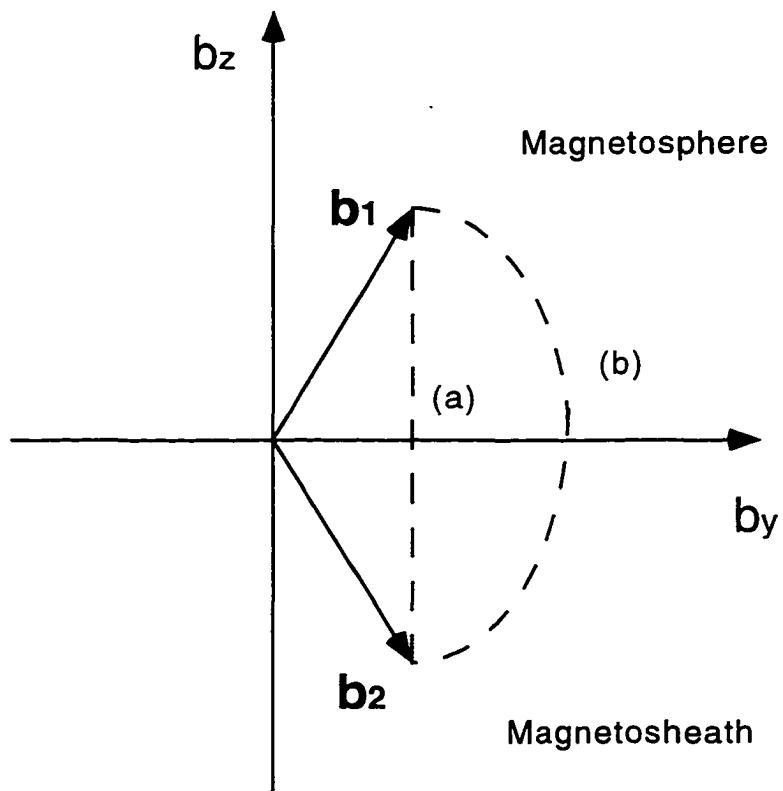


Figure 4.3 A sketch of the hodogram for the b_y and b_z components for a trajectory through the current layer.

I use either the KH or the tearing type, so that I can easily compare 2-D cases with 3-D cases where both modes are present. Note that 2-D KH simulations are carried out in the xy plane, and 2-D tearing simulations are carried out in the xz plane.

The δv perturbation is given:

$$\delta v_{zT} = v_{z1} \cos(\pi/L_z) \cos(y\pi/L_z) \cosh^{-2} x \quad (4.12)$$

$$\delta v_{xKH} = v_{y1} (\pi/L_y) \sin(\pi y/L_y) \cosh^{-2} x \quad (4.13)$$

$$\delta v_{yKH} = -v_{y1} \cosh^{-2} x [1 - 2x \sin(y\pi/L_y) \tanh x] \quad (4.14)$$

$$\delta v_{zT} = -2v_{z1} \cos(\pi z/L_z) \tanh x \cosh^{-2} x \quad (4.15)$$

where v_{z1} and v_{y1} are respectively the initial magnitudes of tearing and KH type perturbation. The perturbation is chosen such that the wave vector of the tearing mode is perpendicular to that of the KH mode. The tearing perturbation is chosen in the cuts along the xz plane, and that of KH perturbation is chosen in the cuts along the xy plane. Note that it is straight forward to rotate the perturbation in the yz plane to excite an additional mode.

The perturbations are not true eigen modes, but they have the same symmetry as the related eigen modes, and they are chosen such that $\nabla \cdot \mathbf{v} = 0$. Thus they are very suited to excite the corresponding eigen mode.

A current dependent resistivity is used in the simulation, which is of the form

$$\eta = \eta_0 + \begin{cases} \alpha(|j| - j_c) & |j| \geq j_c \\ 0 & |j| < j_c \end{cases} \quad (4.16)$$

The time evolution of the magnetic field and plasma parameters is calculated

by solving the 2-D and 3-D normalized MHD equations as described in Chapter 2. Again, the numerical method I used is a leapfrog scheme [Potter, 1973]. Free boundary conditions are applied to the two boundaries in the x direction. Periodic boundary conditions are used at the two boundaries along the y and z directions.

The volume of the three dimensional simulation box is defined as $|x| \leq 20$, $|y| \leq 10$, and $|z| \leq 15$. The angle of magnetospheric field and interplanetary magnetic field is 179° . That will introduce a very small magnitude b_y component, which has a negligible influence on the dynamics, but is very useful for illustrative and diagnostic purposes. The grid is chosen to be uniform along the y and z directions and nonuniform along the x direction with a minimum grid separation of ϵ_x in the center of the system to resolve the evolution of thin current layers during the dynamical evolution. The number of grid points and the maximum resolution is varied for different simulations. In the simulations I use $63 \times 43 \times 43$ grid points with a resolution of $\epsilon_x = 0.05$, $\epsilon_y = 0.5$, and $\epsilon_z = 0.75$.

4.3 Simulation Results

The interaction of the two instabilities obviously requires an excellent understanding of each individual instability. Some of the basic 2-D properties have been studied by various authors. Here I will first review and complement the properties of the instabilities, and then I will discuss the full 3-D system. It should be noted that each linear instability with a single wave vector k is two-dimensional by definition. For several k vectors the resulting linear modes can simply be superimposed. Thus the linear phase of the 3-D KH/reconnection system is a superposition of 2-D

modes. For this reason, and also to test the three-dimensional results, I will discuss the growth of the tearing mode and the KH modes separately in the following subsections before I discuss the 3-D results.

4.3.1 Properties of the Tearing Instability

The dispersion relation of the tearing mode depends mostly on the resistivity and wavelength [Otto and Birk, 1992]. Figure 4.4a shows a typical tearing mode, where the solid lines and the arrows respectively represent the magnetic field lines and velocity vectors. For $\beta = 3.0$ and $k = 0.2$, I evaluate the tearing mode growth rate as a function of the resistivity in a 2-D simulation in the xz plane (Note that the resistivity is the effective resistivity in this case. See Chapter 3). Figure 4.4b shows the tearing mode growth rate as a function of resistivity. The solid line is corrected for effects from diffusion. The dashed line is from analytical results, which are calculated for wavelength $\lambda = 30$. The dotted line is from $\frac{d(\ln(\max(b_x) - \min(b_x)))}{dt}$. Analytically, q is proportional to $\eta^{-\frac{1}{2}}$. There is little difference between the solid line and the dashed line, but some difference between the dashed line and the dotted line. In the simulation, the current sheet width increases because of the resistive diffusion, which increases the characteristic time (which is based on the current sheet width) and leads to a slower growth of the mode. To make the simulation result comparable to the analytical result, it is necessary to correct the diffusion effects. From Figure 4.4b, the growth rate obtained from $\frac{d(\ln(\max(b_x) - \min(b_x)))}{dt}$ is smaller than that of the analytical result, but the corrected growth rate is very close to the analytical result. This result serves as a test for the simulation method.

From the figure, it is evident that the growth rate of tearing instability increases with resistivity. The linear growth rate of the tearing mode is not affected by flow shear $\Delta \mathbf{b}$ (note that $\Delta \mathbf{v}$ is perpendicular to $\Delta \mathbf{b}$), by the value of b_y , and by compressibility. However, for nonlinear results, magnetic islands saturate earlier as the shear velocity increases.

The magnetic field component b_y which is parallel to the shear flow stabilizes the KH instability. Even though the growth rate of the tearing mode is not affected by shear flow perpendicular to the simulation plane, some magnetic field component along the y direction will be generated by shear flow if there is no b_y component initially [La Belle-Hamer *et al.*, 1994]. From my analytical analysis, the generated b_y by the shear flow is proportional to the shear flow gradient and b_x . It will grow at the tearing growth rate. It can be deduced from the formula:

$$\frac{\partial \mathbf{b}}{\partial t} = \nabla \times (\mathbf{v} \times \mathbf{b}) + \eta \nabla^2 \mathbf{b}$$

In the linear stage, diffusion is a very slow process and the diffusion term can be eliminated from the above equation. For the y component,

$$\frac{\partial b_y}{\partial t} = -\frac{\partial(v_x b_y - b_x v_y)}{\partial x} + \frac{\partial(v_y b_z - b_y v_z)}{\partial z} = -b_x \frac{\partial v_y}{\partial x} + b_z \frac{\partial v_y}{\partial z} + \frac{\partial v_x b_y}{\partial x} - \frac{\partial b_y v_z}{\partial z}$$

Note that, in equilibrium, $v_x = b_x = v_z = b_y = 0$. With perturbation analysis in b_y , just first-order terms are kept in the equation:

$$\frac{\partial b_{y1}}{\partial t} = -b_{x1} \frac{dv_{y0}(x)}{dx}$$

where 0 and 1 denote zero and first order magnitudes. Because $b_{x1} = \delta b_x(x) e^{qt+iky}$,

$$\frac{\partial b_{y1}}{\partial t} = -\delta b_x(x) e^{qt+iky} \frac{dv_{y0}(x)}{dx}$$

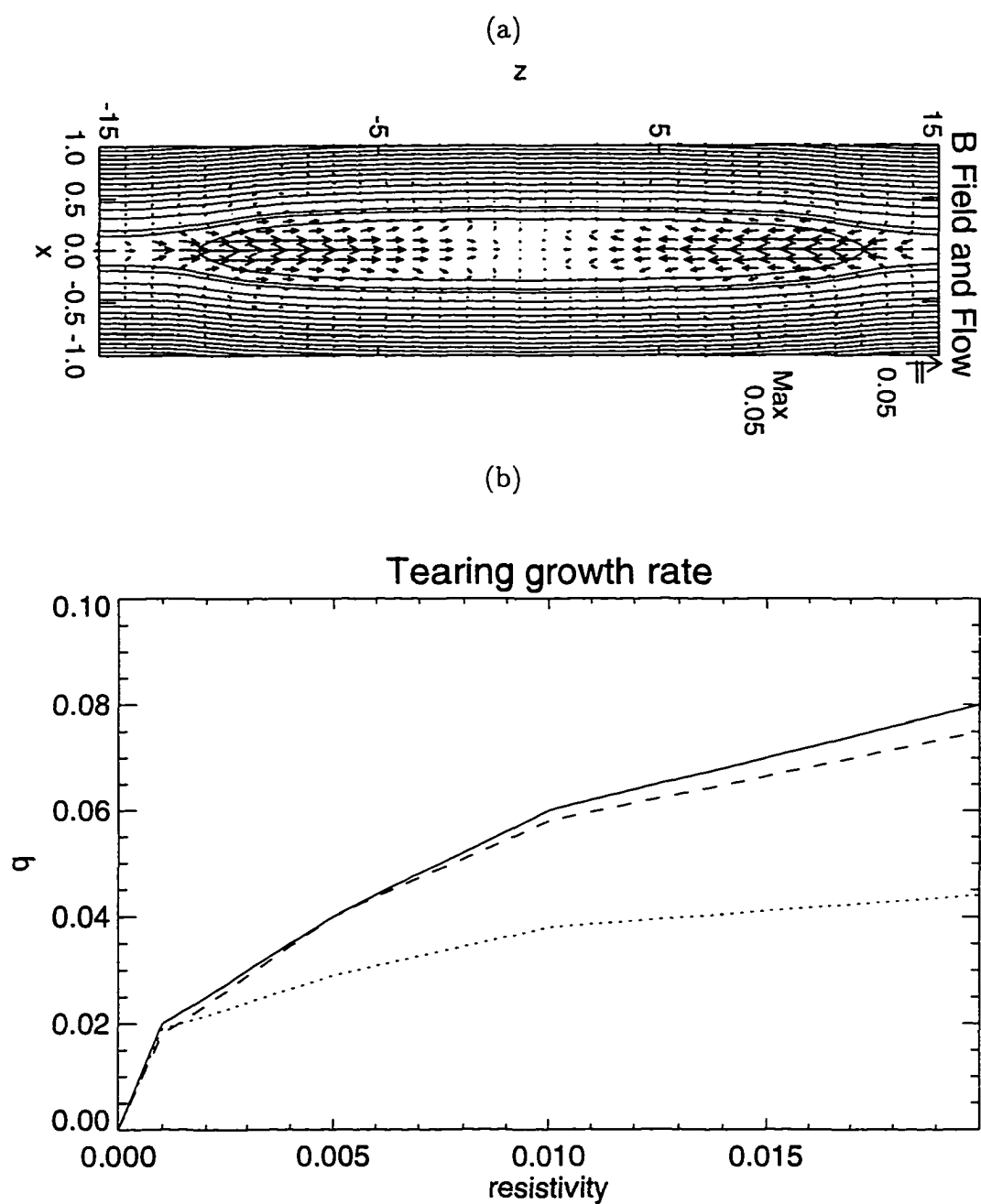


Figure 4.4 (a) A typical tearing mode, (b) tearing growth rate as a function of resistivity ($k = 0.2$). The solid line is from the normalized unit current width, the dashed line is from analytical results, and the dotted line is from the $\frac{d \ln(\max(b_x) - \min(b_x))}{dt}$.

Consistent with *La Belle-Hamer's* results, the growth of b_y occurs only in the reconnection region. If initially there is some b_y component, it will be modified. In the nonlinear stage, the shear layer itself will also be modified, and it will become wider near the magnetic neutral point and thinner near the reconnection region.

4.3.2 Properties of the Kelvin-Helmholtz Instability

The KH instability is affected by the magnitude of shear flow (V_0), and by the wavelength of the KH mode (see Chapter 1). In a magnetized plasma, the KH instability is also affected by the magnetic field component parallel to the shear flow (b_y) and the ratio of thermal pressure to magnetic pressure (β) (see Miura, 1982). Here 2-D simulations are carried out to evaluate the KH growth rate as functions of b_y , β (the ratio of dynamical pressure to magnetic pressure), and V_0 in the xy plane. The growth rate is calculated from $\frac{d(\ln(\max(v_x) - \min(v_x)))}{dt}$. From equation 4.2, initial b_y is dependent on background value b_{yc} and the force-free coefficient κ . There is also another factor, the finite shear layer width, which affects the growth rate of the KH mode. This factor and compressibility make it very difficult to analytically calculate the growth rate of the KH mode. The results from this section are mainly based on the simulations.

Figure 4.5a shows a typical KH mode, where the solid and dashed lines represent the magnetic field lines and the arrows represents the velocity vectors. Figure 4.5b shows that the growth rate decreases with the increased b_{yc} at both cases ($k = 0.31$ and $\kappa = 0$. $V_0 = 1.2$, $\beta = 3$ for the dotted line; $V_0 = 0.3$, $\beta = 0.8$ for the solid line). Figure 4.5c shows that the growth rate decreases with the increased κ at

both cases ($k = 0.31$ and $b_{yc} = 0$. $V_0 = 0.6$, $\beta = 3$ for the dotted line; $V_0 = 0.3$, $\beta = 0.8$ for the solid line). The KH instability is stabilized by b_y , as can also be seen from the analytical dispersion relation of the KH mode. The magnetic field component aligned to the shear flow stabilizes the KH instability. Thus the results of Figure 4.5 confirm and quantify the stabilizing influence of the magnetic field component parallel to the flow shear $\Delta \mathbf{v}$.

Figure 4.6a shows the growth rate as a function of shear flow V_0 . When shear flow increases, the growth rate first increases then decreases until a cutoff shear velocity ($b_y = 0$, $\beta = 3$). The cutoff velocity occurs at the limits of fast mode speed. Figure 4.6b shows the growth rate as a function of β . When $\beta \leq 0.2$, the variation is very large. After β is larger than 0.5, the growth rate changes very little ($V_0 = 0.3$, $b_y=0$). The growth rate of the KH mode increases with the shear velocity and the ratio of thermal pressure to magnetic pressure.

In summary, the growth rate of the KH mode increases then decreases with the shear flow until a cutoff shear velocity. The KH instability is stabilized by compressibility and the magnetic field component parallel to the shear flow. In the nonlinear stage, the shear flow will change the profile of the magnetic shear, which will be discussed in Chapter 5.

4.3.3 Simultaneous Growth of the Kelvin-Helmholtz and Tearing Modes

Now I turn to the interesting case where both the tearing mode and the KH mode operate in one 3-D frame. As outlined above, a clear understanding of the linear

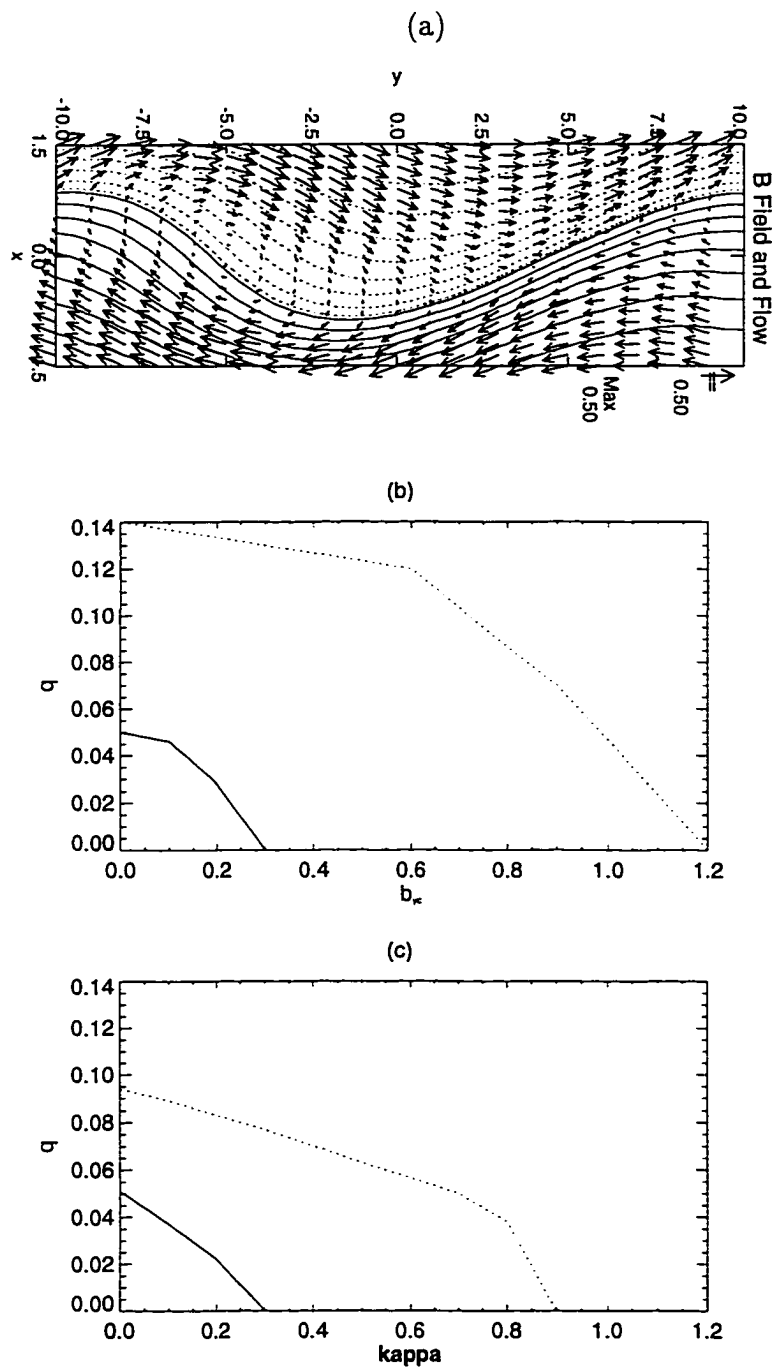


Figure 4.5 (a) A typical KH mode, and the KH growth rate as a function of (b) $b_{y\kappa}$ (for $k = 0.31$, $\kappa = 0$) and (c) κ (for $k = 0.31$, $b_{y\kappa} = 0$).

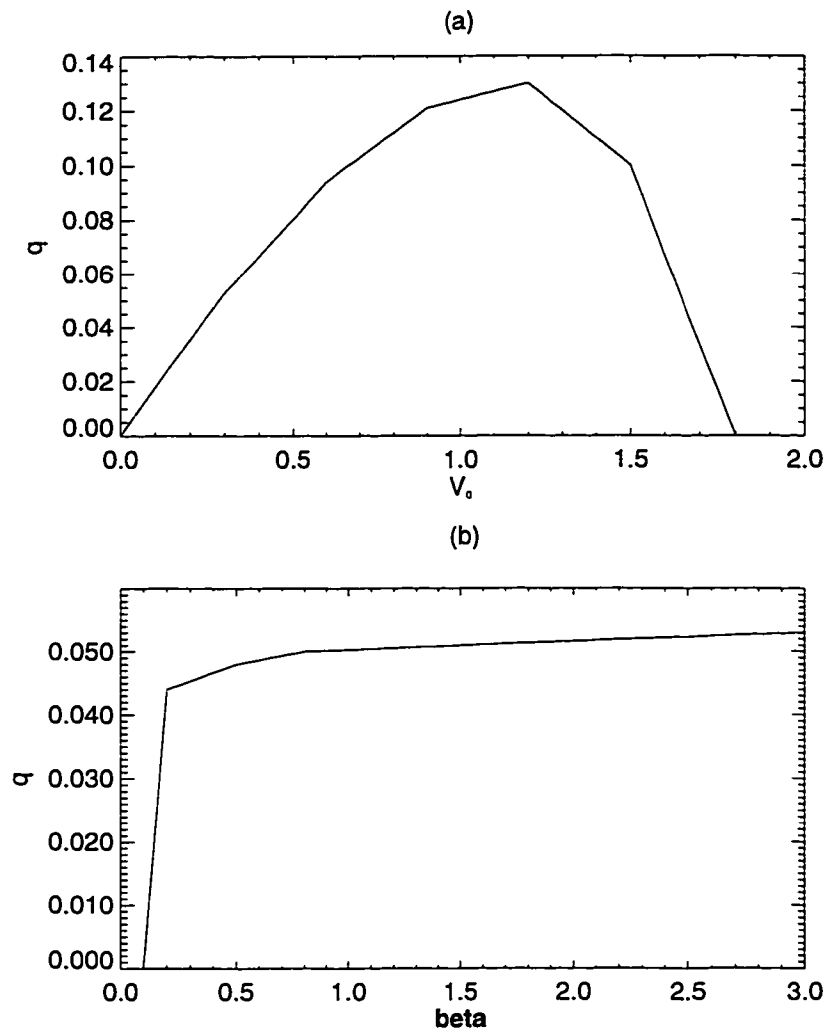


Figure 4.6 The KH growth rate as a function of (a) V_0 (for $b_y = 0$ and $\beta = 3$) and (b) β (for $V_0 = 0.3$ and $b_y = 0$).

Table 4.1 Summary of 3-D Simulation Cases.

Case	V_0	κ	α	j_c	v_{x1}	v_{z1}	q_{KH}	q_T
1	0.5	0.1	0.005	0.8	10^{-4}	10^{-3}	0.0704	0.031
2	0.3	0.15	0.02	0.8	10^{-3}	5×10^{-4}	0.0212	0.0434
3	0.5	0.1	0.005	0.8	10^{-3}	10^{-4}	0.0705	0.0303
4	0.3	0.15	0.02	0.8	5×10^{-4}	10^{-3}	0.0213	0.0441

properties will be very helpful to investigate the nonlinear interaction of the two modes. Here I focus on the basic case of two modes perpendicular to each other. In my 3-D simulations, the wave vectors of the KH and tearing modes are chosen along the y and z directions respectively. A summary of the cases discussed in this section is provided in Table 4.1 where the first column presents the case number. The next two columns give the magnitude of the shear flow V_0 , and the force-free coefficient κ . The fourth and fifth identify the properties of the resistivity model. The sixth and seventh are the magnitude of the KH and tearing perturbation. The last two columns identify the parsed KH and tearing growth rate.

The three-dimensional analysis is not straight forward. For example, growth rates for both the tearing and KH instabilities are not related to the magnitude of the initial perturbation. But the magnitude of the perturbation can affect the time evolution of the nonlinear interaction of the tearing and KH modes. If the tearing mode perturbation is initially smaller than the KH perturbation, the KH instability may dominate first. Controlling the magnitude of perturbation, I can see how those two kinds of instability develop in this situation.

In order to determine the growth rate in the 3-D system, in Figure 4.7, the

solid line represents $\ln(\max(b_x) - \min(b_x))$ as a function of time in the entire 3-D system. The dotted line represents the value of $\ln(\max(b_x) - \min(b_x))$ from the growth of the tearing mode as a function of time. The dashed line represents the value of $\ln(\max(b_x) - \min(b_x))$ from the growth of the KH mode as a function of time. (In Figure 4.7c and 4.7d, the dotted line and dashed line can not be seen because they are almost the same line as the solid lines.) The cases represent four typical mode-mode combinations. For these cases, I will see how the tearing mode and the KH mode coordinate with each other in one 3-D simulation domain.

Figure 4.7a shows the growth of b_x for case 1 in which the tearing mode has a larger initial magnitude of the perturbation but a smaller growth rate than the KH mode. Note that the solid line is not straight. At about $t = 50$, the curve assumes a different slope. In the diagnosis, I calculated the clean b_x growth from the KH mode to get the dotted line which has a growth rate of 0.07, and calculated the clean b_x growth from the tearing mode to get the dashed line which has a growth rate of 0.03 (without diffusion correction). In this way, I parsed a tearing mode and a KH mode from the system. The early part of the dashed line coincides with the solid line, and the later part of the dotted line coincides with the solid line. The separation point is around $t = 50$. The effect of the growth of b_x is the superposition of two modes. The tearing mode is dominant before $t = 50$, and at a later time the KH mode becomes dominant.

In order to prove that the dotted line and the dashed line for case 1 are indeed contributed from the growth of the tearing and KH modes respectively, I carried out 2-D simulations to test these results. As mentioned in section 4.2, all of the parameters in the 2-D simulations are the same as those in case 1 except for the

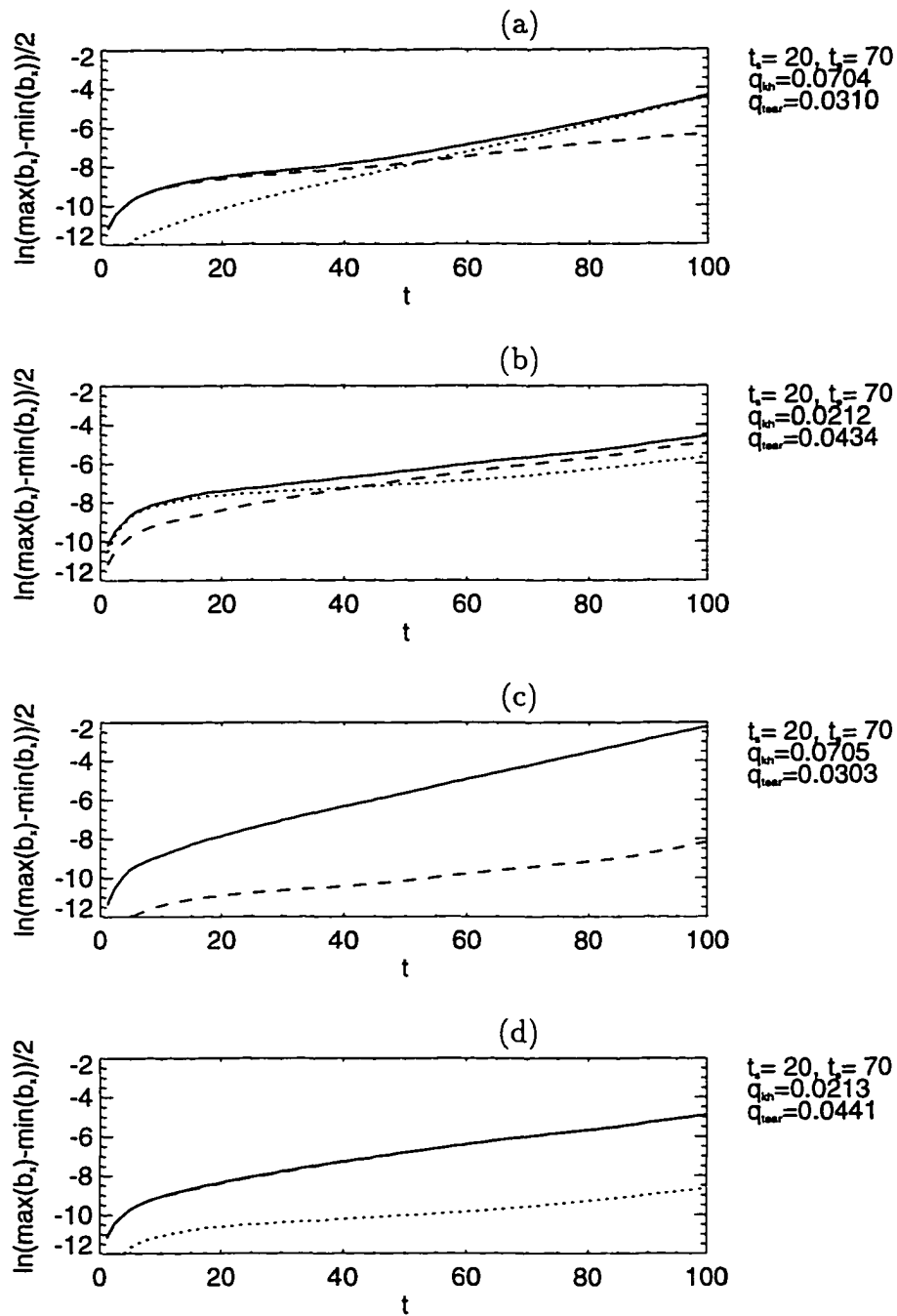


Figure 4.7 Parse the KH and tearing modes from the coupled mode for (a) case 1, (b) case 2, (c) case 3, and (d) case 4.

perturbation, which is either the KH perturbation or the tearing perturbation determined by the corresponding tested mode. A successful comparison of the 2-D and 3-D results is a confirmation for the 3-D method. In addition, this illustrates, in the linear stage, that one mode (the tearing or KH) will develop at its own growth rate without the intervention from the other mode (the KH or tearing).

For the same initial conditions as case 1, in a 2-D simulation, the growth rate of the KH mode (with $V_0 = 0.5$ and $\kappa = 0.1$) is about 0.07; In another 2-D simulation, the growth rate of the tearing mode (with $\alpha = 0.005$) is about 0.029 (without diffusion correction). They are very close to parsed mode's values of case 1. It can be concluded that the tearing mode and the KH mode develop at their own growth rates in this case.

For case 1, the KH and tearing perturbation magnitudes are 0.0001 and 0.001 respectively. Because the perturbation for the tearing mode is initially larger, the growth is mainly from the tearing mode, and the growth from the KH mode is hidden initially. But the growth rate of the KH instability is larger than that of the tearing mode, the growth of KH will eventually surpass the tearing mode. So the total growth in the figure turns sharply at $t = 50$.

Figure 4.7b shows the growth of b_x for case 2 in which the tearing mode has a smaller magnitude of perturbation but a larger growth rate than the KH mode. It exchanges the position of the tearing mode and the KH mode compared to case 1. Initially the KH growth dominates because of its larger magnitude. At $t = 45$ the tearing growth surpasses the KH growth because of its larger growth rate. At $t = 45$, the b_x growth turns sharply. The same techniques as used in case 1 have been used to prove that the tearing mode and the KH mode develop at their own

growth rates in this and the following two cases.

Figure 4.7c shows the growth of b_x for case 3 in which the tearing mode has a smaller magnitude of the perturbation and a smaller growth rate than that of the KH mode. Figure 4.7d shows the growth of b_x for case 4 in which the tearing mode has a larger initial perturbation and a larger growth rate than that of the KH mode. The plots show either the tearing mode dominant or the KH mode dominant in the case when both their perturbation magnitude and growth rate are high. So the dominant mode initially depends on the initial perturbation and growth rate.

From all cases above, the KH mode and the tearing mode increase at their own growth rates in the linear stage. They do not interfere with each other. The total evolution depends on the magnitude of the initial perturbation and the growth rate.

4.4 Discussion and Conclusion

The linear properties of the KH and tearing modes are very important to understand the nonlinear interaction of the KH and tearing instabilities. The KH instability can be stabilized by the magnetic component aligned to the shear flow. The growth rate of tearing is mainly dependent on resistivity model. It is almost not affected by plasma β , b_y , and the perpendicular shear flow. But the perpendicular shear flow will generate a magnetic field component along the same direction, and the component will grow at the same growth rate as the tearing mode.

In three dimensions, if the tearing and KH modes' wave vectors are perpendicu-

lar to each other, the KH mode and the tearing mode will grow at their own growth rates. The dominating instability depends on the initial perturbation magnitudes and the growth rates of the modes. For cases 1 and 2, if the KH/tearing growth can not surpass the tearing/KH growth until the nonlinear phase of the KH/tearing mode, I count them to the category of cases 3 or 4.

It is interesting to investigate possible KH and tearing modes at the magnetopause. In Figure 4.8, the solid arrows denote the wave vectors of the tearing modes, and the dashed arrows denote the wave vectors of the KH modes. Cases with magnetic shear, velocity shear, and both magnetic and velocity shear are present. If the normal of the current sheet is along the x direction, and the antiparallel magnetic field and flow field are along the y and z directions, the wave vectors are confined in the yz plane. If there is no shear flow, the tearing mode wave vectors may be along every direction except the y direction. If there is no magnetic shear and shear velocity is smaller than the fast mode speed, the possible KH mode wave vector are along every direction except the z direction. If the shear velocity is larger than the fast mode speed, the KH wave is stabilized in the vicinity of the y direction. If the magnetic and the flow shears intersect at a non-zero angle, both tearing and KH modes can grow in a separated angle range of directions. For arbitrary perturbations in a configuration with both magnetic shear and flow shear, tearing and KH modes can only grow in a separated range of directions. A lot of these modes can exist simultaneously.

From this reasoning, the tearing and KH modes are actually dependent on the direction of the wave vectors, but the maximum growth rate occurs for k vectors along the direction where there are maximum Δb or Δv . The tearing instability

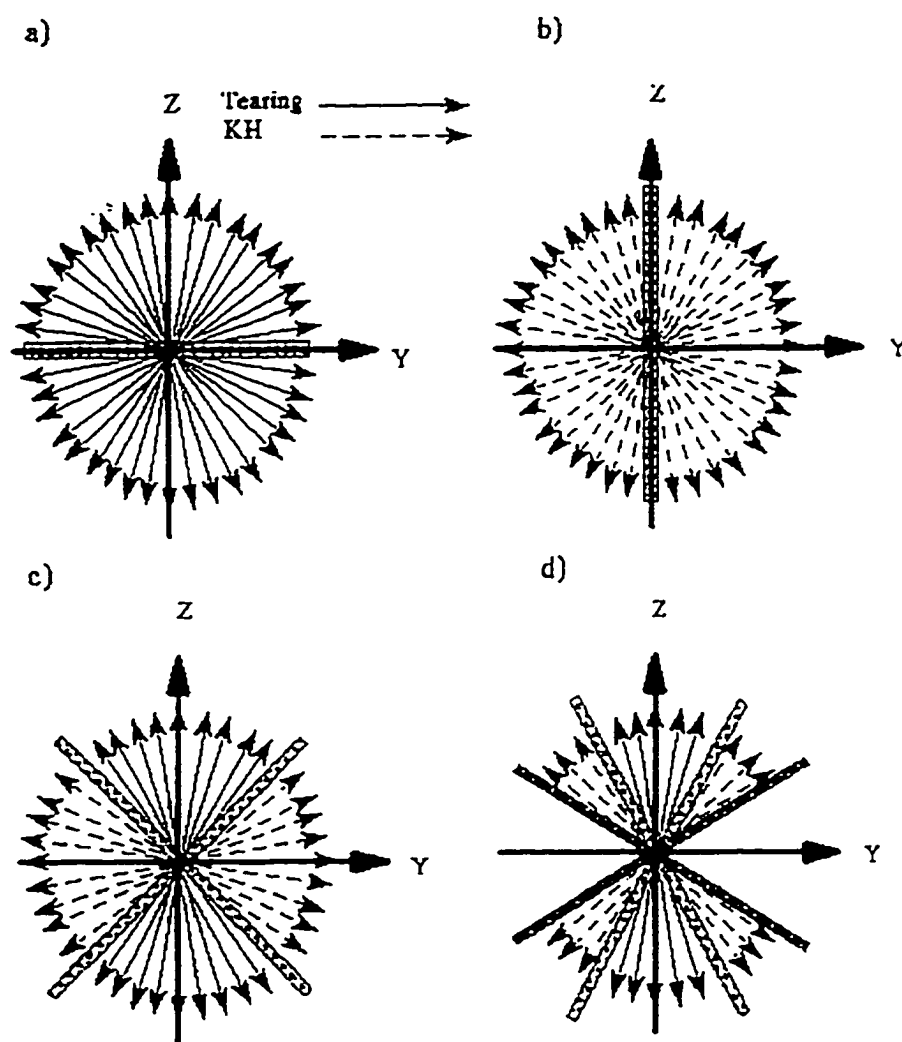


Figure 4.8 The possible tearing modes and KH modes in the yz plane for (a) only the magnetic shear, (b) only the flow shear, (c) both the magnetic and flow shears, (d) both the magnetic and flow shears where the shear velocity is larger than the fast mode speed.

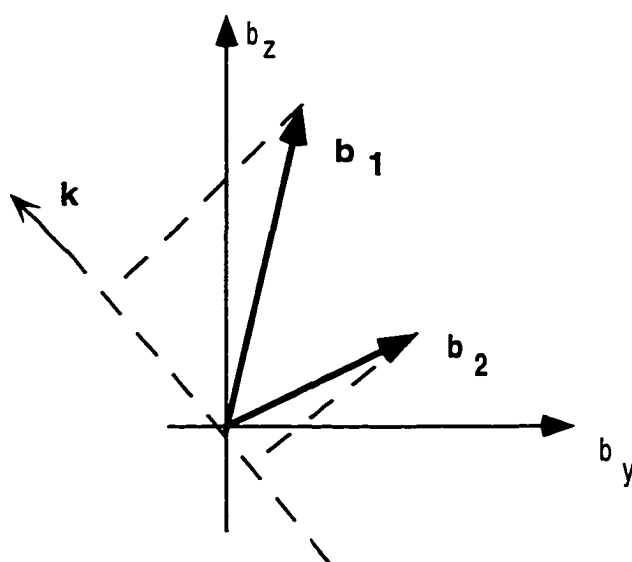


Figure 4.9 The tearing mode for northward IMF.

is still possible even when the IMF is northward. If there is a nonzero angle between the IMF and the geomagnetic field, there exist some directions along which antiparallel magnetic field components (see Figure 4.9). Along those directions, the tearing mode instability can still operate. This explains that FTEs can sometimes be observed when the IMF is northward. But the range of directions for the tearing mode's wave vectors is much smaller than for a southward IMF condition. Thus it is more likely to observe FTEs for a southward IMF.

In the nonlinear stage, the dominant instability may affect the topology and dynamics of the system much stronger than the other one. The study of the linear properties of the tearing and KH instabilities is the starting point for the investigation of the nonlinear processes, which will be discussed in detail in Chapter 5.

Chapter 5

Nonlinear dynamics of the interaction of KH and tearing instabilities in three dimensions

5.1 Introduction

One of the major unanswered questions of magnetospheric physics is the structure of the dayside magnetopause and the low-latitude boundary layer. This topic is important for the transport of magnetosheath plasma into the magnetosphere and the transport of magnetic flux from the dayside magnetosphere to the magnetotail. Two fundamental processes of the solar wind-magnetosphere interaction are magnetic reconnection [*Dungey, 1961*] and viscous diffusion [*Axford and Hines, 1961*]. Most studies of this interaction treat only one of these processes and ignore the other. The interaction of the KH and tearing mode instabilities provides a better

understanding of processes at the magnetopause where magnetic and flow shears are equally important.

The linearization of the MHD equations is very helpful to understand the basic properties of the KH and tearing modes, but it is not sufficient to understand the nonlinear dynamics and the associated plasma, energy, and magnetic flux transport through the magnetopause. In fact the most important processes at the magnetopause and the low latitude boundary layer are large-scale, time-dependent, and highly nonlinear. Nonlinear aspects of the interaction of the KH and tearing mode instabilities are central in this exploration.

Many authors studied the nonlinear aspects of the KH instability or the tearing instability. The nonlinear aspects of the KH instability can be related back to *Rosenhead's* paper [1931]. In a vortex sheet with no density difference across it, he carried out a calculation taking non-linear terms into account which should be validated at later times. An originally sinusoidal interface (or vortex sheet) wound up into a spiral form due to the interaction of the various parts of the vortex sheet and the distortion of the wave form by the mean flow. This result provided the basic topologic and dynamic characteristics of the nonlinear KH instability. Even though it was investigated in a nonmagnetized fluid, it is very helpful to understand the nonlinear characteristics of the KH instability in the magnetized plasma. *Miura et al.* [1987] studied viscous transport at the magnetopause through investigating the nonlinear KH instability. The anomalous viscosity from the KH instability increases with the Alfvén Mach number at a critical value. The nonlinear aspects of the tearing instability have been studied by many authors [*Fu and Lee*, 1986; *Otto*, 1990; *Ma et al.*, 1993; etc.] mostly in numerical simulations. Their results were

connected with observations of layers of accelerated plasma [*Sonnerup et al.*, 1981; *Paschmann et al.*, 1986; *Gosling et al.*, 1990; *Sonnerup et al.*, 1990] and magnetic flux transfer events or flux erosion events [*Russell and Elphic*, 1978; *Paschmann et al.*, 1993] during periods of southward interplanetary magnetic field orientation. Most of these and many other studies are related to magnetic reconnection.

Even though these studies have been completed, no work successfully correlated magnetic reconnection with viscous transport at the magnetopause. The connection between magnetic reconnection and viscous diffusion can happen in a configuration where both magnetic shear and flow shear exist. There are several studies which considered magnetic shear and flow shear [*La Belle-Hamer et al.*, 1988; *Pu et al.*, 1990a and 1990b], but all of these are limited to two dimensions. When the magnetic field is parallel to the flow field, there is no coupling of the KH and tearing mode instability (see Chapter 3). *La Belle-Hamer et al.* [1988] investigated a current sheet with a magnetic field perpendicular to the flow field in a two-dimensional incompressible simulation. In this study, the KH vortices twisted the current sheet and lead to the presence of several separated pinched current sheets. The shear flow generates a magnetic field component in the invariant direction if it is initially zero. In the simulation, the interaction of tearing and KH instability can not be realized, but it is assumed that reconnection occurs where vortices pinch the current sheet. Note that 2-D simulations are able to demonstrate the modification of the tearing mode by shear flow and the modification of the KH made by finite resistivity and magnetic shear. However, obviously three dimensional simulations are needed to study the nonlinear coupling of the two instabilities.

In this chapter, I will first discuss how the nonlinear evolution of the KH instability operated along a k vector induces the growth of tearing modes along wave vectors perpendicular or not aligned to the KH wave vector. I will also discuss how several growing tearing modes interact with each other just as the growth of tearing modes in multiple current layers [Yan *et al.*, 1994]. The second subject will contribute to the understanding of the nonlinear interaction of the KH and tearing instabilities. I will discuss how the tearing instability affects the KH instability and how the KH instability affects the tearing instability.

5.2 Simulation Model

Three-dimensional resistive MHD equations, initial equilibrium, boundary conditions, and initial two-mode perturbation are quoted as Chapter 4.

A current dependent resistivity is used in the simulation.

$$\eta = \eta_0 + \begin{cases} \alpha(|j| - |j_c|) & |j| \geq j_c \\ 0 & |j| < j_c \end{cases} \quad (5.1)$$

The time evolution of the magnetic field and plasma parameters is calculated by solving the 2-D and 3-D normalized MHD equations as described in Chapter 2. The numerical method I used is a leapfrog scheme [Potter, 1973]. Free boundary conditions are applied to the two boundaries in the x direction. Periodic boundary conditions are used at the two boundaries along the y and z directions.

The grid is chosen to be uniform along the y and z directions and nonuniform along the x direction with a minimum grid separation of ϵ_x in the center of the system to resolve the evolution of thin current layers during the dynamical evolution. The number of grid points and the maximum resolution is varied for different

simulations. In the simulation for case 1, I use $143 \times 103 \times 103$ grid points with a resolution of $\epsilon_x = 0.05$, $\epsilon_y = 0.2$, and $\epsilon_z = 0.3$. Here ϵ denotes the minimum grid separation for each cartesian coordinate, which is chosen such that the current sheet and the KH vortices are better resolved. In the simulation for case 2, I use $103 \times 53 \times 53$ grid points with a resolution of $\epsilon_x = 0.05$, $\epsilon_y = 0.4$, and $\epsilon_z = 0.6$.

5.3 Simulation Results

5.3.1 The KH instability Induces the Tearing Instability

Overview of case 1

The basic configuration has been illustrated in section 2 (see Figure 4.1). The volume of the three dimensional simulation box is defined as $|x| \leq 20$, $|y| \leq 10$, and $|z| \leq 15$. The angle of magnetospheric field and interplanetary magnetic field is 179° . That will introduce a very small magnitude b_y component, which has a negligible influence on the dynamics, but is very useful for illustrative and diagnostic purposes. The other quantities are $\beta = 3.0$, $B_0 = 1$, $V_0 = 0.3$, $\rho_0 = 1$, $j_c = 1.1$, $\alpha = 0.01$. Also the initial tearing mode perturbation is $v_{z1} = 0.001$, and the initial KH mode perturbation is $v_{x1} = 0.01$.

Figure 5.1 shows the evolution of normal velocity/magnetic field components and maximum current density. The critical current is set to a high value ($j_c^2 = 1.1$) such that the resistivity in the initial configuration is negligible. The resistivity between $t = 0$ and $t = 100$ remains very small, so the tearing growth rate during that period is very very small compared with the KH growth rate. The initial

perturbation for the tearing mode is smaller than that of the KH mode. The dominant mode is the KH mode (see Chapter 4). There is a gradual increase of current density from $t = 50$ to $t = 100$ caused by the KH instability. From the evolution of v_x and b_x , the growth rate of the KH instability is about 0.051. After $t = 100$, the nonlinear phase of the KH instability is shown. At about $t = 155$, all of the three variables increase very rapidly. This change indicates the occurrence of a fundamental process, which is quite different from the KH instability. In this case, two physics processes are well separated at $t = 155$. After $t = 155$, the resistivity and the current density reach very high values indicating the onset of very fast reconnection. The later sections will discuss this in detail.

A. Current thinning processes

From $t = 0$ to $t = 155$, the KH instability is the dominant mode. In Chapter 3, I discussed the thinning process in a configuration with reversed magnetic field parallel to the shear flows. Now the geometry is changed to a configuration with reversed magnetic field and shear flow perpendicular to each other. When resistivity is very small, it can be shown from equation 2.3 [e. g., *Siscoe*, 1983] that the magnetic flux through a closed loop moving with fluid is conserved. Mathematically, this statement can be expressed as

$$\Phi_b = \mathbf{b} \cdot \mathbf{A} = \text{const} \quad (5.2)$$

where \mathbf{A} is an arbitrary cross-section of magnetic flux. Because there is very little change for magnetic field b_z component in the early stage, a cross-section chosen in the xy plane and moving with the fluid shows almost no change.

To demonstrate the mechanism of the current sheet thinning, in the xy plane, I

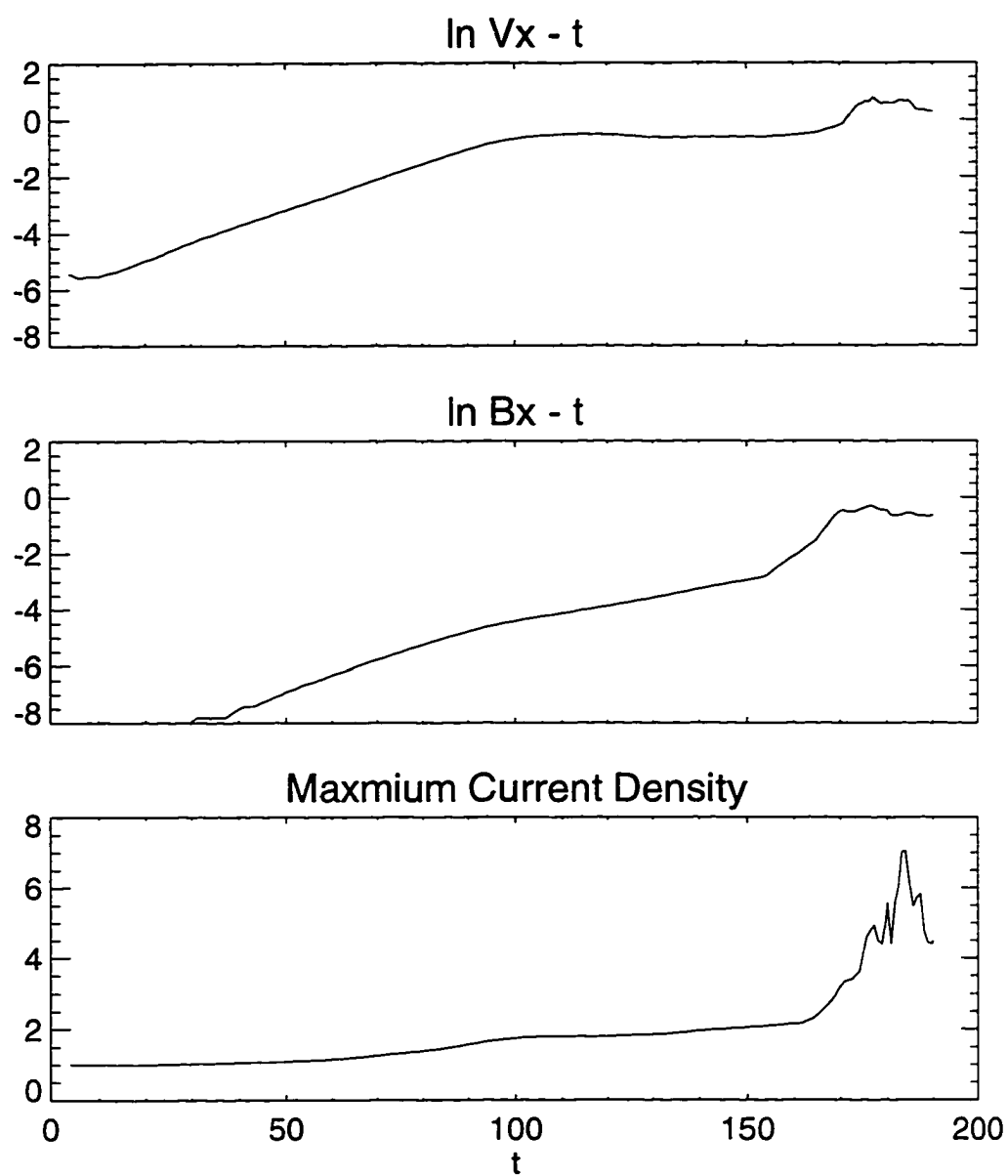


Figure 5.1 time evolution of normal velocity, magnetic field components, and maximum current density of case 1.

choose an area $ijkl$ to which the magnetic field is perpendicular, as in Figure 5.2a. At $t = t_1$, curve ij and kl follow two contour lines of b_z , which presents the profile of the current sheet. ik and jl can be regarded as the half width of the current sheet. At $t = t_2$ ($t_2 > t_1$), the area is changed to $mnop$. Figure 5.2b shows that the length of the contour line increases rapidly with time. So the width of the current sheet decrease. This process is not a uniform process along the current sheet. The magnetic field in a different region along the current sheet is different, such that the width will vary along the contour line.

B. Current sheet winds up to a spiral form.

Figure 5.3 shows the early evolution of the central-surface of the current sheet where isosurfaces of $b_z = 0$ at several different times are presented. At $t = 0$, it is located at $x = 0$. At $t = 75$, it becomes twisted. At $t = 100$, three layers are formed. If an observer moves along $y = -7$, he will encounter the current sheet three times. At $t = 125$, five layers are formed. This process can extend to a saturated state. As long as there is no z variance in the system, the current sheet will be twisted by the shear flow continuously, and the plasma at the two sides of the center-surface are well separated.

In an ideal magnetic fluid there are no dissipative effects; this means that fluid structures cannot diffuse freely. A change in the field pattern due to physical recombination or reconnection of magnetic fluid structures cannot take place without resistive or other nonideal terms in Ohm's law. The magnetic field line topology is frozen in the ideal fluid while the structure of the current sheet, in continuous motion, can be highly distorted by the background flow as in Figure 5.4. Gradually it will become thinner and wind up with several layers. If resistivity is zero

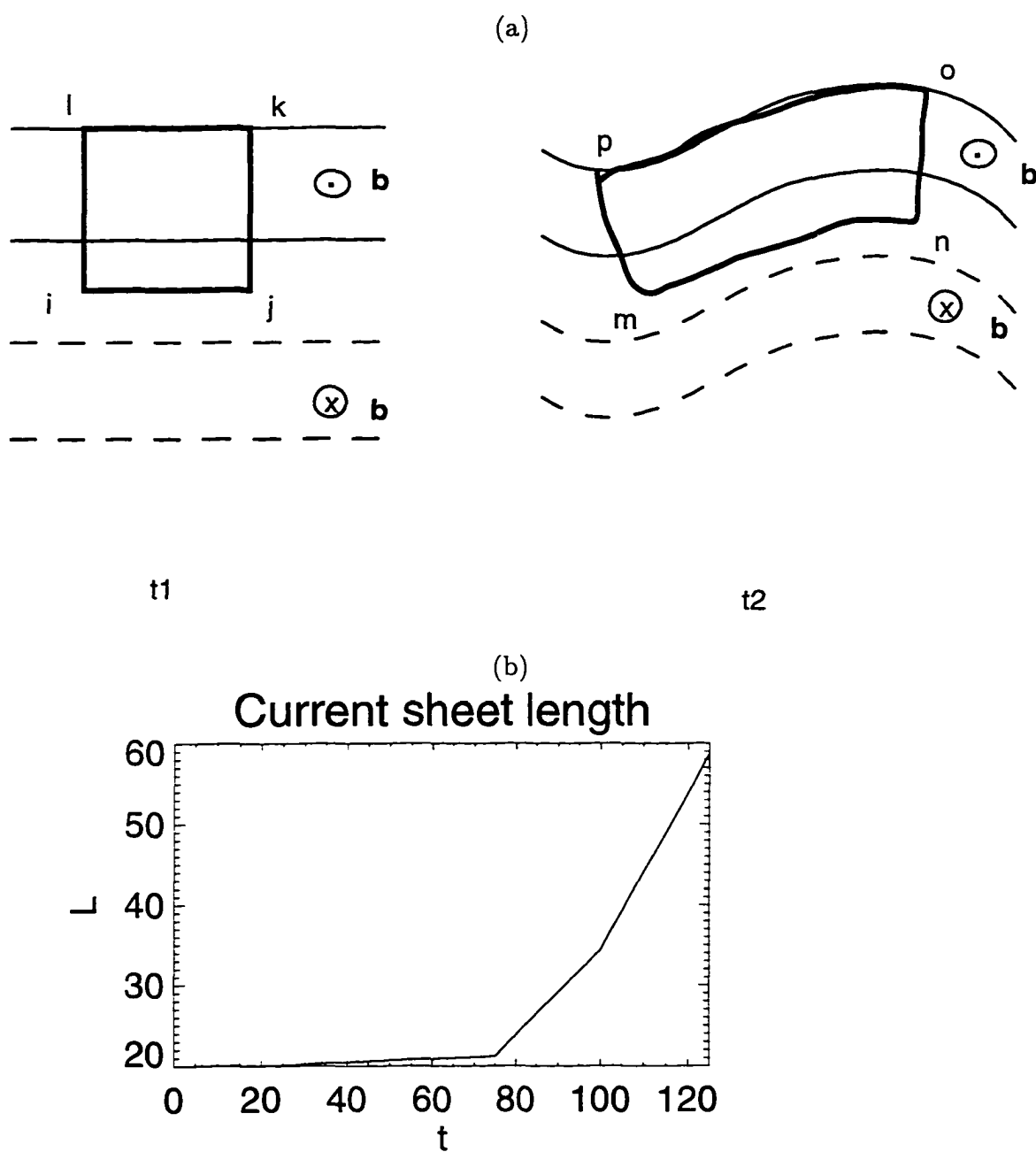


Figure 5.2 (a) The change of flux tube cross-section from t_1 to t_2 . (b) The length of the contour line for $b_z = 0$ as a function of time.

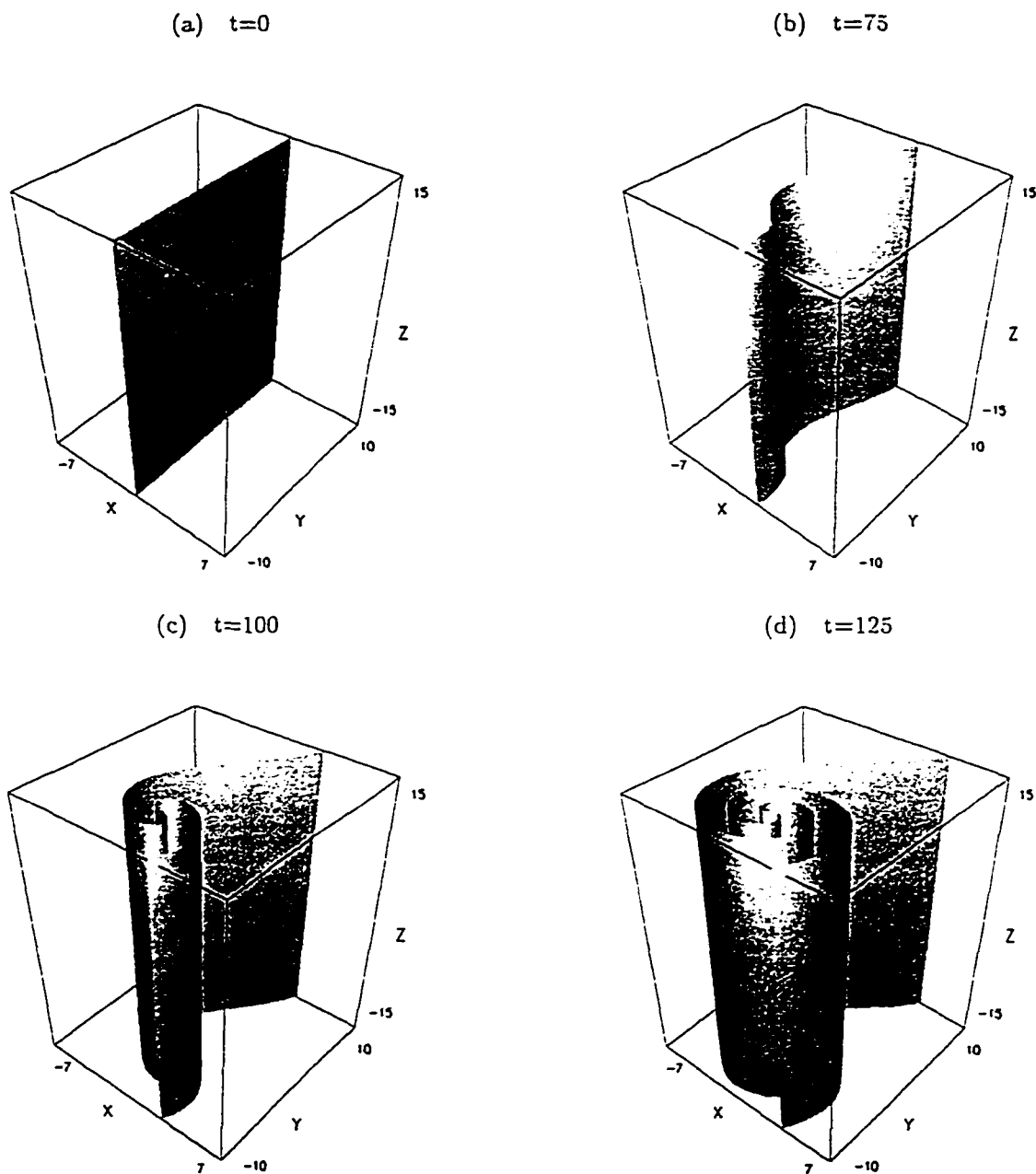


Figure 5.3 Winding-up processes of the current sheet and formation of multiple current layers due to Kelvin-Helmholtz vortices, where isosurfaces of $b_z = 0$ at (a) $t = 0$, (b) $t = 75$, (c) $t = 100$, and (d) $t = 125$ are shown.

or sufficiently small, antiparallel magnetic field lines are maintained on the two sides of those layers. Plasma, magnetic field, and flow field still can be identified across the current layers. As long as the frozen-in condition applies (with negligible resistivity), multiple current layers must form. The presence of the multiple current layer structure is a generic feature of organized fluid patterns. Because of dissipative effects, the lifetime of these structures is limited. If the resistivity is large, resistive diffusion will destroy these current layers. However, if the resistivity is small (as it is in space plasma), the tearing mode is a much faster process than resistive diffusion. The induced tearing instability will happen in those very thin regions, provided a suitable perturbation is presented. This process is called multiple current layer reconnection, which was previously investigated for multiple plane current layers by several authors [Matthaeus *et al.*, 1986; Scholer, 1990; Otto and Brik, 1992; Yan *et al.*, 1994].

C. Multiple current layer reconnection

After $t = 155$, the current density increases very fast. Resistivity has approached a relatively high value to trigger the tearing instability in multiple locations where the thickness of the current layer is very thin. Figure 5.5 shows the current sheet evolution after $t = 155$. The striking feature is the increasing deformation of the current sheet along the z direction. From $t = 155$ to $t = 170$, the number of layers are almost unchanged, but the current layers are strongly modified by fast-growing tearing modes. At some later time, current layers are broken, fragmented, or disappear completely. Those current layers can not be identified again. On the two sides of the current layers, magnetic field lines are reconnected, and plasma is mixed.

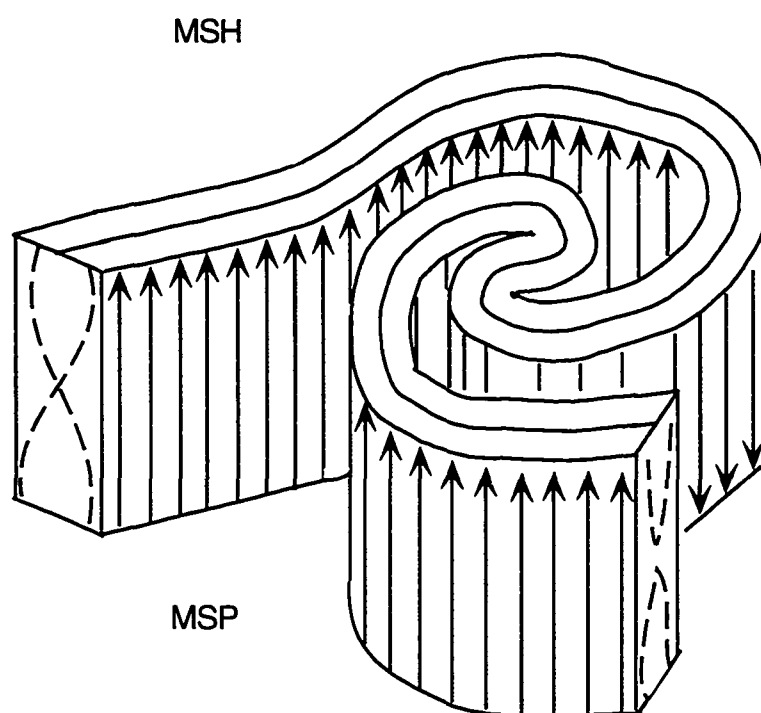


Figure 5.4 The mechanism of the formation of multiple current layers.

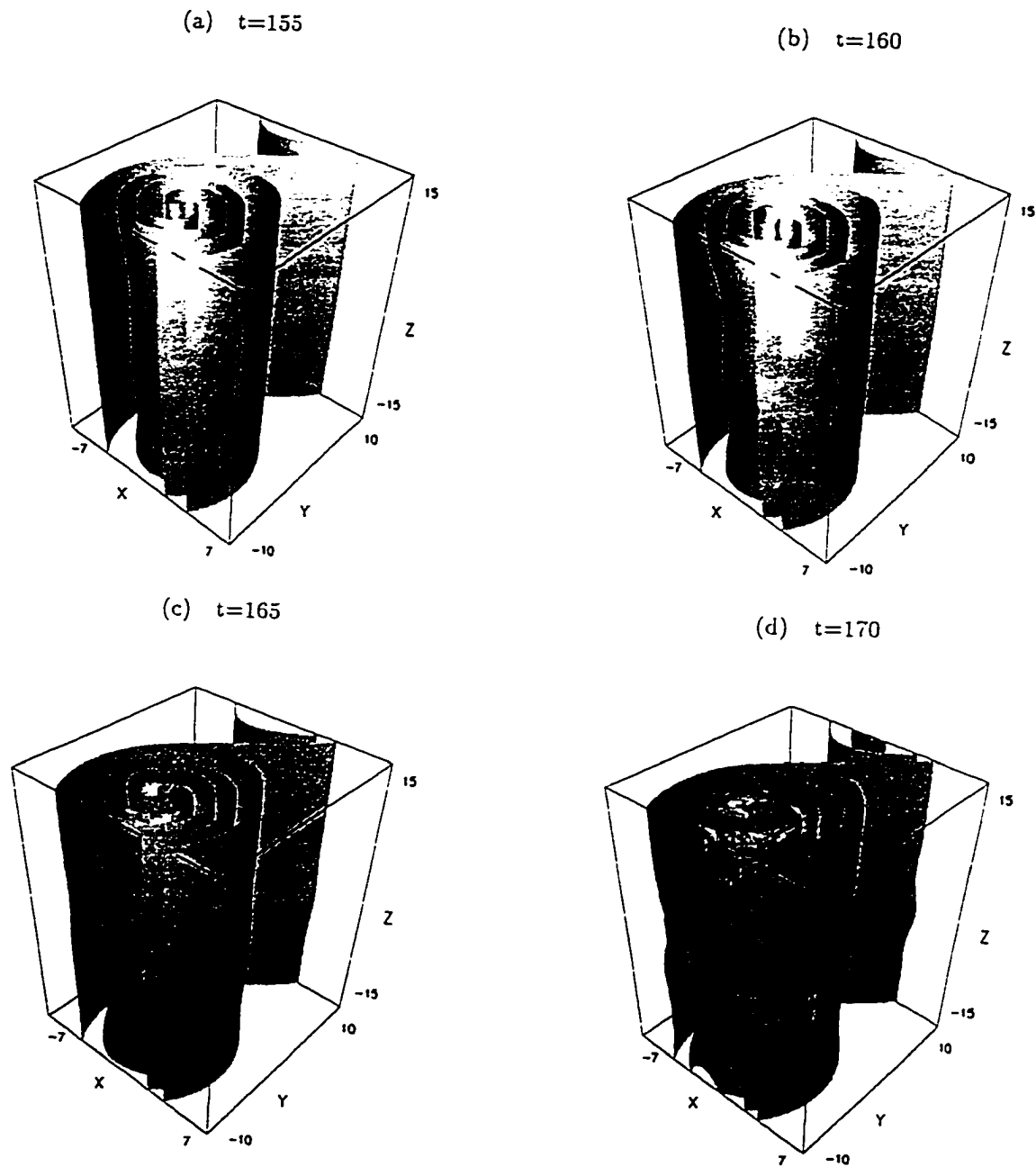


Figure 5.5 When multiple current layer reconnection is triggered, the current sheet is modified, where isosurfaces of $b_z = 0$ at (a) $t = 155$, (b) $t = 160$, (c) $t = 165$, and (d) $t = 170$ are shown.

Figure 5.6 presents snap shots of the magnetic field vectors across the surface $y = -7$ at times $t = 160$, $t = 165$, and $t = 170$, where part of the x range is shown. At $t = 160$, seven layers exist. At $t = 165$, some layers are broken. At $t = 170$, most of the layers are difficult to identify. Along the lines $x = 5$ and $x = -4.5$, reconnection is more active because in those regions, the width of the current sheets is very thin. We can see the growth of magnetic islands. At $t = 160$, two islands at $x = -4.5$ can be identified. The length in the z direction is about 7.5, and the width in the x direction is about 1. We also can identify these structures from the snapshots of resistivity and v_z at the same time (see Figure 5.7 and 5.8, where solid contour lines have high resistivity and positive v_z and dashed contour lines have low resistivity and negative v_z , respectively). Resistivity is high at $(x = -4.5, z = -15)$ or $(x = -4.5, z = 15)$. A pair of antiparallel flows along the z direction develop from almost the same locations, which is another strong indication of the tearing mode instability. Magnetic reconnection happens at those locations. At $t = 165$, the island grows to about 2 in width. At $t = 170$, the width is about 3 and resistivity and v_z also increase.

The reason for the fast increase of b_x between $t = 155$ and $t = 180$ is the interaction of tearing modes at different layers. The mutual interaction of modes in neighboring current layers will cause a fast growth for the instability. From Figure 5.6, at about $x = -4.5$, there are four islands operating. At $t = 170$, islands 3 and 4 have a little distance over islands 1 and 2 along the x direction. At the connection region between island 2 and island 3, magnetic field components favor each other. This introduces a large b_x component. The same conditions maintain for islands 3 and 1 and exist for islands 1 and 4. From the contour lines of resistivity

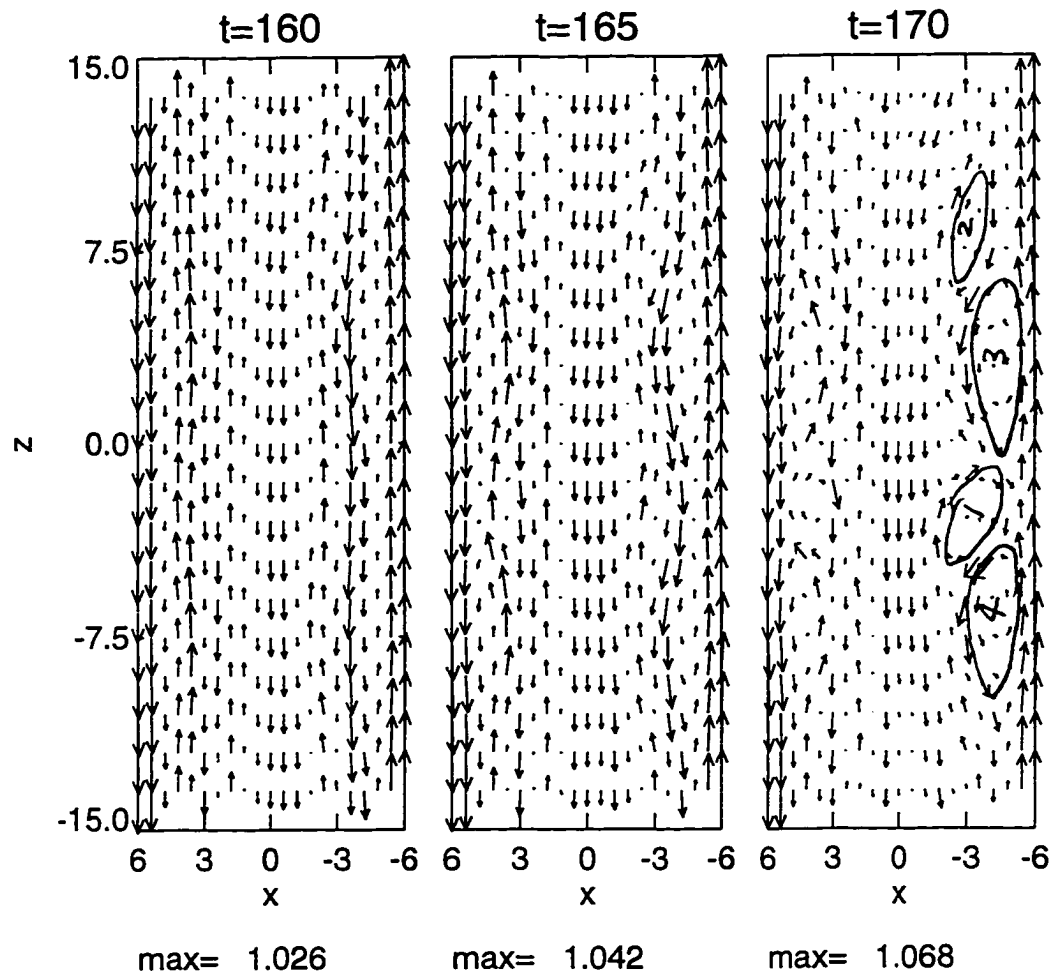


Figure 5.6 Snap shots of the magnetic field vectors across the surface $y = -7$ at times $t = 160$, $t = 165$, and $t = 170$, where part of x range is shown.

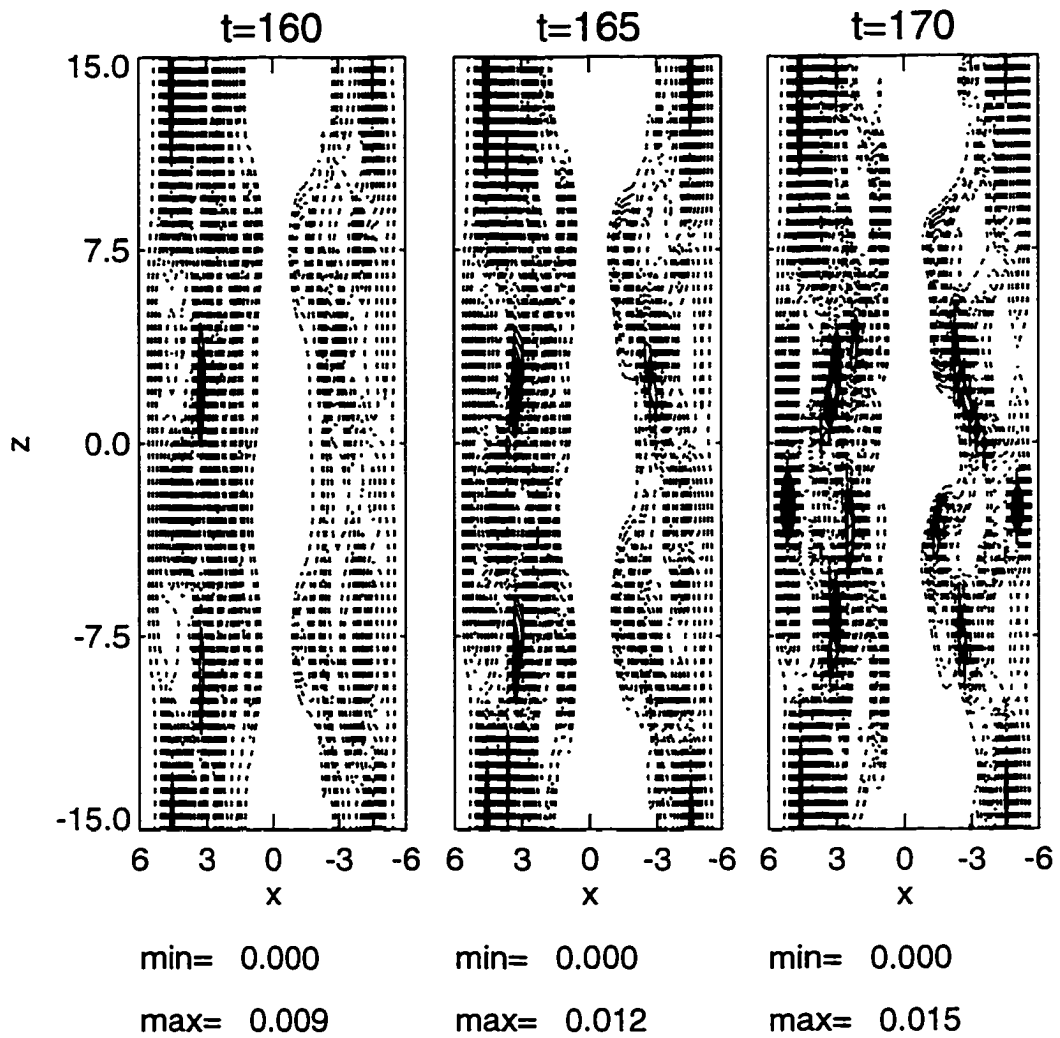


Figure 5.7 Snap shots of the contour lines of resistivity across the surface $y = -7$ at times $t = 160$, $t = 165$, and $t = 170$, where part of x range is shown. The solid and dashed contour lines denote high and low resistivity regions respectively.

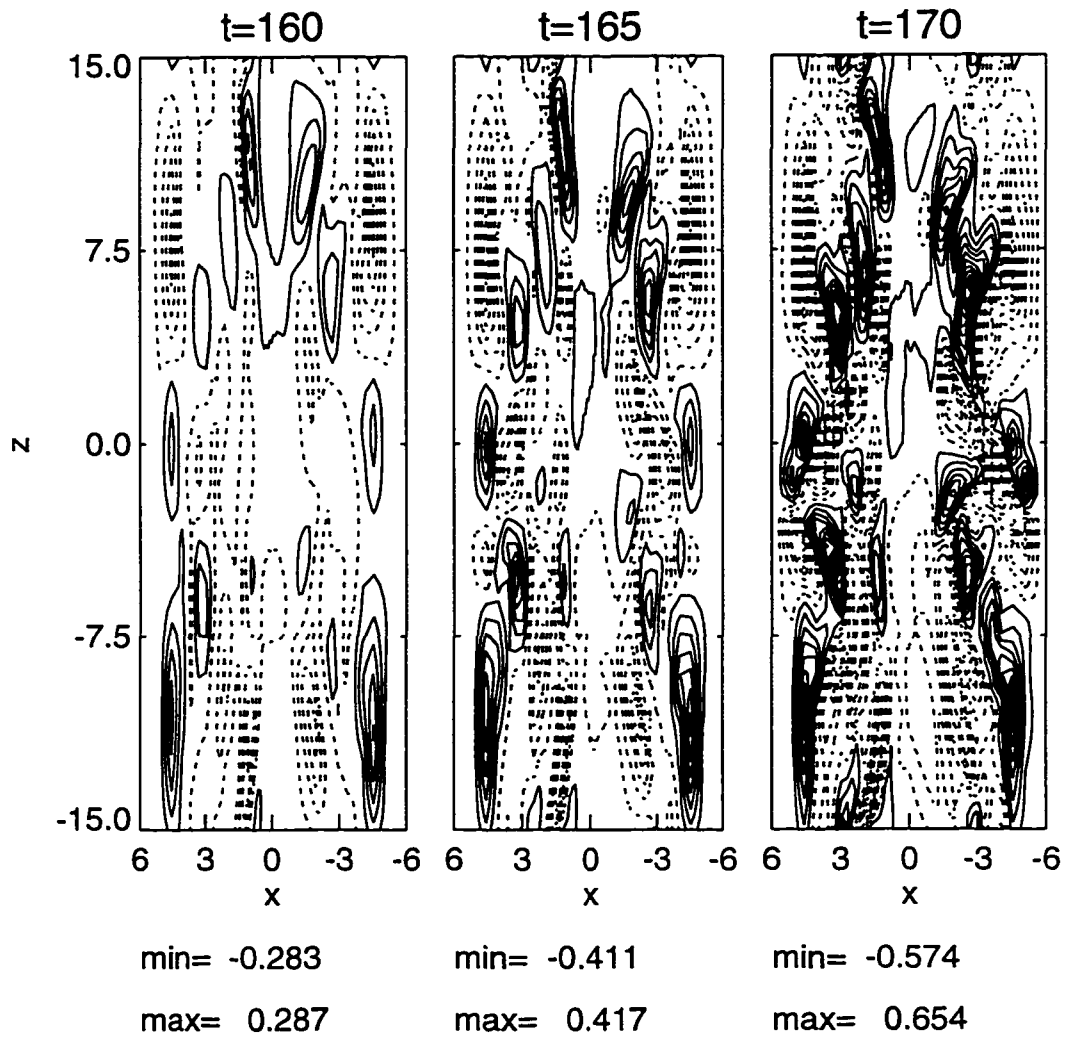


Figure 5.8 Snap shots of the contour lines of velocity component v_z across the surface $y = -7$ at times $t = 160$, $t = 165$, and $t = 170$, where part of x range is shown. The solid and dashed contour lines denote regions with positive and negative v_z respectively.

at this time, multiple layer reconnection can also be identified. Around the four islands, there are four regions with high resistivity. At $t = 170$, some magnetic flux transfer between layers can be seen, which is another characteristic of multiple layer reconnection. Note that the island truly is truly a three-dimensional structure (flux tube).

In this process, magnetic reconnection occurs in localized regions of the multiple current layers. The arrangement of some islands favor reconnection and leads to a faster growth. Because many islands form in a short time interval, the multiple current layer reconnection process proceeds very fast. Accelerated flow along the z direction also can be seen near the reconnection regions.

D. Dynamics and topological aspects

Before magnetic reconnection operates, magnetic field lines on the two sides of the current sheet are almost antiparallel along the z direction. But the topology is completely changed after $t = 155$. Figure 5.9 shows three magnetic field filaments from different views at $t = 165$. Those lines pass through $(-4.5, -7, 3.5)$, $(-4.5, -7, 1.5)$, and $(-4.5, -7, 0)$ respectively. Each line rotates in the xz plane, but extends in the y direction and shifts along the x direction. It can be seen that they almost uniformly twist around a core field line. They are contained in a tube with a cross-section approximately 2×7 . Each line commutes with the other two. There are no knots. There is a zero braid pattern among the three of them. From the top, the structure follows the profile of the outermost current layer.

There are also many examples of complex magnetic field structures. Figure 5.10 shows an example of a magnetic field filament viewed from three different angles. It passes through $(-3, -7, -2)$. From the top and at an angle, it is easy to see that

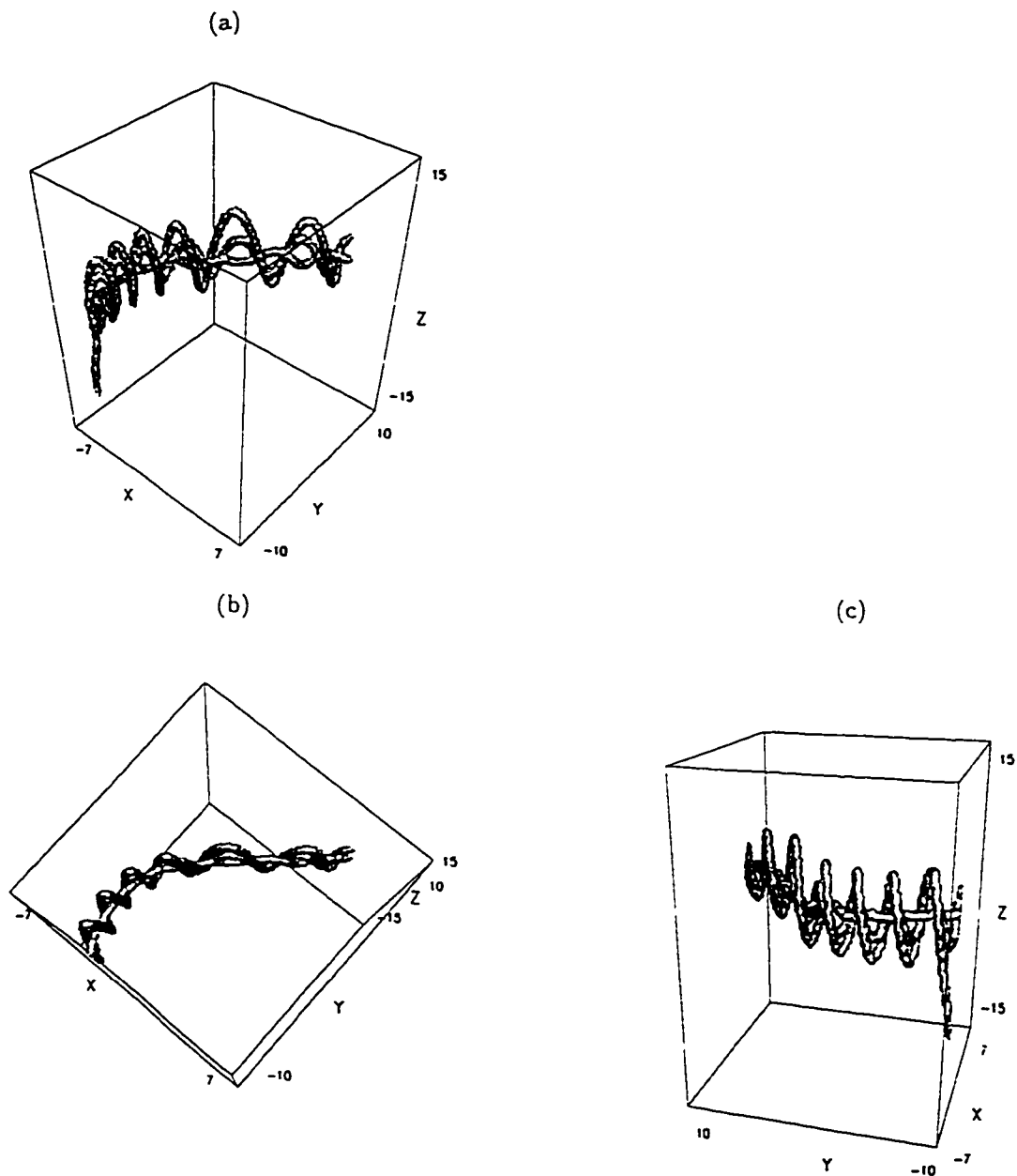


Figure 5.9 At $t=165$, three magnetic field filaments pass through $(-4.5, -7, 3.5)$, $(-4.5, -7, 1.5)$, and $(-4.5, -7, 0)$ in a flux tube viewed from (a) origin (b) top (c) the position turned -40° along the z axis.

a field line goes down along the z direction to the surface $z = 0$, then twists and rotates from the inner layers to outer layers. Figure 5.11 shows a magnetic field filament integrated from a fixed location $(-3, -7, -5)$ at $t = 165$, $t = 170$, and $t = 175$ respectively. At these time intervals, the topology is totally different, illustrating nicely the rapid change in magnetic field topology. It shows that the multiple current layer reconnection process is very fast.

Figure 5.12a and 12c show five current field filaments passing through $(-4.5, -7, 3.5)$, $(-4.5, -7, 1.5)$, $(-4.5, -7, 0)$, $(5.2, -7, 3.5)$, and $(-4.5, -7, -10)$, and 12b shows five velocity field filaments passing through the same five points. It is easy to see current and flow fields all follow vortex motion. 12d shows the regions with $\eta > 0.8$; it is very clear that the high resistivity regions include several patchies and numerous scattered spots. Those patchies are separated layer by layer with finite varied length and have the twisted geometry, which is a generic feature of the vortex motion. Those patchies can not be seen as multiple X lines because they have finite length in three dimensions. This shows the reconnection occurs as a multiple patchy reconnection instead of a multiple X line reconnection.

Figure 5.13 shows three density distributions in cuts along the z and the x direction at $t = 165$ and $t = 170$ respectively. From (a) and (c), the flow vortex motion formed the layer structure before $t = 165$, and some layers are smeared by the magnetic reconnection. At $t = 170$ more layers are broken. From (b) and (d), one can see some reconnection feature for plasma density. One layer structure at the plasma blob is smeared out and becomes difficult to identify. At the thin shear flow layer, one can see that a magnetic island is growing. The pressure presentation also illustrates similar features (see Figure 5.14). At a later time, the current layer

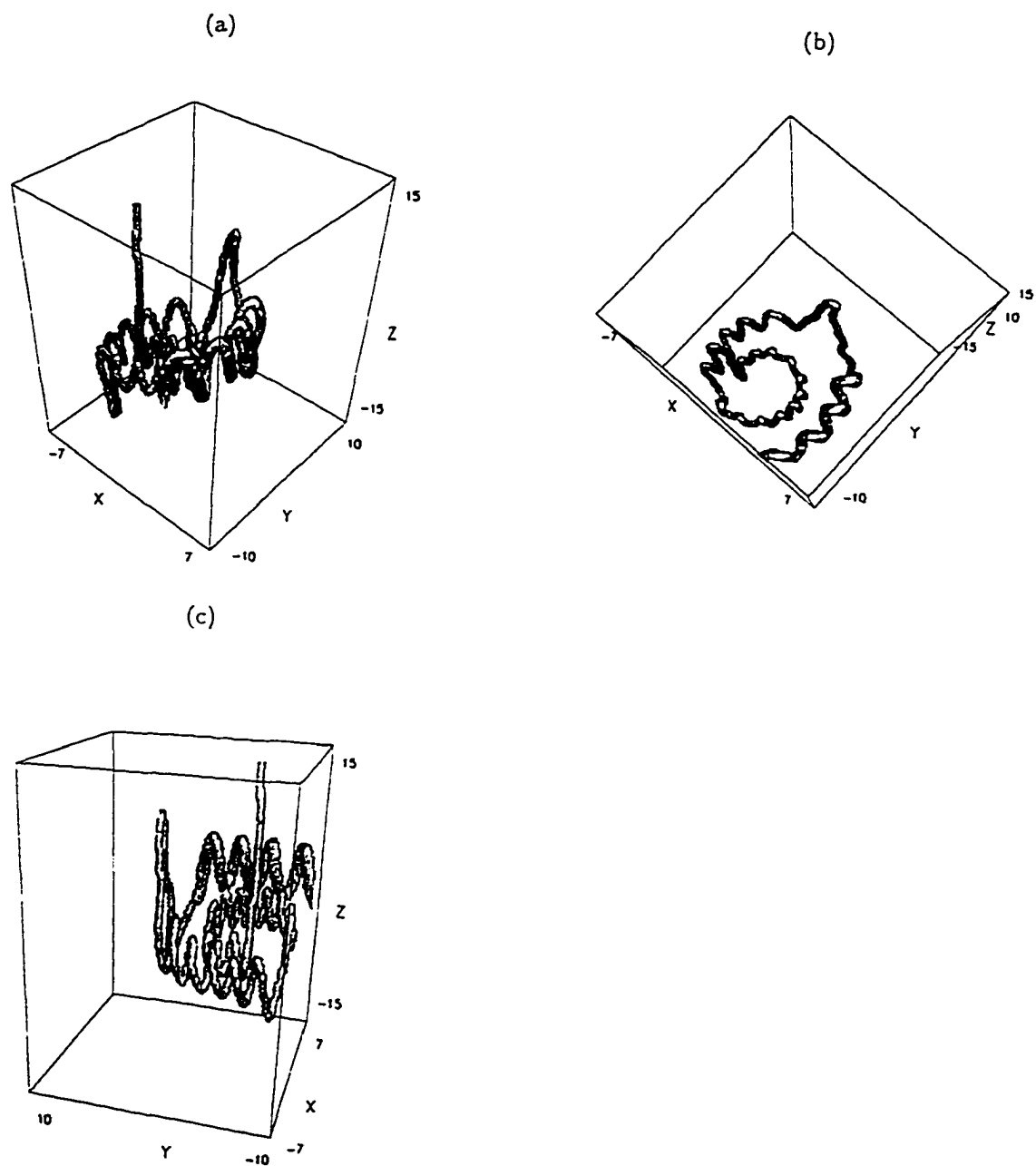


Figure 5.10 At $t=165$, a magnetic field filament pass through $(-3, -7, -2)$ viewed from (a) origin (b) top (c) the position turned -40° along the z axis (d) the position turned -90° along the z axis.

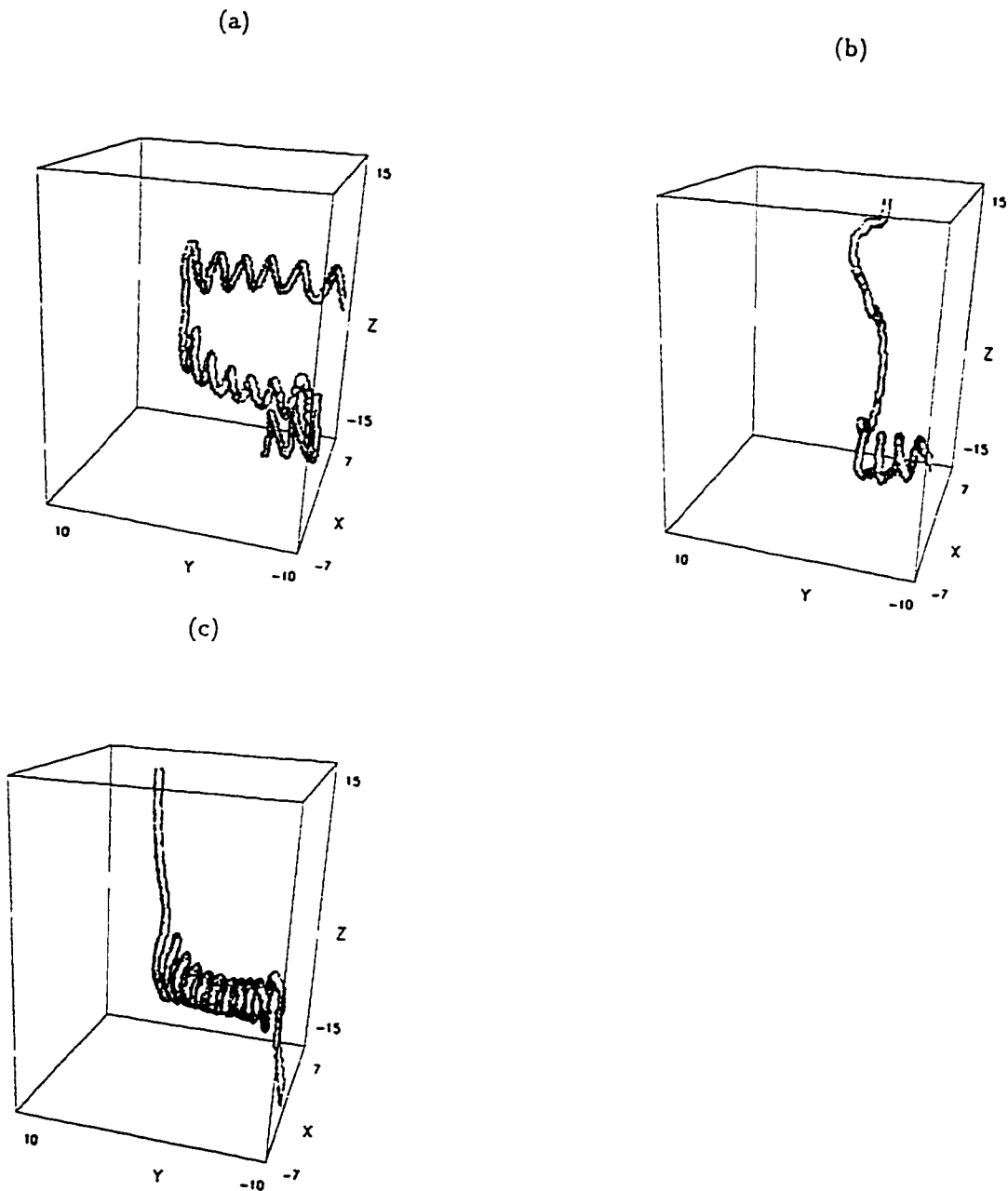


Figure 5.11 A magnetic field filament pass through $(-3, -7, -5)$ viewed at (a) $t=165$ (b) $t=170$ (c) $t=175$.

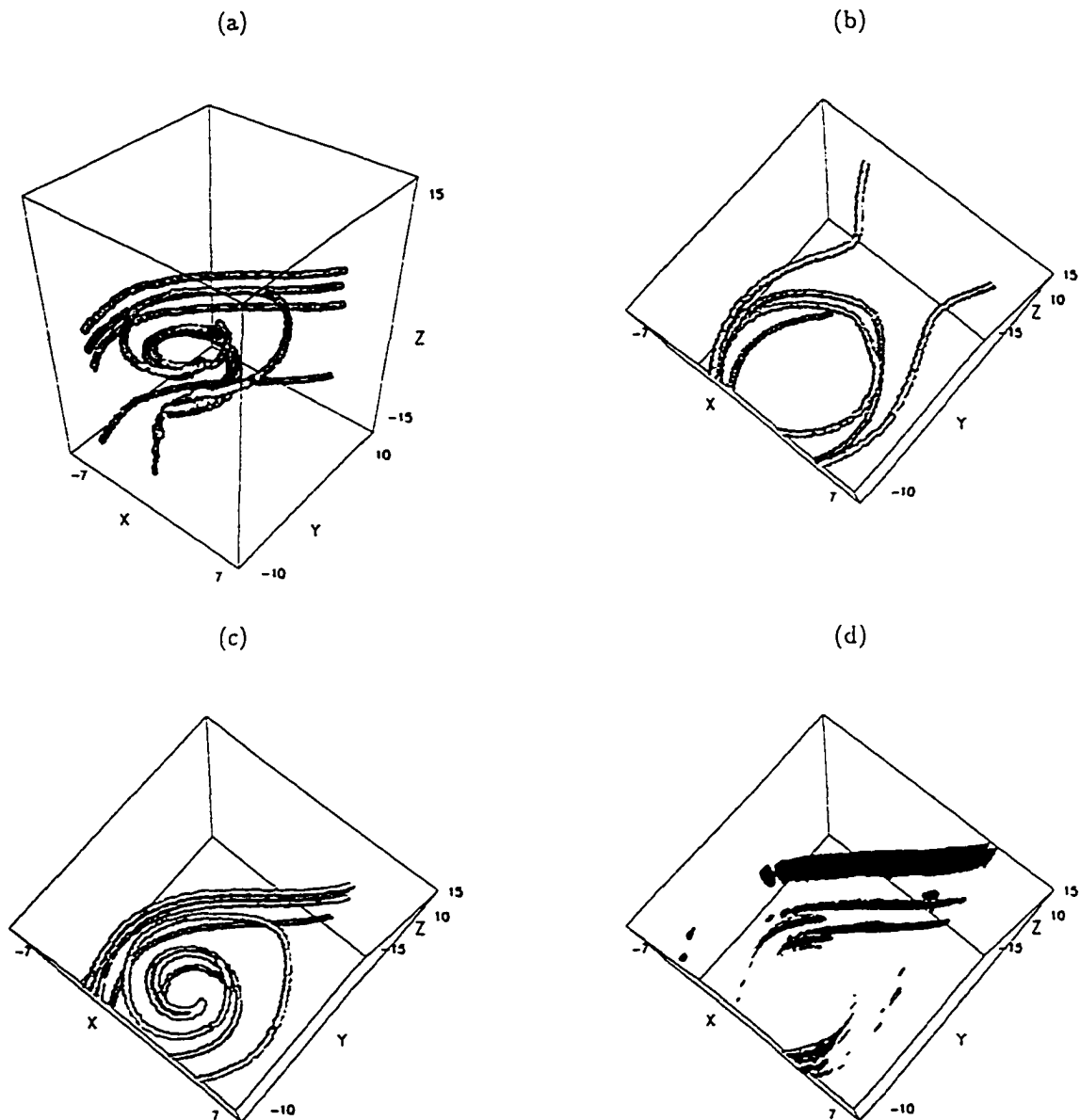


Figure 5.12 At $t=165$, five current field filaments viewed from (a) origin (b) top; five velocity field filaments viewed from (c) top; and reconnection patches viewed from (d) top.

structure disappears. The plasma of two sides become easy to mix with each other.

The field topology display shows the combined field features of the KH and tearing modes. Multiple current layer reconnection happens in different patches. Those patches are located in different current layers, and have finite lengths with twisted feature in three dimensions. After the multiple current layer reconnection, the topology of magnetic field lines is very complex. There are field lines contained in magnetic flux tubes, and field lines follow the flow vortex motion. The magnetic field line topology defined by a fixed point can change very fast. Current and stream lines follow vortex motion. The process leads to a very efficient mixing of plasma.

5.3.2 Coupling of the Kelvin-Helmholtz and Tearing Instabilities

Overview of this case:

Again, the basic field configuration is mentioned in section 2. The size the simulation has is the same as before, that is, $|x| \leq 20$, $|y| \leq 10$, and $|z| \leq 15$. The angle of magnetospheric field and interplanetary magnetic field is 179° . The other quantities are $\beta = 3.0$, $B_0 = 1$, $V_0 = 0.3$, $\rho_0 = 1$.

The major difference from the first case is that the critical current density ($j_c^2 = 0.8$) is lower than before ($j_c^2 = 1.1$). With a larger value of j_c , the tearing mode instability could not operate in the initial configuration. The present choice allows an faster growth of the tearing mode, and $\alpha = 0.005$ introduces a tearing growth rate of value about 0.036. Initially, there is some b_y distribution in the current sheet

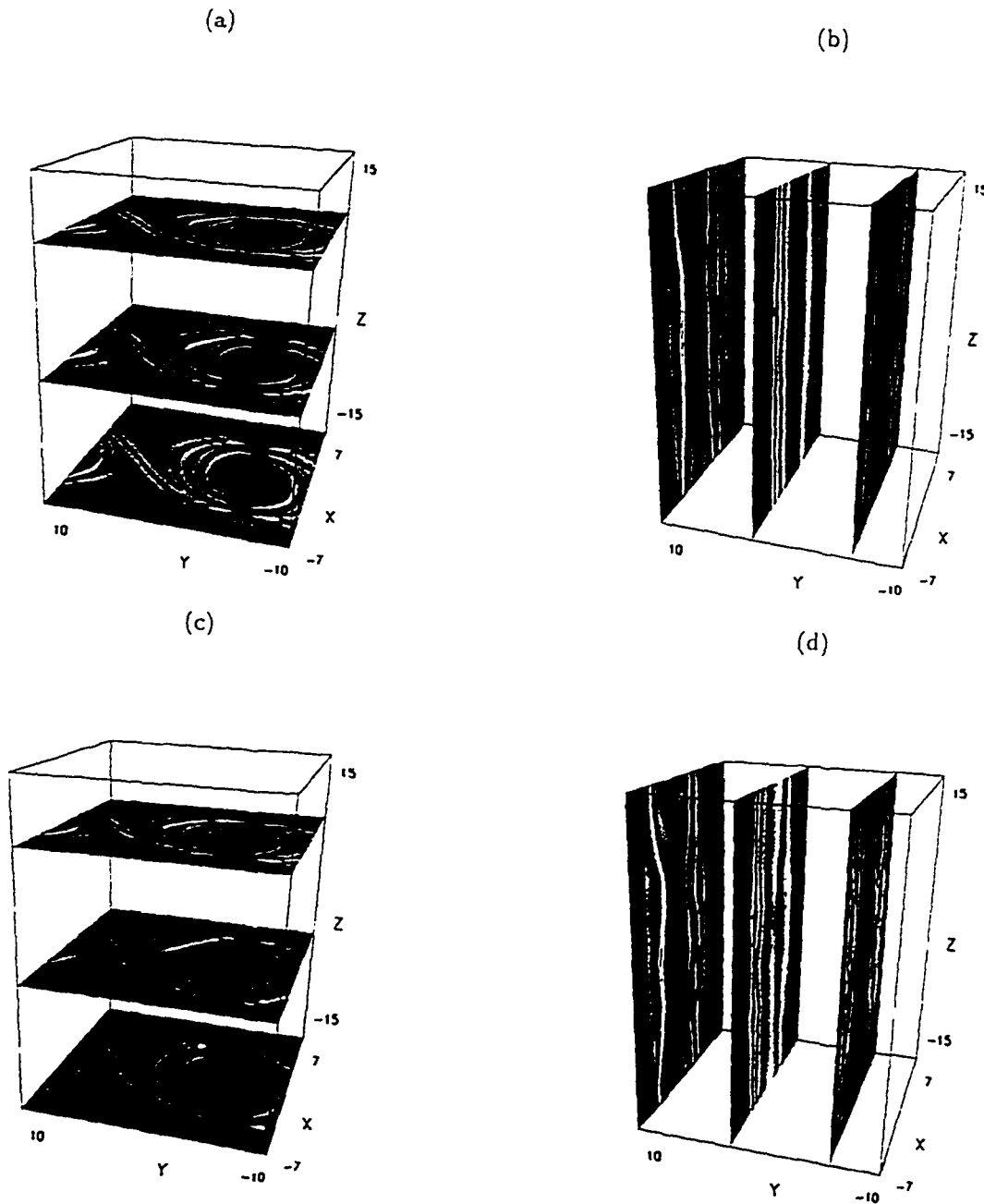


Figure 5.13 At $t=165$, three density distribution cuts along (a) the z direction, (b) y direction, and three pressure distribution cuts along (c) the z direction, (d) the y direction.

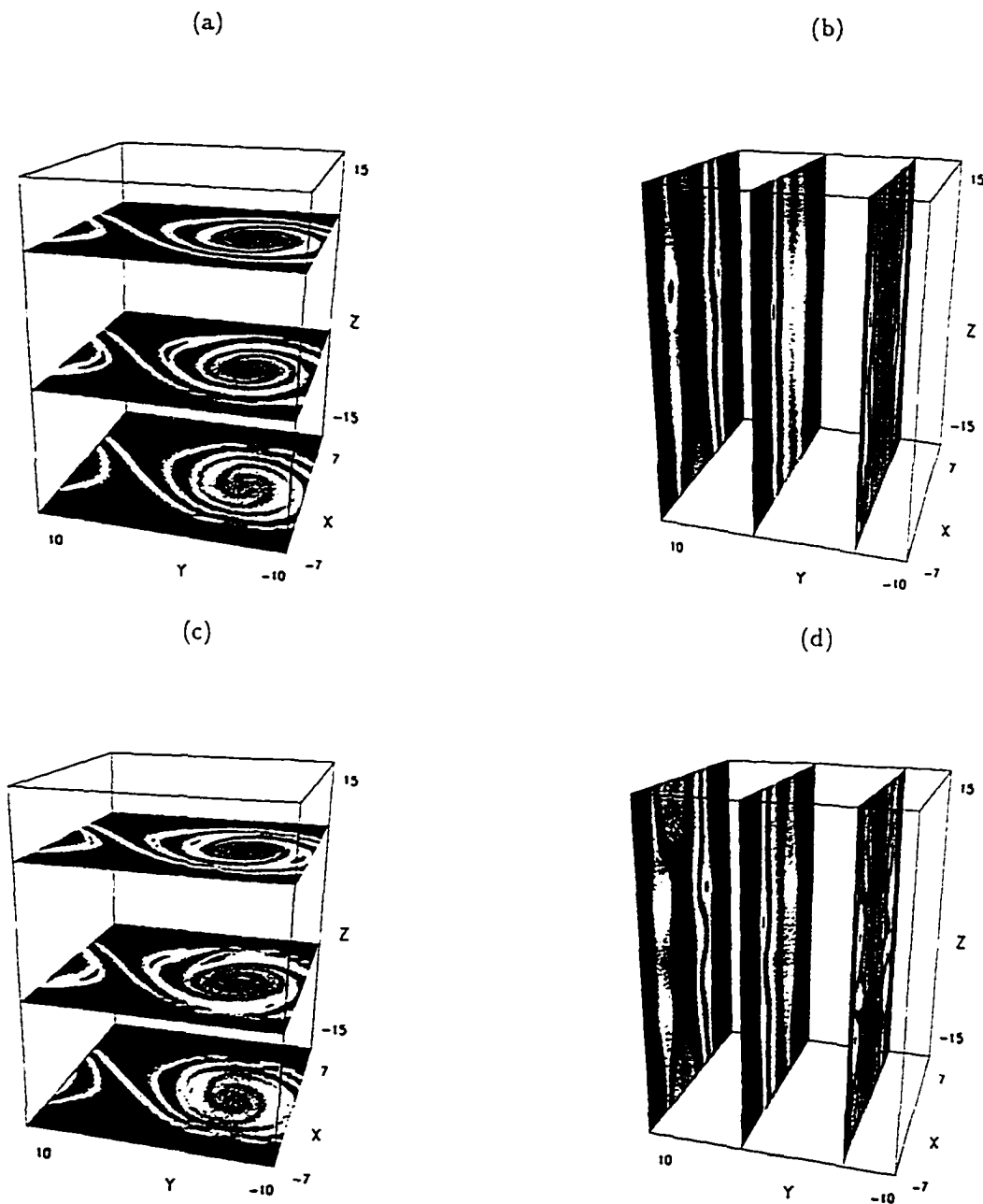


Figure 5.14 At $t=165$, three pressure distribution cuts along (a) the z direction, (b) y direction, and three pressure distribution cuts along (c) the z direction, (d) the y direction.

caused by the choice $\kappa = 0.1$. This field component partially stabilizes the KH mode and decreases the growth rate to a value about 0.027. Also, the initial tearing mode perturbation is $v_{z1} = 0.01$, and the initial KH mode perturbation is $v_{x1} = 0.001$. In this way, the tearing mode and the KH mode will grow simultaneously with their perpendicular wave vectors.

Figure 5.15 presents the evolution of normal velocity/magnetic field components and maximum current density. Because the growth rate and the initial perturbation magnitude of the tearing mode are larger than those of the KH mode, the growth is mainly determined by the tearing mode. After $t = 160$, there is a sharp increase of maximum current density. It indicates that magnetic reconnection develops very fast, and the process is highly nonlinear. There are topological and dynamic changes in the system.

For comparison, two two-dimensional simulation have been done, that is, one simulation of the evolution of the tearing mode in the xz plane and the other simulation to test the evolution of the KH mode in the xy plane. All of the parameters are set up in the same way as the three-dimensional simulation except that only one perturbation related to the particular mode is used. Thus, each single mode can be investigated with high resolution for the same initial conditions, however, limited to a two-dimensional frame. The tearing mode develops in the xz plane and affects the shear flow layer in the xy plane. In the other two-dimensional simulation, the KH mode developed in the xy plane has some influence on the current layer in the xz plane. This allows me to test the three-dimensional simulation and to determine the effects of the three-dimensional interaction.

Figure 5.16 presents the results of the two-dimensional simulation for the tear-

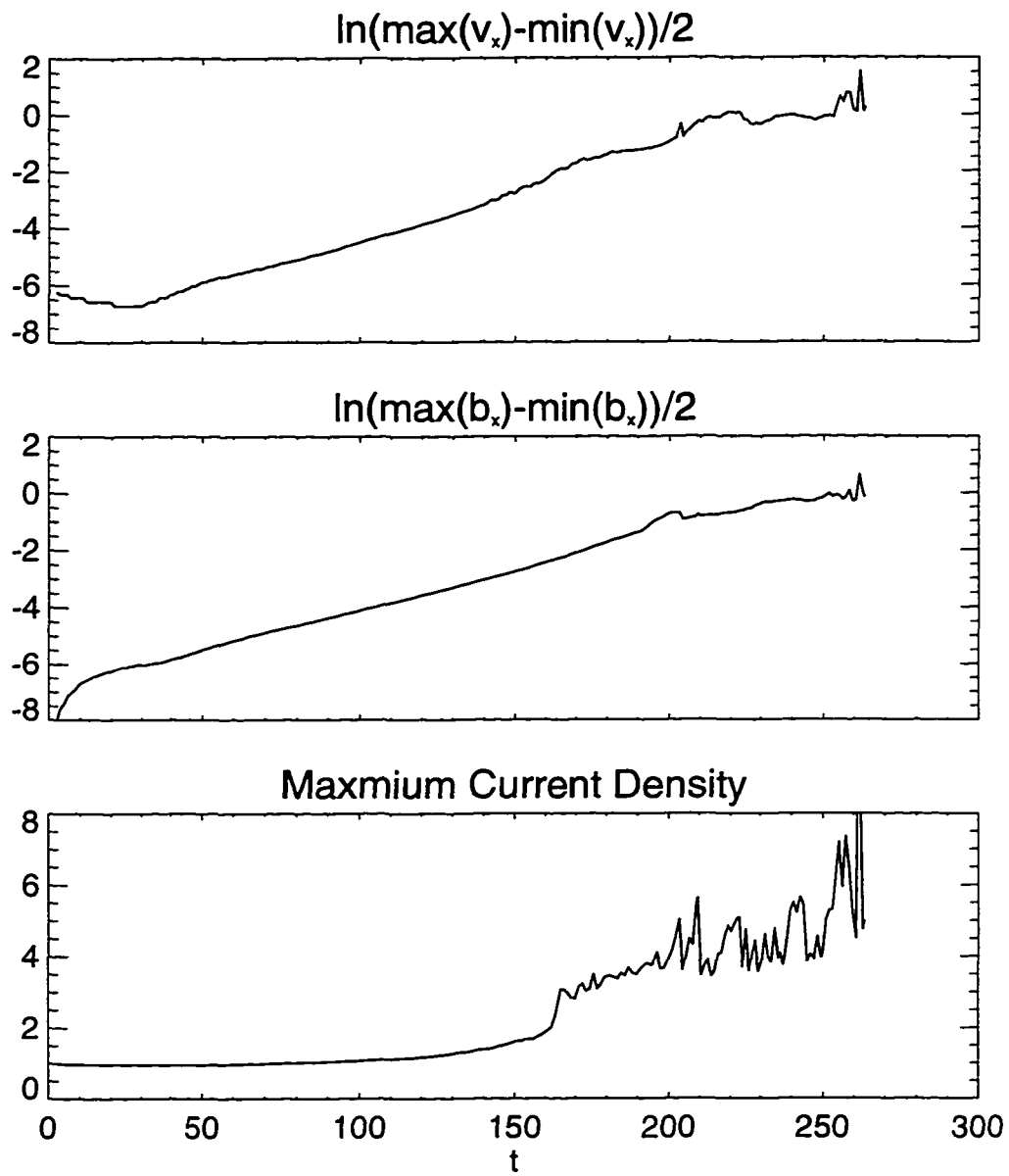


Figure 5.15 Time evolution of normal velocity, magnetic field components and maximum current density of case 2.

ing mode at $t = 210$. Magnetic field vectors, contour lines of magnetic field component b_y and velocity component v_y are presented in the xz plane, where the solid contour lines have positive values and the dashed lines have negative values. The wavelength of the tearing mode is $\lambda = 30$, and the size in the x direction is approximately 4. The contour lines of b_y and v_y also have the profile of the island in the current layer. The flow shear layer width is very thin near the reconnection region, and very wide near the neutral point.

Figure 5.17 shows the results of a two-dimensional simulation for the KH mode at $t = 210$. Flow field vectors, contour lines of magnetic field component b_z and resistivity are presented in the xz plane, where the solid contour lines resemble positive b_z and high resistivity and the dashed lines resemble negative b_z and low resistivity. The thin shear layer of the flow vortex (or mode) is about 7, and the size in the x direction is about 6. The contour lines of η and b_z also are twisted by the flow vortex. The magnetic shear layer width is very thin in the thin shear layer, and very wide in the blob. Also the current sheet oscillates along the original center line $x = 0$.

In the nonlinear stage, there is no accurate way to evaluate growth rates because the shear flow layer and the magnetic shear layer widths are varied in different locations. There is no single criteria to compare the growth rate of one mode with the other. An increase of b_y leads to a decline of the growth rate of the KH mode, but the thinner shear layer is helpful to speed up the the growth of the mode. When the shear layer becomes wider and b_y decreases, it also makes the relation complex. The similar thing will happen to the tearing mode. So the better way is to look at the shape and topology of the magnetic flux tube and the vortex tube.

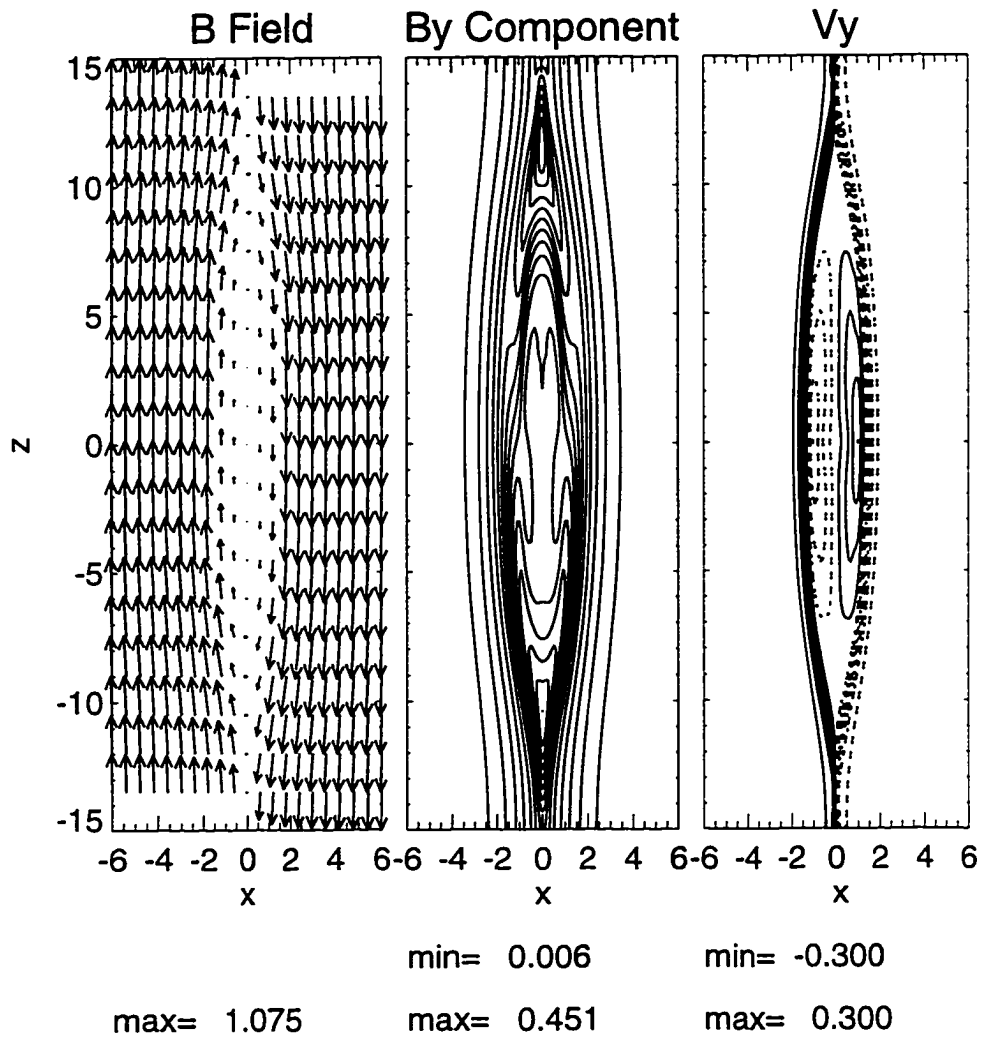


Figure 5.16 Magnetic field vectors, contour lines of magnetic field component b_y and velocity component v_y in the xz plane are shown at $t = 210$ in a two-dimensional simulation.

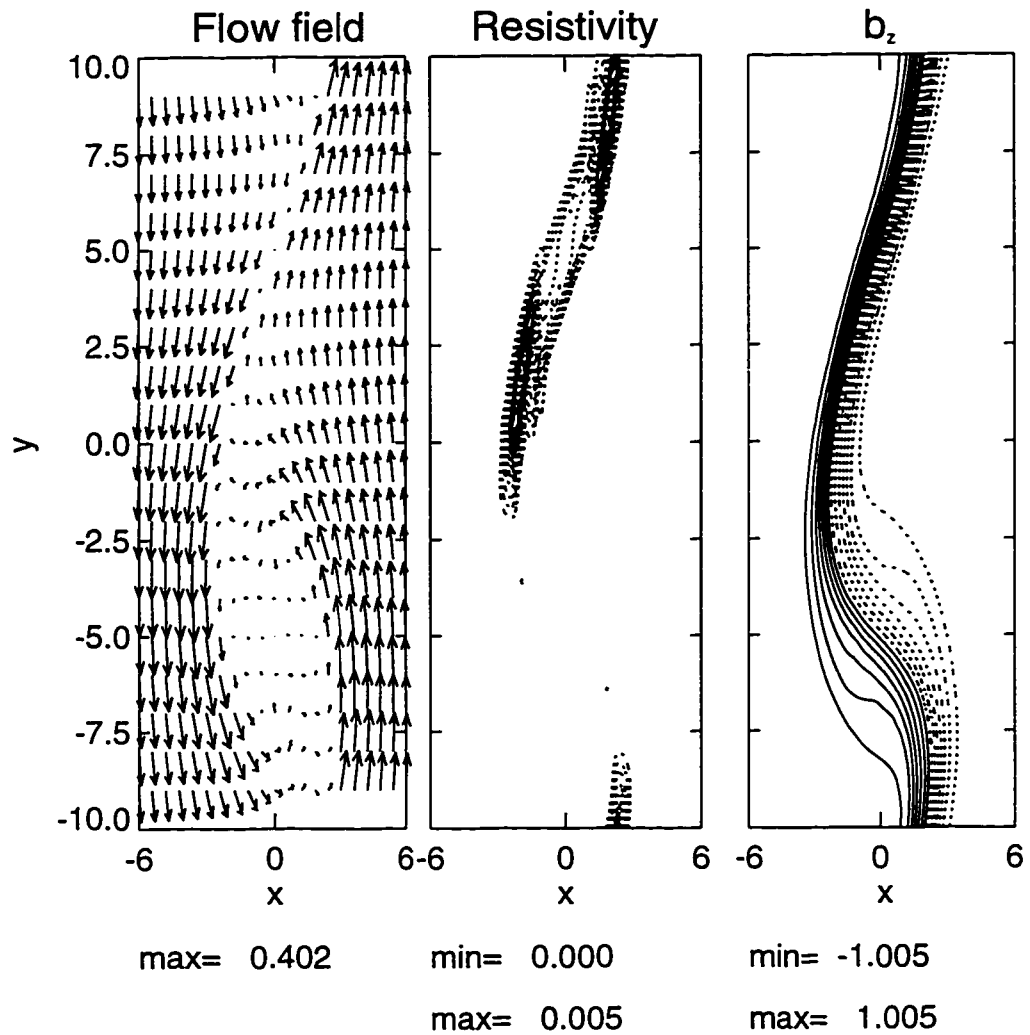


Figure 5.17 Velocity vectors, contour lines of resistivity and magnetic field b_z in the xy plane are shown at $t = 210$ in a two-dimensional simulation.

Figure 5.18 shows, at $t = 210$, three cuts of magnetic field vectors, three cuts of resistivity, and three cuts of v_y contour lines along the y direction in the three-dimensional simulation. The cut at $y = -8$ shows that the wavelength of an island is 26 and the size in the x direction is 3. The cut at $y = 1$ shows the wavelength of an island is 22 and the size in the x direction is 3.5. Those two islands shift away from $x = 0$. In Figure 5.18, three cuts are from the thin shear layer of the flow vortex in the xy plane. The width of magnetic shear layers becomes thinner. So the wavelength and the size decrease. The cut at $y = -4$ shows the wavelength of an island is larger than 30 and the size in the x direction is approximately 6. From Figure 5.18, the cut is from the blob of the flow vortex in the xy plane. The width of the magnetic shear layer becomes wide. So the wavelength and the size increase. It is seen that the tearing mode whose wave vector is along the z direction is affected by the KH mode whose wave vector is along the y direction. The sizes and wavelengths of islands cut along the thin shear layer of the flow vortex are smaller and shorter, and bigger and longer along the blob of flow vortex. At some regions, the magnetic islands shift away from the surface $x = 0$, which is the center of the current sheet in the two-dimensional simulation.

The influence of the KH mode on the tearing mode also can be seen from the time evolution of the magnetic island along some cuts. Figure 5.19 gives magnetic field vectors at $y = -8$ for $t = 150$, $t = 180$, and $t = 210$. The cut crosses the thin shear layer of the KH mode operated in the y direction. Because the vortex motion makes the current sheet at that location move away from the original place, it is obvious that the magnetic island growing with time gradually shifts away from the surface $x = 0$ when the KH instability operates. The sizes and wavelengths

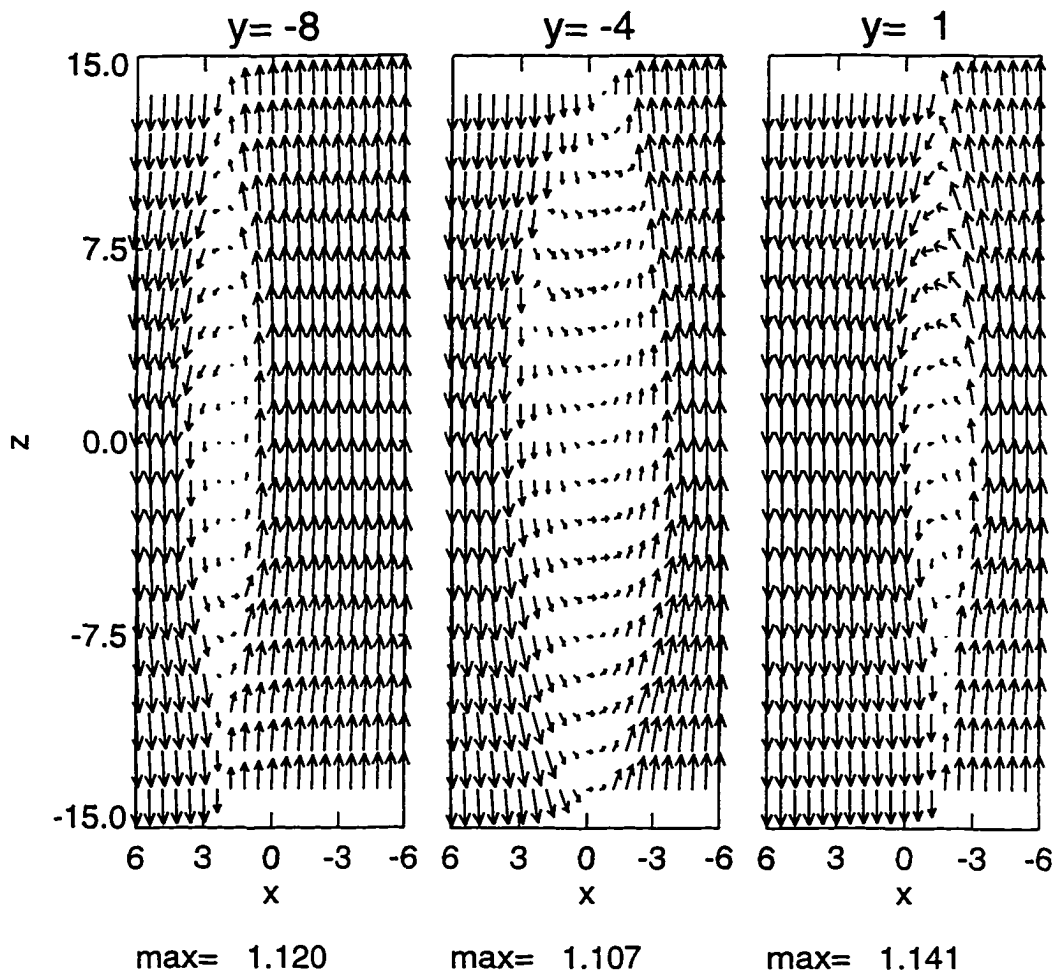


Figure 5.18 At $t = 210$, three cuts of magnetic field vectors along $y = -8$, $y = -4$, and $y = 1$ in the three-dimensional simulation.

of islands are still smaller and shorter than those at the corresponding times in the two-dimensional tearing-related simulation. The reason is that the length scale for the tearing mode is a thinner current sheet width than that used in 2-D simulations. Correspondingly, the wavelength of the fast-growing tearing mode will become shorter, and the size of the mode becomes smaller as well. For similar reasons, the sizes and wavelengths of islands cut in the blob regions are larger and longer than those at the corresponding times in the two-dimensional tearing-related simulation.

The KH mode is also affected by the tearing mode because the tearing instability changes the shear flow layer structure, which is most important for the KH instability. Figure 5.20 shows, at $t = 210$, three cuts of flow field vectors at $z = -13$, $z = -7$, and $z = 11$ in the three-dimensional simulation. The cut at $z = -13$ shows that the size of a vortex in the x direction is 4.5, and the thin shear layer is about 10. The cut at $z = 11$ shows the size of a vortex in the x direction is 5, and the thin shear layer is approximately 9. Those cuts are closer to the reconnection regions. The shear layers are thinner, and the length scale for the tearing mode is a thinner current sheet width. The wavelength of the fastest growing KH mode becomes smaller. The cut at $z = -7$ shows that the size of a vortex in the x direction is 8, and the thin shear layer is about 6. The cut is close to a neutral line of flux tube, so the thin shear layers are shorter but the widths are wider than that of two-dimensional KH-related simulation. The tearing mode affects the KH mode by modifying local shear layer width, wavelength and the size of the KH mode.

Based on the knowledge of the interaction of the tearing and KH instabilities,

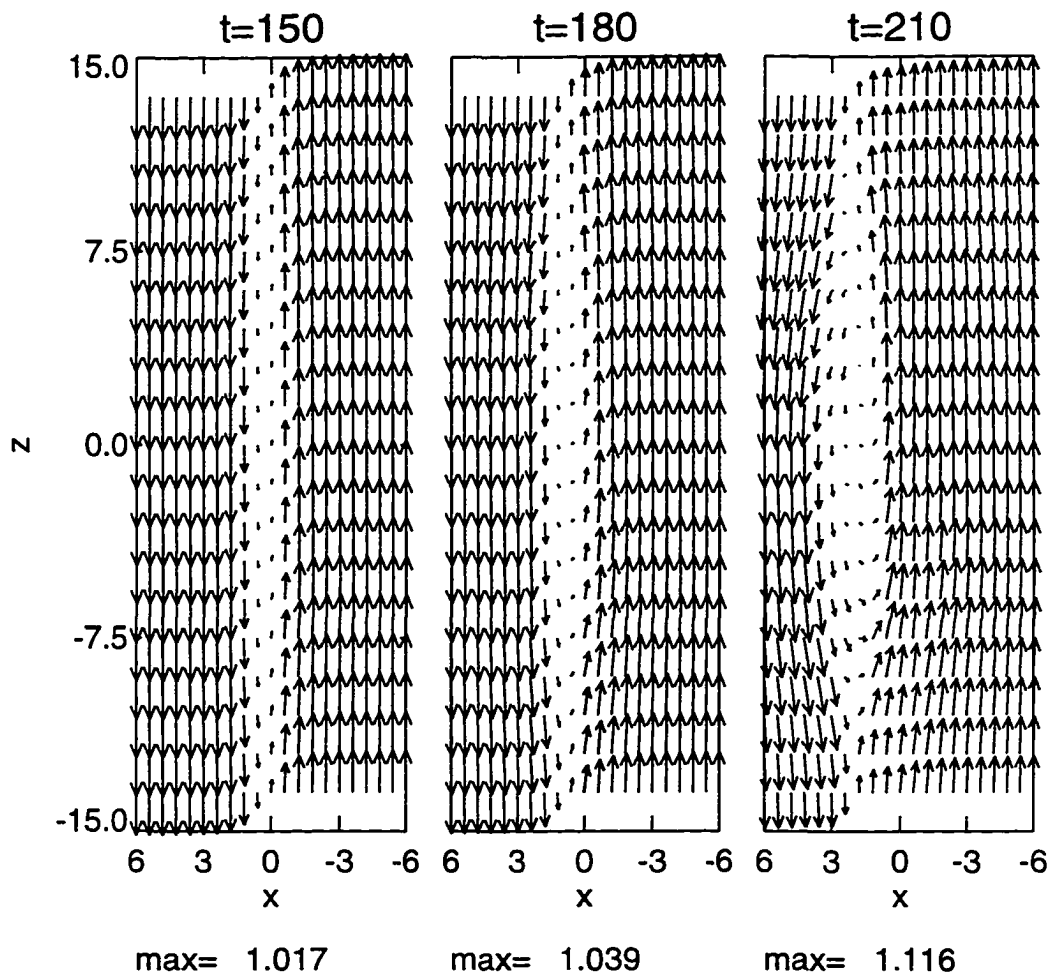


Figure 5.19 Magnetic field vectors comparison cut along $y = -4$ at $t = 150$, $t = 180$, and $t = 210$ in the three-dimensional simulation.

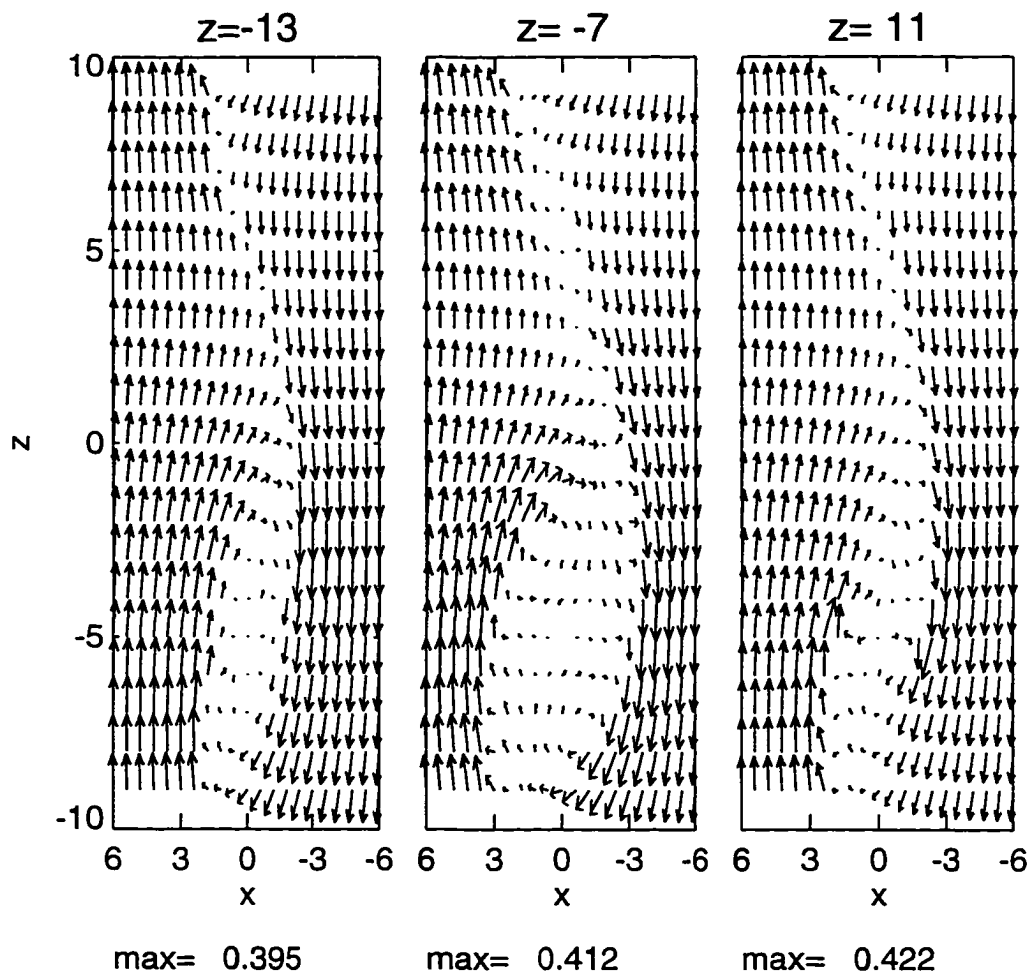


Figure 5.20 At $t = 210$, three cuts of flow field vectors along $z = -13$, $z = -7$, and $z = 11$ in the three-dimensional simulation.

it is worthwhile to get a full view of the magnetic flux tube. Figure 5.21 shows the topology of the magnetic flux tube at $t = 210$, which is presented with the isosurface of pressure $p = 3.7$. When b_y is small, the magnetic flux tube is a region with weak magnetic field and high thermal pressure. The isosurface of pressure can give a reasonable profile of the magnetic flux tube. The tube extends in the y direction. The body oscillates along the surface $x = 0$. Some parts of it are fat, and others are thin. From the top, it is seen that the tube follows the vortex motion.

Such a structure of the magnetic flux tube results from the nonlinear interaction of the KH mode and the tearing mode. The KH instability changes the profile of the current sheet. The current sheet follows the vortex motion and becomes twisted. Some regions become thinner to form smaller magnetic islands, and others become wider to form larger magnetic islands. Alternatively, the tearing mode instability modifies the flow shear layer. The shear layer width near the reconnection site becomes very thin, and the shear layer width near the neutral line becomes wider. This structure modifies the KH instability such that the region with thinner shear layer width develops smaller vortices, and the region with a wider shear layer width, develops larger vortices. The flux tube will become multiple length-scale structure. Those processes continue to reform the structure of the magnetic flux tube in a cycle of continuous interaction of the tearing and KH modes. The large structure will become larger and the small structure will become smaller. At last, the magnetic flux tube will break up.

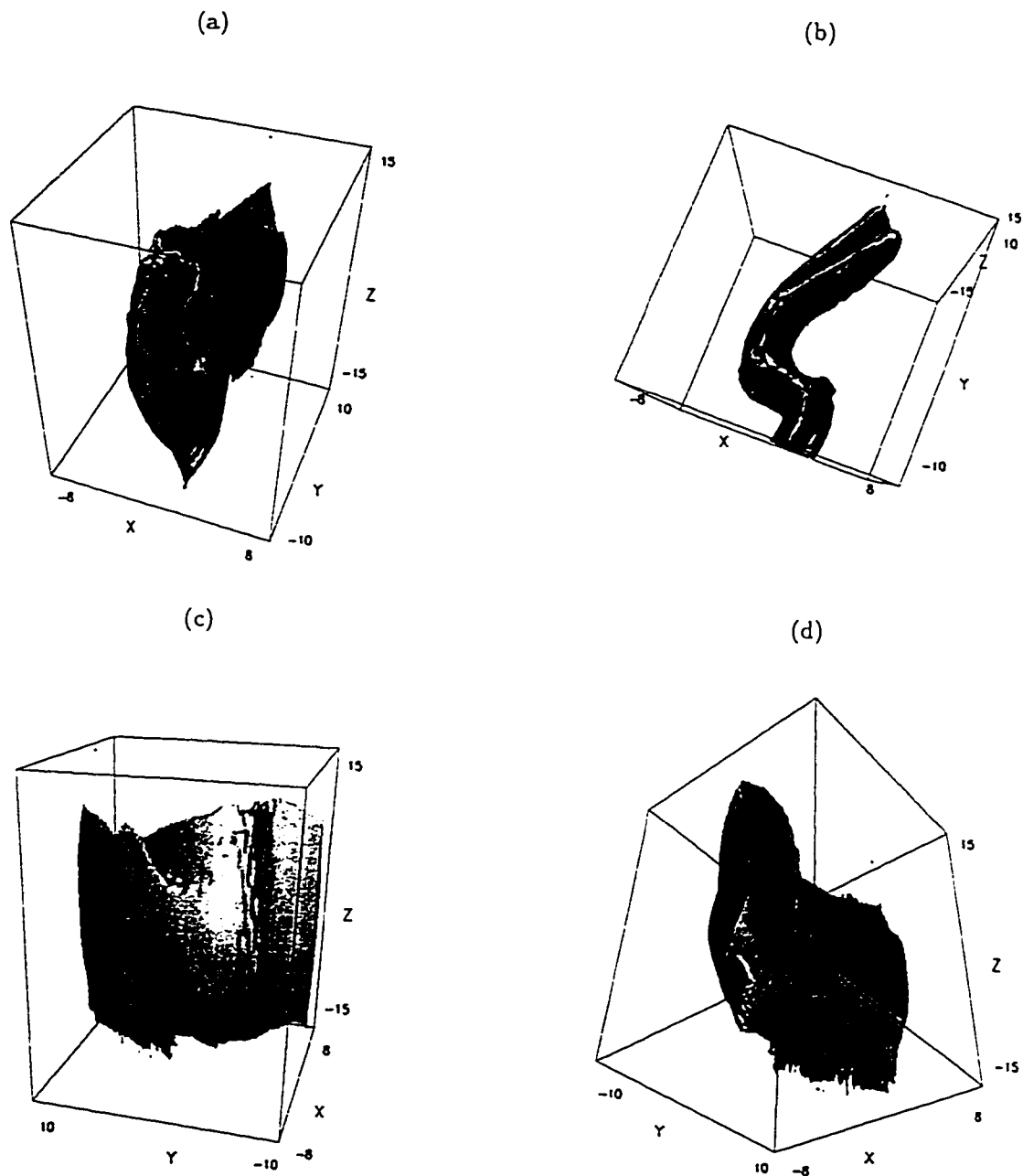


Figure 5.21 The topology of magnetic flux tube at $t = 210$ viewed from (a) the original place (b) top (c) left (d) the low bottom.

5.4 Discussion and Conclusion

Vortex-induced reconnection is realizable in a field configuration with a reversed magnetic field and a shear flow perpendicular to the magnetic field, where the wave vectors of the tearing KH modes follow the directions of the magnetic field and the flow field. This is totally different from the 2-D picture of vortex-induced reconnection (Hu and Liu, 1986, see Chapter 3), in which the flow shear is parallel to the magnetic shear. To make a difference, I call the new process 3-D KH-induced reconnection. If the KH instability operates first, nonlinear KH vortices lead to current sheet thinning and to the formation of multiple current layers. Thus the KH vortices can generate multiple current layer reconnection in a three-dimensional configuration. The mutual interaction of neighboring tearing islands leads to fast growth of the tearing mode. This process is turbulent reconnection. The topology of the magnetic field, the current density, and the flow field shows the combined features of the KH and tearing instabilities. This three-dimensional vortex-induced tearing instability is a highly efficient process of mixing magnetospheric and solar-wind-origin plasma.

In this sense, if the tearing mode instability is initially weaker than the KH instability, the KH instability can generate another tearing mode instability at a later time. The basic mechanism is the 3-D KH-induced reconnection. The 3-D KH-induced reconnection might be a very important process at the magnetopause when IMF orientation is southward. It is a very useful mechanism to relate the magnetic reconnection to the viscous transport at the magnetopause. The most possible location is tailward LLBL. The KH instability is easy to operate first

because of the high shear velocity and field configuration. For a southward IMF, the multiple current layers will be formed by the KH instability.

If the growth rates of the KH and tearing modes are comparable, the KH and tearing instabilities affect each other. The KH instability changes the profile of the current layer. The current sheet follows the vortex motion to become twisted. Some regions become thinner to form smaller magnetic islands; others become wider to form larger magnetic islands. The tearing mode instability modifies the shear flow layer. The shear layer width near the reconnection site is thin, and the shear layer width near the neutral line becomes wider. This reconfiguration modifies the KH instability. In the region with a thinner shear layer width, vortices are smaller, and in the region with a wider shear layer width, vortices are larger. Those processes continue to reform the structure of the magnetic flux tube and vortex tube in a cycle of mutual interaction of the tearing and KH modes. The nonlinear interaction can be one of the physical process that occurs at the magnetopause. The most possible location is the low latitude dayside magnetopause with a southward IMF, where magnetic flux tubes are easily formed and weak KH instabilities still have a chance to reform the structure of the magnetic flux tubes.

Chapter 6

The Kelvin-Helmholtz instability: Comparison with observation

6.1 Introduction

In the proceeding chapters, I have discussed the tearing instability, the KH instability, and the interaction of both modes in two dimensions and three dimensions. This chapter will compare the simulation results with observations at the magnetopause and the magnetotail boundary.

In the first part, I will use the 3-D simulation data from Chapter 5 to analyze the expected magnetopause structure. The second part will contribute to the case study of an observation event from the magnetotail boundary.

6.2 Structure of the Magnetopause

The study of macroscopic and microscopic plasma processes occurring at and in the magnetopause is an important task in magnetospheric physics because such processes determine the rate of transport of mass, momentum and energy from the solar wind into the magnetospheric cavity. The magnetopause is almost constantly moving because the magnetopause location is determined both by the solar wind dynamic pressure or momentum flux and also by the southward component of the IMF. Most of the phenomena at the subsolar magnetopause in the mesoscale range of 1000 to 10,000 km are associated with reconnection. Persistent high-speed flows have also been reported from the dusk flank of the magnetopause [*Gosling et al.*, 1986].

Based on three assumptions concerning the local magnetopause, that is, its orientation is constant, its structure is one-dimensional as well as time independent during traversal, the normal direction is that along which the variance of the corresponding measured field component is a minimum. Thus the method consists of finding the eigenvalues and eigenvectors of the variance matrix, and then selecting the normal vector as the eigenvector corresponding to the smallest eigenvalue [*Sonnerup and Cahill*, 1967].

So far few observations can be used to prove the interaction of the KH and tearing instabilities. Some of magnetopause structure observations may give evidence of the interaction of the two instabilities. *Sonnerup et al.* [1987] developed a method to handle spacecraft data using measured convection electric field variance analysis, where $\mathbf{E}_c = -\mathbf{v} \times \mathbf{B}$ was used. The method is similar to the minimum

variance analysis commonly performed on \mathbf{B} data, except that the direction of maximum variance of E_c , rather than minimum variance of \mathbf{B} is used to determine the normal. This method can be particularly reliable if plasma is moving at a high velocity tangential to the magnetopause as expected for a reconnection event.

If the structure of magnetopause is time-independent, there exists a deHoffmann-Teller (HT) frame in which the electric field vanishes. The electric field in the frame could then also be written as $\mathbf{E}_{HT} = -\mathbf{v}_{HT} \times \mathbf{B}$. If the magnetopause structure were one-dimensional and time independent, the deHoffmann-Teller velocity would remain the same as before.

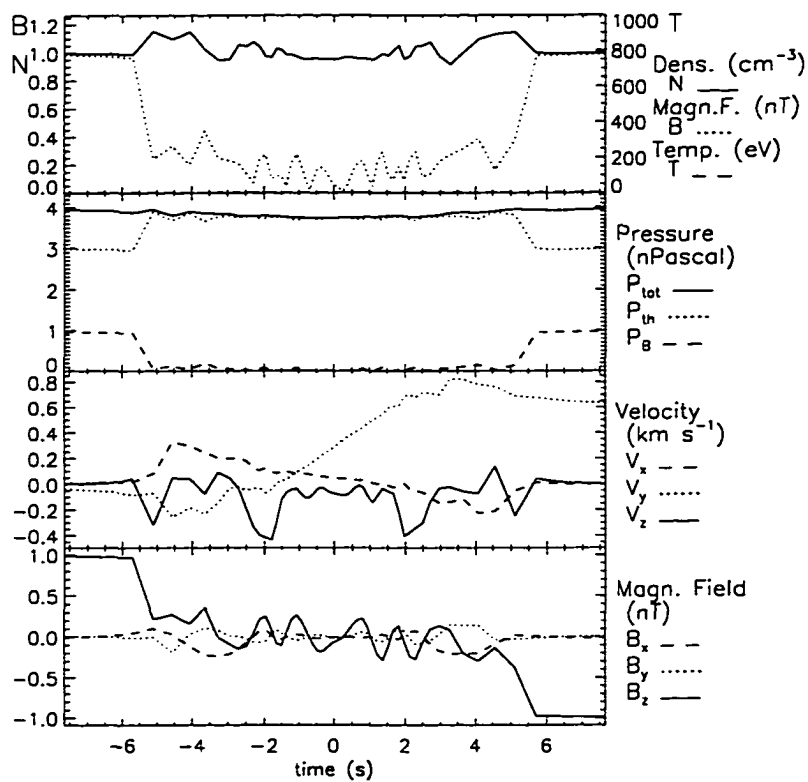
The application of the Walén relation to the normal components of flow and magnetic field at a boundary can determine whether it is a rotational discontinuity or not. Thus $\mathbf{v} - \mathbf{v}_{HT} = \pm \frac{\mathbf{B}}{\sqrt{\mu_0 \rho_0}}$ can be taken as an indication for a rotational discontinuity (RD). It is very useful in determining whether it is TD or RD. The test of the Walén relation will clearly be negative in the case of a tangential discontinuity. In other words the Walén relation provides a good test of stationary magnetic reconnection. Note, however, that this relation is also approximately satisfied for an intermedial or a slow shock. All of these discontinuities (RD, intermedial shock, slow shock) are indicative of a reconnection layer.

These techniques are very useful in evaluating the structure of the magnetopause. In this study, I try to confirm that the vortex induced reconnection based on three-dimensional configuration can account for some typically observed magnetopause structures. The simulation results are from case 1 in Chapter 5. I choose the period after the induced tearing instability had started to operate. The next section shows my results.

6.2.1 Simulation Comparison

To look at the structure of the magnetopause, the easy way is to investigate the magnetic field and plasma data properties across the magnetopause. Figure 6.1 shows a cut along $z = -8$, $y = -5.3$. This magnetopause is formed at $t = 180$ in case 1. Again the first panel shows the plasma density, and plasma beta (ratio of thermal and magnetic pressure), the second presents total, thermal, and magnetic pressure, the third shows the three plasma velocity components, and the fourth shows the three magnetic field components. The magnetic field components show that the B_z reversed several times and B_x, B_y also have some distributions. It seems that the magnetopause has multiple layer structure. The magnetosheath flow is about 0.6. If there is only the KH instability happened, there would be no or only very small B_x component observed. Because the tearing instability is induced after $t = 155$, the B_x component became larger. This crossing shows a typical interaction between the KH and tearing instabilities.

The other way is to look at the hodogram of magnetic field through the cut across the magnetopause. Figure 6.2 shows the hodogram representation of magnetic field during the analysis interval, and B_i, B_j, B_k are the field components along the maximum, intermediate, and minimum variance directions, respectively. B_i is approximately in the z direction, Usually, the minimum variance direction derived from the B field is denoted by k_B . In many cases this vector provides a good approximation to the magnetopause normal vector. For the present crossing this is not so. The figure shows the presence of large amplitude magnetic noise-like information in the magnetopause region, which looks like the magnetopause



Probe index: 15 Rotation angle for y,z comp.: 0

Initial probe location and vel. (simulation frame., normalized):

$$x = -7.7 \quad y = -5.3 \quad z = -8.0$$

$$V_x = -0.013 \quad V_y = 0.298 \quad V_z = 0.019$$

Initial probe location and vel. (MSP frame, in km and km/s):

$$x = -4592 \quad y = -3200 \quad z = -4800$$

$$V_x = 0 \quad V_y = 0 \quad V_z = 0$$

DATA is plotted in the probe rest frame in rotated (MSP) coord.

Figure 6.1 Plasma and magnetic field simulation data presentation through a cut $z = -8$, $y = -5.3$ at $t = 180$.

crossing by the AMPTE/IRM spacecraft on September 4, 1984, investigated by *Sonnerup et al.* [1987].

Prior to this work, two dominant interpretations for this structure were made. One of these was that the observed fluctuation were caused by a back and forth motion of the current layer over the satellite. However, this alone is insufficient to explain the observation. If the magnetic structure of a one-dimensional current layer does not change, a back and forth motion would always give the same and simple trajectory of the magnetic field in hodogram. Thus this model can not explain the observed chaotic trajectories of the magnetic field.

The other possible explanation is magnetic percolation [*Galeev et al.*, 1986]. magnetic percolation is the occurrence of very small scale tearing modes in multiple layers in a single current sheet. Although this may generate reconnected flux through a stochastic meandering of magnetic field lines in the magnetopause current sheet, this can not explain the observed field fluctuations for a very simple reason. The tearing mode in this configuration saturates at an extreme small amplitude such that all local perturbation are necessarily very small. However the observed magnetic perturbations are of large amplitude. Thus the process of multiple current layer formation and random reconnection discussed in Chapter 5 is the first consistent explanation for the observed magnetopause structure. The multiple current layer structure is formed because of the nonlinear KH vortex thinning process. The width of those current layers is relatively thin. The probe passed through those current layers. At the same time, the tearing instability is going on. So the hodogram gives such kind of interesting information. From this simulation, I can conclude that many high resolution observations showing large

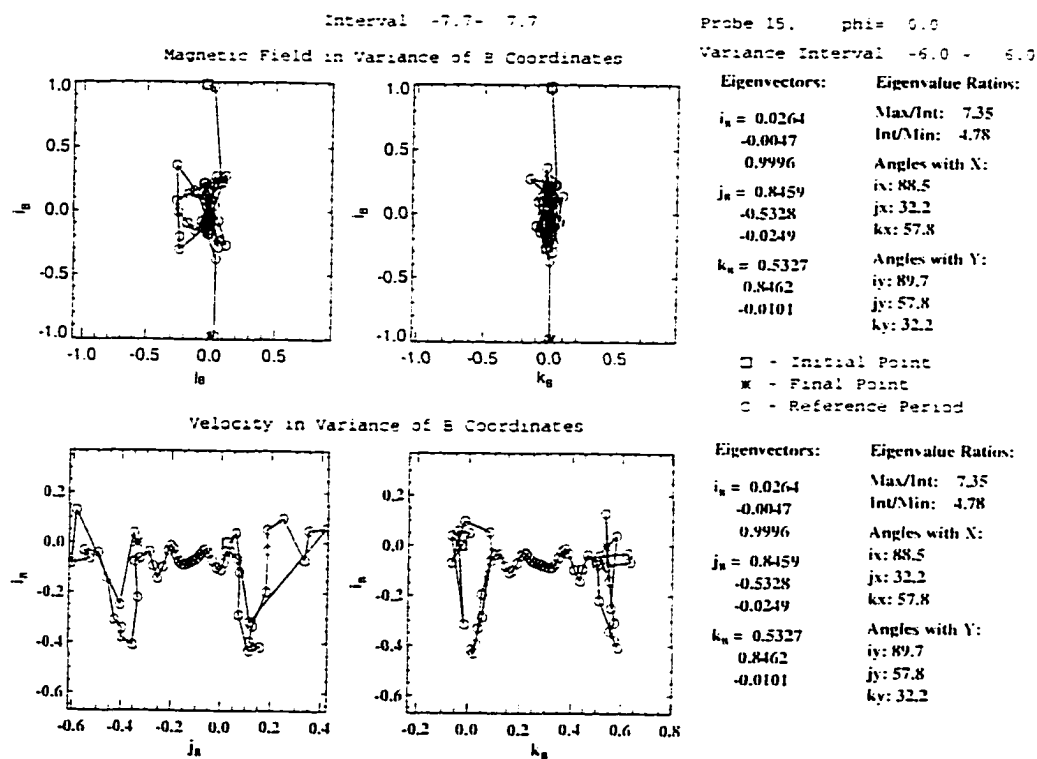


Figure 6.2 Magnetic field hodogram.

amplitude magnetic noise may indicate thin structures of the magnetopause. The thinning process of the KH instability might be one of the sources.

Figure 6.3a shows the test of Walén relation to determine which type of boundary the magnetopause belongs to. A linear proportionality should exist between the three components of the plasma velocity in the deHoffmann Teller frame and the corresponding components of the Alfvén velocity. The solid line shown represents the least squares fit to the data using orthogonal distances and the constraint that the line passes through the origin. It has a slope almost zero and the correlation coefficient is also almost zero. That implies that the large scale structure of this current layer is that of a tangential discontinuity, not a rotational discontinuity.

If the magnetopause is a time independent or Alfvénic structure, the correlation coefficient of convection electric field with deHoffmann-Teller electric field should be 1. Figure 6.3b shows the correlation of the convection electric field with the deHoffmann-Teller field $\mathbf{E}_{HT} = -\mathbf{v}_{HT} \times \mathbf{B}$. Again, the solid line shown represents the least squares fit to the data using orthogonal distances and the constraint that the line passes through the origin. It has a slope 0.4, which is much smaller than 1 (If the slope is 1, it means the structure is time-independent). In this condition, the magnetopause is changing with time.

In summary, the observed magnetic field turbulence of the magnetopause is explained as the coupling of the KH and tearing instabilities. The KH instability makes very thin multiple current layer. The tearing mode instability occurs when those layers become sufficient thin. Satellites crossing those structures would observe this regular change in all physical parameters. It is different from an oscillation of the magnetopause or a percolation tearing instability. The large scale

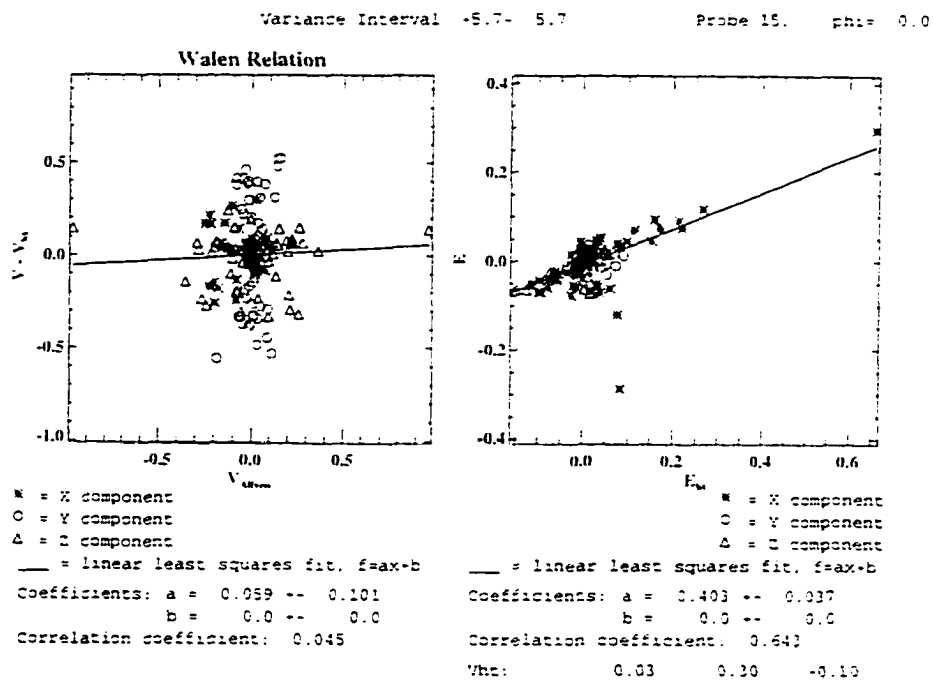


Figure 6.3 Walen relation presentation.

magnetopause appears as a tangential discontinuity. These properties are similar to actual magnetopause observations.

6.3 The Kelvin-Helmholtz Instability at the Magnetotail Boundary

It is well accepted that the low-latitude boundary is a location of entry of mass, momentum, and energy from the magnetosheath to the magnetosphere. *Mitchel et al.* [1987] and *Traver et al.* [1991] reported that the topology of the field lines in the low-latitude boundary layer (LLBL) is controlled by the IMF B_z component, closed (open) when northward (southward). Observations in LLBL showing the mixture of magnetospheric and magnetosheath ions on closed field lines have been known for some time [e.g., *Sckopke et al.*, 1981]. However, the mechanism of this mixing is still under debate.

The KH instability has long been thought of as an important process at this magnetotail boundary. The solar wind impinging upon the magnetosphere creates a velocity shear across the magnetopause current sheet. The configuration of the magnetic field and flow field in LLBL makes the KH instability easy to operate. Early observations found that tailward propagating surface waves have wavelengths from half an R_E to 10 R_E at the terrestrial magnetopause [*Aubry et al.*, 1971; *Fairfield*, 1979; *Lepping and Burlaga*, 1979; *Song et al.*, 1988]. A particular form of a surface wave that often develops in the magnetotail boundary is the KH wave. So far there have been a number of observations related to the KH wave. However,

an unambiguous identification of KH wave is often difficult.

The most fully analyzed event is the one that occurred on the outbound orbit of the ISEE 1 and 2 spacecraft, located at $(12.5 R_E, 40^\circ, 0800\text{LT})$, on November 6, 1977 near 0530 UT. The characteristics of the waves and the relation to the structure of the boundary layers were first described by *Sckopke et al.* [1981]. Irregular intervals of wave-like fluctuations around that time identify wave cycles in which the spacecraft moved between different plasma regimes. The interpretations on the physical mechanism for the quasi-periodic variations and on the origin of the plasma in these regions include: temporally modulated bursts of strong diffusion across the magnetopause [*Sckopke et al.*, 1981], FTEs on open field lines [*Paschmann et al.*, 1982; *Saunders*, 1983], and pressure pulses [*Sibeck et al.*, 1990]. The interpretation that the unstable boundary is the magnetopause itself might be closer to the reality, but the variability of the IMF makes the mechanism for this event still unclear.

Another event occurred from 400 to 1800 UT on February 15, 1978 during northward IMF [*Chen et al.*, 1993] at a time when ISEE 1 and 2 were near apogee on the dawn flank of the magnetotail. *Chen et al.* [1993] found 5 minute non-sinusoidal periodic waves of plasma and field with steep leading edges, which is different from the waves with steep trailing edges in the two-dimensional MHD simulations [e.g. *Miura*, 1990].

Recently, *Fairfield et al.* [1996] found that, from the Figure 6.4 and 6.5 which shows the plasma and magnetic field data respectively, for several hours on March 24, 1995 the Geotail spacecraft remained near the duskside magnetotail boundary some $15 R_e$ behind the Earth while the solar wind remained very quiet ($V=330\text{km/s}$).

$n=14$ to $21/\text{cc}$) with a very northward 11 nT IMF. Geotail experienced multiple crossings of a boundary between a dense ($n=19/\text{cc}$), cool ($T_p=40\text{eV}$), and rapidly flowing ($V=310\text{km/s}$) magnetosheath plasma and an interior region characterized by slower tailward velocities ($V=100 \text{ km/s}$), lower but substantial densities ($n=3/\text{cc}$) and somewhat hotter ions (220eV). The crossings recurred with a roughly 2 minute periodicity and all quantities were highly variable in the boundary region. The magnetic field exhibited some of the largest fluctuations seen anywhere in space, despite the fact that the exterior magnetosheath field and the interior magnetosphere field were both very northward and nearly parallel. They speculated that the multiple crossing are due to a KH instability at the boundary generating vortices that convect past the spacecraft.

In this study, I focus on the last mentioned event, and attempt to model it using observed plasma parameters for the magnetosphere and the magnetosheath. It seems that tailward magnetosheath flows have little influence on the northward magnetic field. But the flow direction and the wave vector of the KH mode are two different things. If the KH mode has a k vector not exactly aligned with tailward direction, the projections of IMF and geomagnetic field onto the k vector are nonzero. When the KH instability operates, the magnetic field configuration is also changed significantly. It will be shown that this can account for a strong magnetic oscillation.

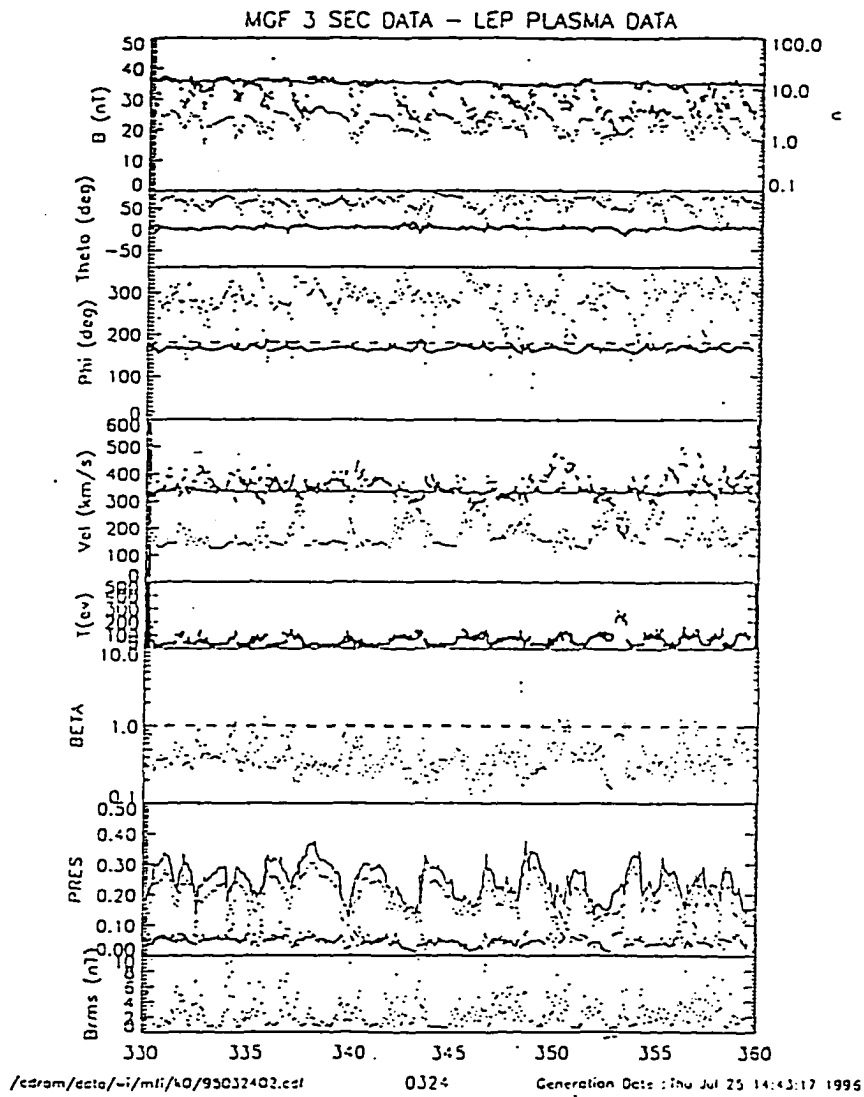


Figure 6.4 Observational plasma data near the duskside magnetotail boundary on March 24, 1995 (from Fairfield).

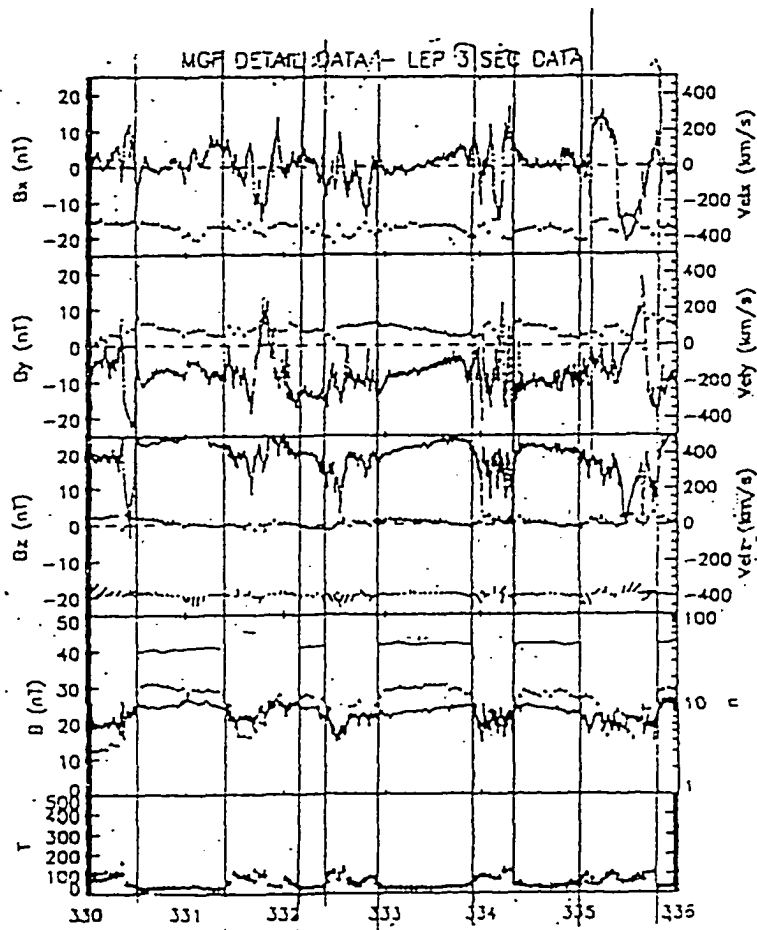


Figure 6.5 Observational magnetic field data near the duskside magnetotail boundary on March 21, 1995 (from Fairfield).

6.3.1 Simulation Model

The basic configuration for this study consist of a strongly northward magnetic field on both sides of the boundary layer and a fast tailward flow on the magnetosheath side. While a magnetic field perpendicular to the velocity shear ΔV favors the KH instability, it would be difficult to explain the reversal of b_z if the magnetic field were purely perpendicular to the plane in which the KH instability operates.

In particular, these large magnetic fluctuations with intermittent periods of southward b_z (although the IMF is strongly northward and the plasma sheet magnetic field is northward) shed initially some doubt on the interpretation in terms of KH waves.

A magnetic field reversal can result from KH waves if a small magnetic field tangential to the wave vector k of the KH instability exists. I, therefore, assume in this study the general case that the wave vector has a small component out of the equatorial plane. This turns out to be central for the interpretation of the observed signatures in terms of the MHD simulation. Thus this configuration combines aspects from chapters 3 and 4. A small magnetic field component in the plane of the KH instability does not alter the growth rate significantly. However, this field component will get twisted and thus aspects of two-dimensional vortex induced reconnection can be important.

Figure 6.6 shows the coordinate system used in the simulation. The dark region (or the simulation region) crosses the duskside tailward magnetopause, and is in the equatorial plane of the Earth. The z direction is northward, and the y direction is along the magnetopause normal. The x direction closes a right hand system.

This is the GSM coordinate system. The k vector of the considered instability is at some angle ϕ with the tailward direction (the x direction), so the projections of IMF and geomagnetic field onto the k vector are nonzero. The simulation plane is in the plane formed by the k vector and the y axis.

For this investigation, two-dimensional MHD equations are used. The simulation domain is a rectangular box with $|x| \leq L_x$ and $|y| \leq L_y$. Free boundary conditions are applied to the two boundaries in the y direction. Periodic boundary conditions are used at the two boundaries along the x' direction.

The plasma is initially uniform in total pressure (including dynamical and magnetic pressure). The equilibrium is determined by

$$B_{x0}(y) = 0 \quad (6.1)$$

$$B_{y0}(y) = 0 \quad (6.2)$$

$$B_{z0}(y) = B_{zi} - B_{\Delta} \tanh y \quad (6.3)$$

$$v_{x0}(y) = -V_0 \tanh y \quad (6.4)$$

$$v_{y0}(y) = 0 \quad (6.5)$$

$$v_{z0}(y) = 0 \quad (6.6)$$

$$p_0(y) = \beta_0 + B_{\Delta}^2 \cosh^{-2} y + 2B_{zi}B_{\Delta} \tanh y \quad (6.7)$$

$$\rho_0(y) = 1 + 0.75 \tanh y \quad (6.8)$$

where $B_{\Delta} = 1/2|1 - B_{sh}|$, $B_{zi} = 1/4(1 - B_{sh}^2)/B_{\Delta}$, and β_0 is the ratio of dynamical to magnetic pressure at the boundaries $|x| = L_x$. For all cases, β_0 is chosen to be 2.8 which is consistent with typical values in the magnetosheath and in the dayside low-latitude boundary layer [Phan and Paschmann, 1996]. The normalization for

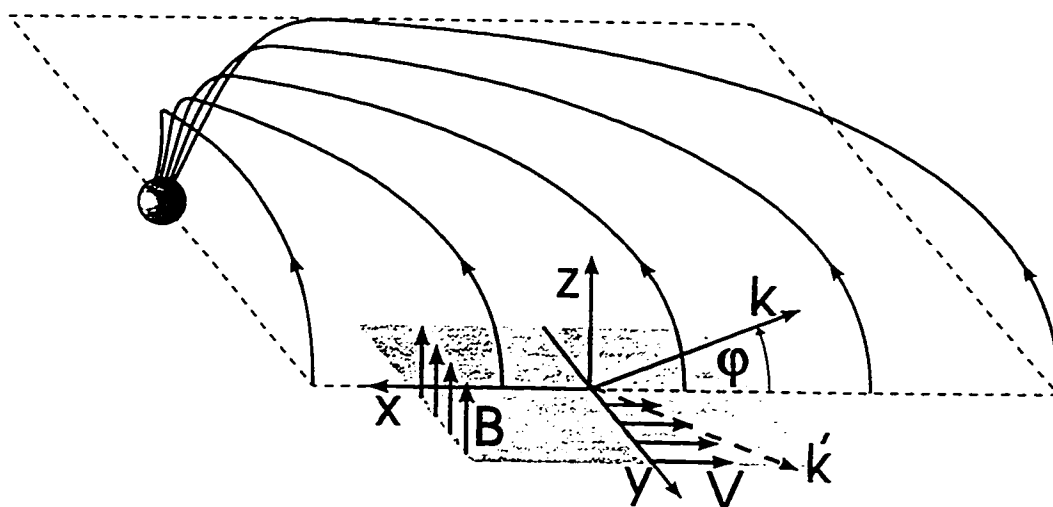


Figure 6.6 The simulation coordinate system.

density is 11cm^{-3} , magnetic field is 16nT , velocity is 105.17 km/s , pressure is 0.1019 nPa , length is 600km , and time is 5.7s .

In the observation, magnetosheath velocity is between 250 and 380 km/s . The angle ϕ (the angle for k vector with the tailward flow) varied between 10 and 25 degrees. In my simulation, I set $V_0 = -310\text{km/s}$, $\phi = 25^\circ$, $B_z = 16\text{nT}$ at the magnetosphere side and $B_z = 24\text{nT}$ at the magnetosheath side. It is unusual that the magnetic field on the magnetosheath side is larger. It is consistent with the observation. The initial velocity perturbation is about 10km/s .

6.3.2 Results and Comparison

The KH instability can develop if the fluid velocity is tangential to a thin layer and changes in magnitude across this layer. In an ordinary fluid the instability has no stability threshold, which means an arbitrarily small change in the flow velocity is sufficient to generate the instability. This is different in a magnetized plasma. Here this instability has to deform the magnetic field which requires a certain amount of energy. Therefore, the instability requires a sufficiently large difference in the flow velocities.

Particularly interesting are the plasma and magnetic field signatures, which a satellite is expected to record if this instability operates at the boundary of the magnetosphere. In the following I will illustrate the evolution of the KH instability as a result of two-dimensional plasma (magnetohydrodynamic) simulations, and then record data along particular trajectories similar to how a satellite would record such data in space.

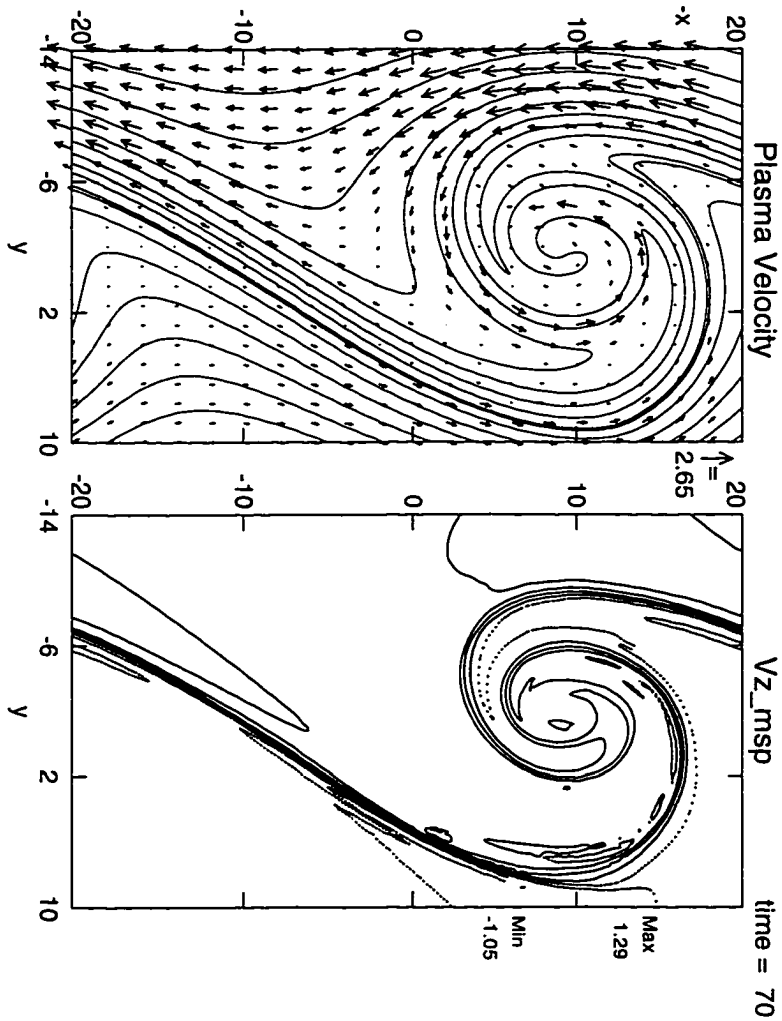


Figure 6.7 The contour lines of plasma velocity v_z in the MSP coordinate system and velocity vectors and streamlines in the simulation plane at $t = 70$.

In the simulation plane, when the shear flow is larger than the Alfvén speed and smaller than the fast mode speed, the KH instability operates. The simulation magnetic field and plasma satisfies the condition. Figure 6.7 shows the contour lines of the plasma velocity v_z component in the MSP coordinate system and velocity vectors and streamlines in the simulation plane at $t = 70$. It is shown that the KH vortex develops with a wavelength of 2 to 2.5 R_E . In the deHoffmann Teller frame, it is measured that the vortex is moving at $v_x = -220\text{km/s}$. The KH vortex develops because the shear flow overcomes the magnetic tension (shear velocity is larger than the local Alfvén speed) and the perturbed KH mode grows with time. The growth time is about 5 minute.

The magnetic field line in the simulation plane will become twisted by the KH vortices, and also the northward magnetic field will be modified. Figure 6.8 shows the magnetic field lines and magnetic field vectors in the simulation plane, and the B_z contour lines in the MSP coordinate system at three different times. Note that the field is well ordered initially (in fact has only one orientation) and becomes twisted by the vortex motion from the KH instability. To twist and deform the magnetic field requires energy. It is shown that the magnetic field lines in the xy plane become twisted by the KH vortex at $t = 45$. B_x is along the positive x direction. At $t = 70$, the nonlinear vortex becomes so strong that there are some regions where B_x becomes negative. It is shown that some field line twisted back. In the MSP system, those negative B_x components contribute to reduce the positive B_z component (Figure 6.9a). If the negative B_x components are very large, B_z may even become negative. In some local regions, at $t = 86$, magnetic reconnection starts to operate.

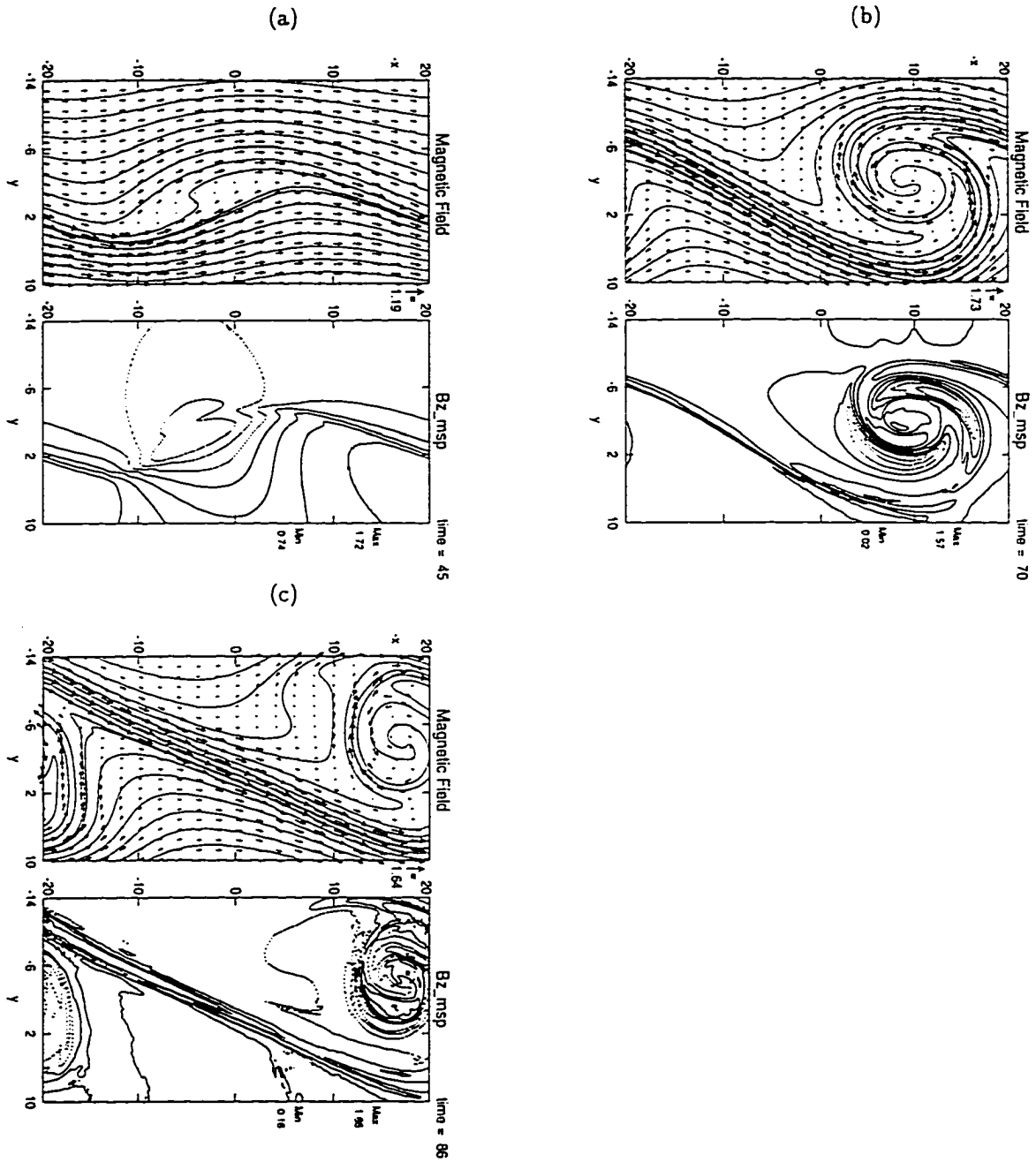


Figure 6.8 B_{z-msp} contour lines, Magnetic field lines, and velocity vectors in the simulation plane at (a) $t = 45$, (b) $t = 70$, and (c) $t = 86$.

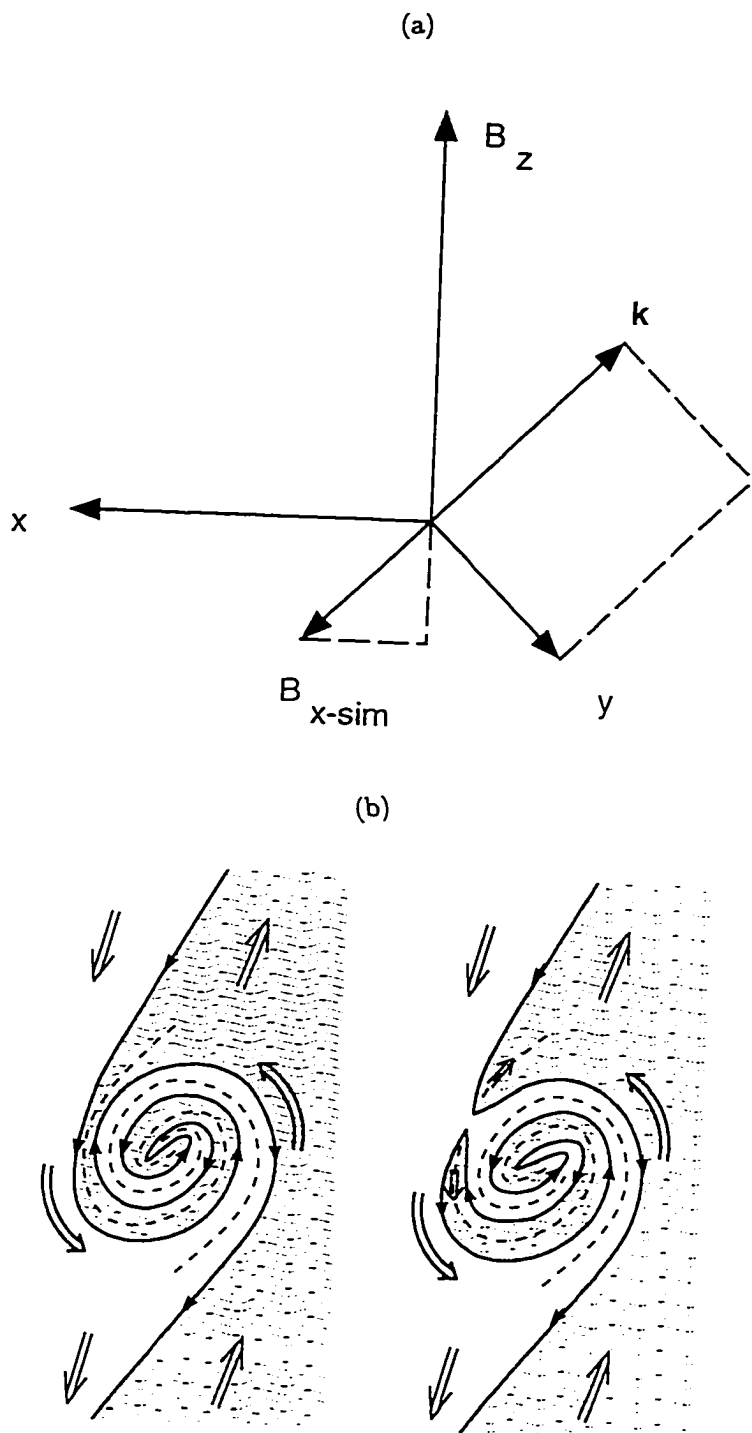


Figure 6.9 (a) B_{x-sim} , which is generated by the vortex motion, deducts the northward IMF B_z . (b) The mechanism of component reconnection and magnetic flux transfer process.

The mechanism of the component reconnection can be easily illustrated in Figure 6.9b. In the simulation plane, the magnetic field is twisted by the nonlinear KH vortex. The vortex motion renders one part of a magnetic field line antiparallel to another, and the associated current sheet becomes stronger as time proceeds. At a critical time, reconnection begins to operate and a twisted loop is formed. If this process occurs in the magnetopause, the loop will be left in the magnetosphere. It presents a very important magnetic flux transport process which is able to capture magnetosheath plasma blobs and transport them into the magnetosphere.

Figure 6.10 shows the contour lines of plasma density and temperature at three different times. Again, the left-hand side in the images represents the magnetosphere, and the right-hand side represents the region with solar wind plasma. It can be seen that vortex shape contour lines are also formed by the KH instability.

The solar wind plasma is denser and cooler than the magnetospheric plasma, and similarly the plasma blob which start to form at $t = 70$ in the eye of the vortex has higher density and lower temperature than the magnetospheric plasma. At the boundary of this blob both the magnetic field and the plasma velocity change rapidly which should be visible as large fluctuations to the satellite traversing this region. This process leads to a very efficient mixing of magnetospheric and magnetosheath plasma, generating a plasma with intermediate properties and strong fluctuations. Interesting are the very thin sheets with varying density, pressure, and magnetic field orientation (which implies strong currents in these layers) which are visible, particularly at $t = 86$.

The KH instability operating in the simulation plane will change the magnetic

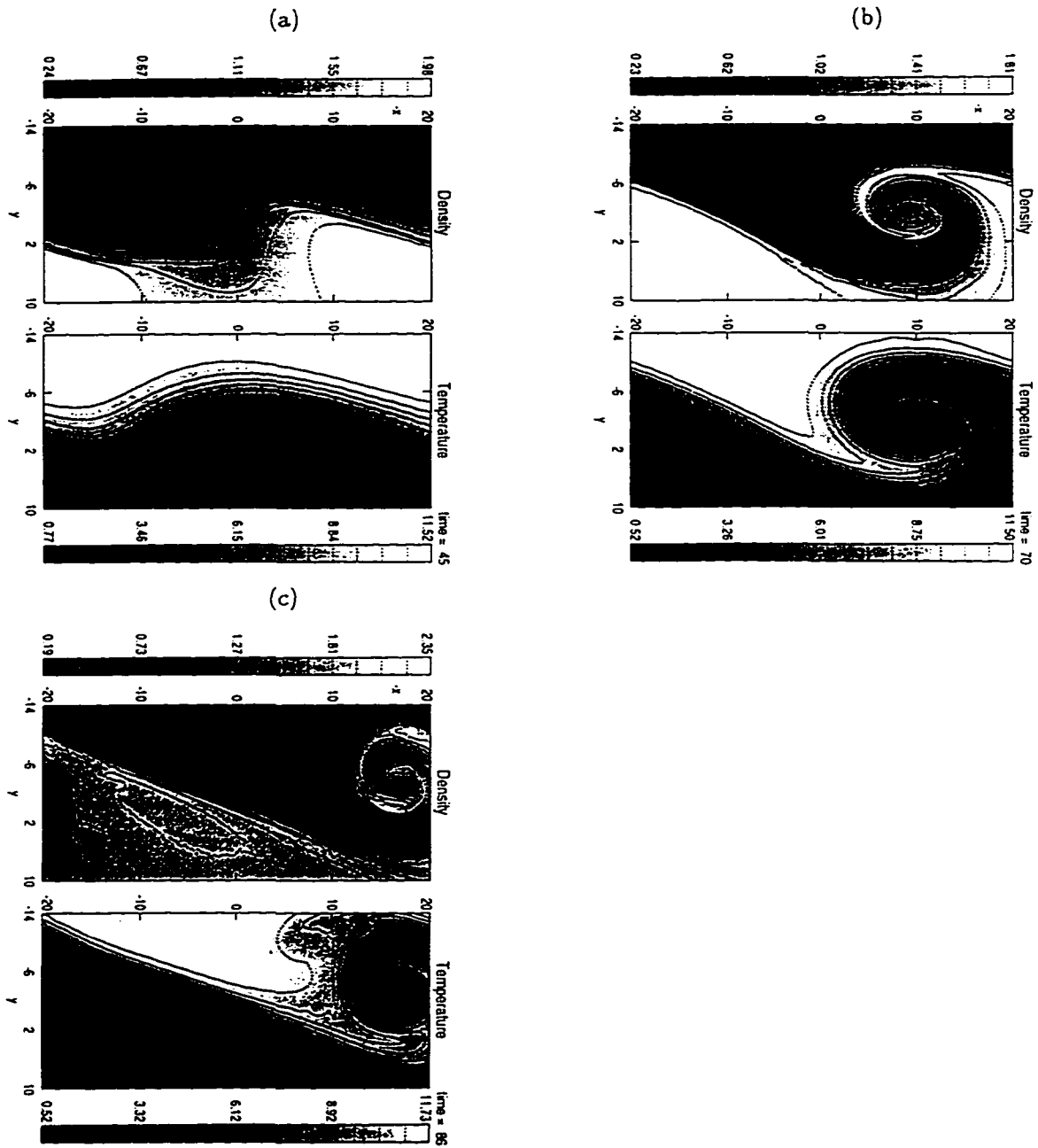
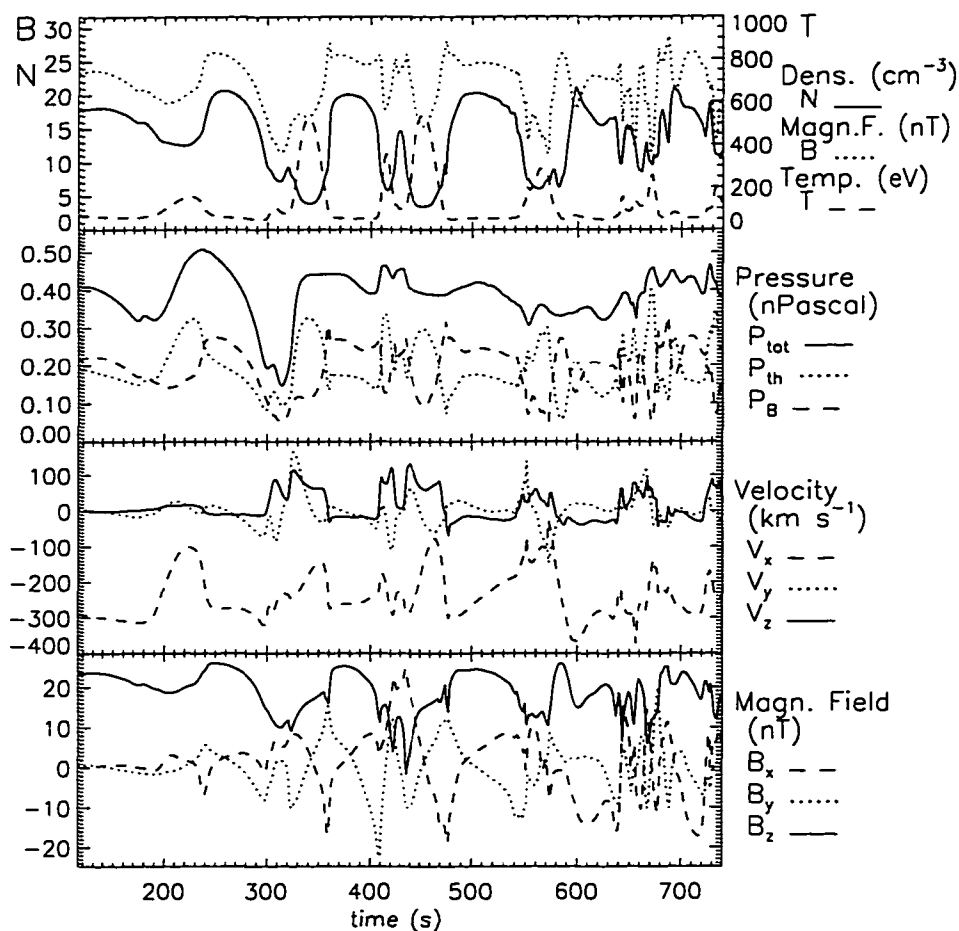


Figure 6.10 Contour lines of plasma density and temperature at (a) $t = 45$, (b) $t = 70$, and (c) $t = 86$.



Probe index: 22 Rotation angle for y,z comp.: 24

Initial probe location and vel. (simulation frame., normalized):

$$x = 3.0 \quad y = 1.5 \quad z = 6.0$$

$$V_x = -0.849 \quad V_y = 0.000 \quad V_z = -0.396$$

Initial probe location and vel. (MSP frame, in km and km/s):

$$x = 3152 \quad y = 900 \quad z = 2501$$

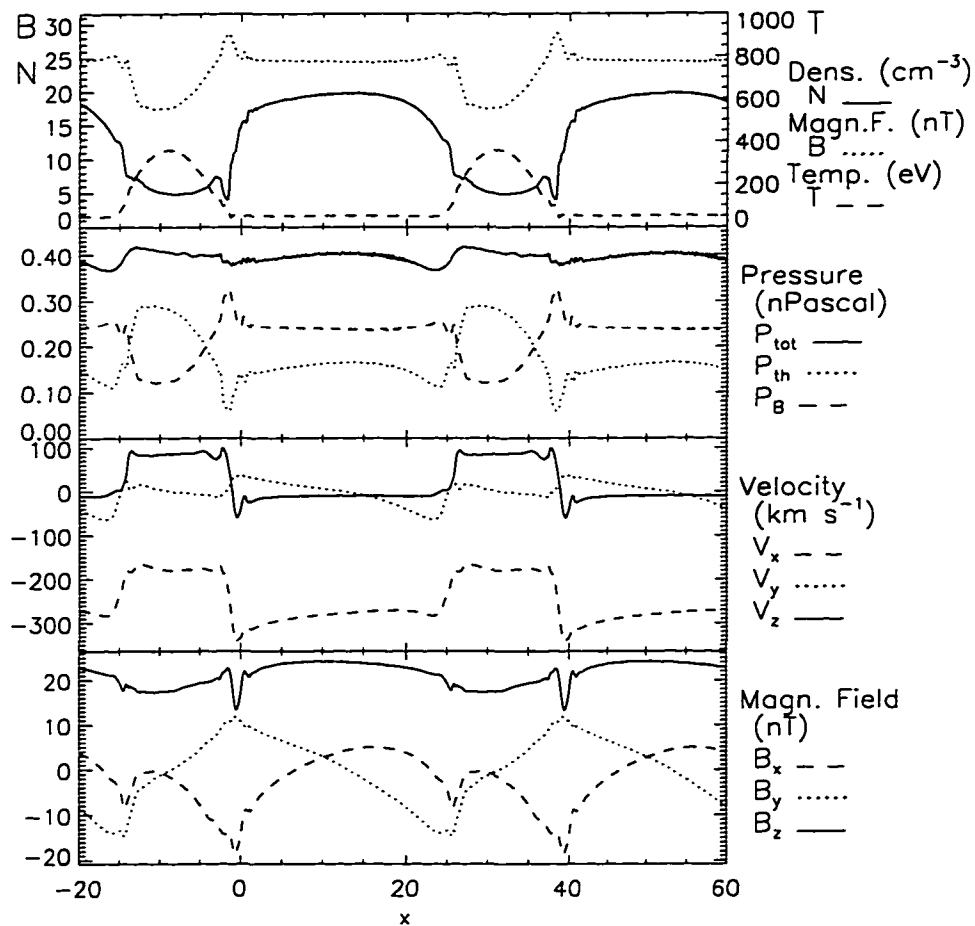
$$V_x = 0 \quad V_y = 0 \quad V_z = 0$$

DATA is plotted in the probe rest frame in rotated (MSP) coord.

Figure 6.11 Plasma and magnetic field signatures for a probe rested at (3152,900,2501) in the MSP frame.

field and plasma data properties. If a probe is at rest in the MSP frame, the moving vortex passing through it will give magnetic and plasma data records which can be compared with the satellite observations. Figure 6.11 shows an example of the signatures which one can record from this instability process. The first panel shows the plasma density and plasma β (ratio of thermal and magnetic pressure), the second presents total, thermal, and magnetic pressure, the third shows the three plasma velocity components, and the fourth shows the three magnetic field components. All quantities are converted to physical units for easier comparison. The initial probe location is $(x = 3152, y = 900, z = 2501)$, and it is stationary in the MSP frame. The figure shows the time interval from 100s to 750s. It can be seen that, at $t = 230s$, plasma density, total magnetic field, b_z component, and magnetic pressure increase, while temperature, thermal pressure, v_x component decrease. The probe begins to move out of the magnetosphere and enters the magnetosheath. In the magnetosheath, there are high density, magnetic field, magnetic pressure and low temperature, thermal pressure. This lasts about one minute. Then at $t = 300s$, plasma density, total magnetic field, b_z component, magnetic pressure begin to decrease, and temperature, thermal pressure, v_x component increase. The probe begins to move into the magnetosphere. In the magnetosphere, there are low density, magnetic field, magnetic pressure and high temperature, thermal pressure. This also lasts about one minute. Then begins another cycle of the interchanging process. In the frame of probe, there are a total of five of those processes. The KH instability generated very strong changes in the magnetic field.

A cut along constant y will show some local structure of the magnetopause for better identification of the plasma and field structure. Figure 6.12 shows a cut



Data represents a cut through system for const y .

Location is in simulation units and velocities are in magnetospheric frame

Cut at $y = 6.0$, $\phi = 25.0$, time = 403.

Figure 6.12 Plasma and magnetic field data representation through a cut $y = 6.0$ at $t = 403$.

through the system for $y = 6.0$, $\phi = 25^\circ$, $t = 403$. The range of x is from -20 to 60. I also find a signature similar to the time series signature in Figure 6.5. On the magnetosheath side, one can see intervals of high plasma density, large magnetic field and B_z component, large tailward flow, low temperature, and few fluctuations. These intervals interchange with intervals of lower density, small total magnetic field, higher temperatures, strong and rapid magnetic field fluctuations, and smaller and sometimes briefly southward B_z . Choosing a probe location further on the magnetospheric side, similar transients are observed but magnetic fluctuations (including B_z) are preferably now in the denser, low-temperature magnetosheath-like plasma. Most of the properties of the simulation can also be seen from the observation (see Figure 6.4 and 6.5).

In summary, the presence of quasi-periodic 2-minute large amplitude waves in the low latitude boundary layer is explained as the development of the KH instability. The KH wave propagates at a small angle toward the tailward direction. the KH instability develops in the plane including the KH wave vector and the boundary normal direction. The formation of vortices will twist the magnetic field lines in the plane. This process, in turn, leads to the observed strong plasma and magnetic field oscillations. The KH instability is a very important macroscopic process at the magnetotail boundary.

6.4 Conclusion and Discussion

In this chapter, I have focused on two particular observations. One refers to the structure of the magnetopause current layer, and the other to the presence of

quasi-periodic large amplitude waves in the low latitude boundary layer.

The intriguing element of structure of the magnetopause current layer is the magnetic fluctuations observed typically in hodogram plots of the magnetic field in the magnetopause. During periods of magnetic reconnection, the magnetopause is typically a relatively simple and well ordered structure. However at other times this current layer often exhibits significant magnetic fluctuations. These can be indicative of a temporal structure, a spatial structure or both.

To understand boundary waves at the low latitude boundary layer, a simple MHD approximation in the simulation is used. The simulation region is a localized region. Where for simplicity, simple periodic boundary conditions are used along the tailward direction. Quantitatively basic magnetic field and plasma data are chosen consistent with the observation. Based on this simple model, the magnetotail boundary events are successfully explained in terms of the KH instability.

During northward IMF, the observed large magnetic field and plasma large fluctuations are due to the KH instability at the boundary generating vortices that convect past the spacecraft. There are a large number of common properties of simulation and observation. On the magnetosheath side, intervals of high plasma density, large magnetic field and B_z component, large tailward flow. low temperature, few fluctuations interchange with intervals of lower density, smaller total magnetic field, higher temperatures, strong and rapid magnetic field fluctuations, smaller and sometimes briefly southward B_z . On the magnetospheric side, there are similar transients but magnetic fluctuations (including B_z) in the denser and low-temperature plasma. The size of high density blobs appears larger on the magnetosheath side. Transitions from low into high density regions are often

associated with a minimum or maximum B_y .

The formed vortex moves at a tailward velocity 200km/s, and its typical wavelength is 2 to 2.5 R_E . According to the growth time for the vortex, the origin is close to the terminator. The mechanism is that the wave vector is not exactly tailward. It makes the projections of IMF and geomagnetic tail field onto the wave vector nonzero. The KH instability operates in a plane including the wave vector and the boundary normal direction. The formation of vortices will twist the magnetic field lines in the plane. Some antiparallel magnetic field lines are produced, and this process leads to strong magnetic field and plasma fluctuations. Simulation also indicates transport of plasma into the magnetosphere due to magnetic reconnection in the KH vortices.

Chapter 7

Summary and discussion

It is widely accepted that magnetic reconnection and the Kelvin-Helmholtz instability are two fundamental processes at the magnetopause. They play crucial roles in the transfer of energy, momentum, and mass from the solar wind into the magnetosphere. The relation between the KH instability and magnetic reconnection, the interaction of the tearing and KH modes, and their applications at the magnetopause are very interesting topics. In this chapter, the main results of those projects are presented. Possible topics for future studies for the interaction of the tearing and KH modes are suggested in the final section.

7.1 Main Results

The KH instability and magnetic reconnection can operate in the presence of antiparallel magnetic field or velocity components, which is present at the magnetopause and the magnetotail boundary layer. Two basic flow and magnetic field configurations are distinguished on the two sides of a plane layer: (1) configura-

tions where the difference in plasma velocity between the two sides of the boundary Δv (velocity shear) is parallel to the difference of the magnetic field Δb (magnetic shear), and (2) configurations where the velocity shear is perpendicular to the magnetic shear. Properties of other configurations can largely be inferred from these basic cases.

7.1.1 Configuration (1): A Tearing-Mode-Dominated Regime for Sub-Alfvénic Flows and the KH-unstable Regime for Super-Alfvénic Flows

For sub-Alfvénic shear flow the reconnection rate decreases with increasing velocity shear.

In Chapter 3, when reversed magnetic field is parallel to the shear flow, for the tearing and KH modes with parallel wave vectors which are realized in two-dimensional simulations, only one mode can grow. If half of the flow velocity jump is smaller than Alfvén speed, only the tearing instability operates; If half of the flow velocity jump is larger than Alfvén speed, only the KH instability happens. For the particular direction, only one mode can propagate. For sub-Alfvénic flow the reconnection rate decreases with increasing velocity shear. I found the KH mode to be stabilized for shear flow less than the Alfvén velocity unless η is very large.

For a super-Alfvénic shear flow, the nonlinear KH vortices generate thin current layers to trigger magnetic reconnection.

If the shear flow is super Alfvénic, the tearing mode is stabilized. The KH

instability evolves largely independently of a sufficiently small resistivity, even if this model is changed to a current dependent form which can generate a locally enhanced resistivity. In its nonlinear evolution the KH instability leads to a significant pinching of the current sheet. The increase in the current density generates a corresponding increase in the resistive electric field. This mechanism generates magnetic reconnection and magnetic islands of the size of the KH vortices. The corresponding reconnection process is obviously strongly driven by the pinching of the current layer. The reconnection process is expected to occur also if the system is initially fully collisionless because the KH vortices would generate arbitrarily thin current sheets if no dissipation is available and thus force the generation of a dissipation process. The evolution of the KH mode even with large nonlinear amplitudes appears largely unaffected by the reconnection process. Because of the fast pinching of the current sheet, I could not identify a tearing mode structure or tearing mode growth during the later times of the KH evolution. The plasma outflow occurs in regions which are created by the KH vortices and do not show the typical reconnection layer structure. A current dependent resistivity appears to be a more realistic choice, particularly for many magnetospheric processes.

The dayside magnetopause is not a location for the KH instability to occur.

Kelvin-Helmholtz vortices can induce magnetic reconnection which is a viable process at the Earth's magnetopause. However, the location for the occurrence of these structures is disputable. First, the formation requires a magnetosheath flow velocity which is larger than the threshold velocity of the KH instability. This condition largely excludes the subsolar magnetopause if the flow is strongly aligned

with the field (which is necessary to obtain a significant reconnection process). Second, the vortices should be almost fully developed otherwise the reconnected flux is small. It excludes the major portion of the dayside magnetopause as a possible location to observe large scale structures (1 or 2 R_E) resulting from the KH instability.

7.1.2 Configuration (2): The 3-D KH-Induced Reconnection and the Interaction of the Tearing and KH Modes.

The tearing and KH instabilities can operate simultaneously in different planes.

In Chapter 4, when reversed magnetic field is perpendicular to the shear flow, for the tearing and KH modes with perpendicular wave vectors which can only be realized in three-dimensional simulations, both modes can grow. In a plane including the current sheet normal direction and a wave vector, the properties of the wave vector-related mode will be seen. In the linear stage, the two modes do not affect each other. One mode's growth behaves as if the other does not exist. The linear behavior of the KH and tearing instabilities is the superposition of two modes. The dominant instability depends on its initial perturbation magnitude and the growth rate of modes. If the growth rate and initial perturbation of the tearing mode are respectively smaller and larger than those of the KH mode, a cross-over time can be identified. Before that time, the growth is dominated from the tearing mode. After that time, the growth is mainly due to the KH mode.

It can also be inferred that, in a plane along which waves can propagate, the

KH and tearing modes can not propagate along the same direction. The range of possible wave vectors of tearing mode are well separated by that of KH mode. For shear flow larger than the fast mode speed, there is a range in which neither tearing nor KH mode operates. If the shear flow is zero, all possible modes are tearing mode; if no magnetic shear exists, all possible modes are KH modes.

In the nonlinear stage, the tearing and KH instabilities interact with each other.

The nonlinear dynamics is governed or strongly influenced by the mode which first reaches a nonlinear amplitude. If the tearing mode grows faster than the KH mode, both modes operates on the same scale. The tearing mode instability modifies the flow shear layer. The shear layer width near the reconnection site becomes thinner, and the shear layer width near the neutral line becomes wider. That will affect the KH instability. In the region with thinner shear layer width, vortex becomes smaller, and in the region with wider shear layer width, vortex becomes bigger. The KH instability changes the profile of the current sheet and makes the current sheet oscillate around its initial position. Those processes continue to reform the structure of the magnetic flux tube in a cycle of interaction of the tearing and KH modes.

Formation of multiple current layers and turbulence reconnection due to the KH instability

In Chapter 5, three-dimensional nonlinear interaction of the KH and tearing modes is investigated. When reversed magnetic field is perpendicular to the shear flow, for the tearing and KH modes with perpendicular wave vectors which can only be realized in three-dimensional simulations, nonlinear KH vortices lead to

current sheet thinning and formation of multiple current layers. Vortices can induce multiple current layer reconnection in a three-dimensional configuration. Mutual interaction of neighboring tearing islands lead to fast growth of the tearing mode. Topology of magnetic field, current, flow field shows the combined features of the KH and tearing instabilities. The three-dimensional vortex-induced tearing instability can make highly efficient mixing of plasma and complex current layer structure.

7.1.3 Comparison with Observations

The 3-D KH-induced reconnection provides the first explanation of the turbulent structure of the magnetopause current layer.

The analysis of the multiple current structure simulated in Chapter 5 shows the correlation with the observations of the magnetic field at the magnetopause. The presence of large amplitude magnetic fluctuations in observed magnetic hodograms is a long standing problem of magnetopause physics. Simple explanations (motion of the magnetopause, magnetic percolation) do not hold up in a more critical examination. The results from Chapter 5 provide an explanation in that the spacecraft passed through complex multiple current layer structure. Typical data analysis tools show that this structure is not a simple one-dimensional, time-independent structure. The observations can be explained as the interaction of the KH and tearing instabilities at the magnetopause.

The Kelvin-Helmholtz instability operates at the magnetospheric boundary at low latitudes.

The presence of quasi-periodic 2-minute large amplitude waves in the low latitude magnetotail boundary on March 24, 1995, which lasted for several hours for a northward IMF nearly parallel to the magnetospheric magnetic field, is simulated in a two-dimensional simulation. The large magnetic field and plasma large fluctuations are due to the Kelvin-Helmholtz instability at the boundary generating vortices that convect past the spacecraft. The formed vortices move at a tailward velocity 200km/s, and its typical wavelength is 2 to 2.5 R_E . According to the growth time for the vortex, the origin is close to the terminator. The mechanism is that the KH wave does not propagate exactly along the tailward. It makes the projections of IMF and geomagnetic tail field onto the KH wave vector nonzero. The KH instability operates in a plane including the wave vector and the boundary normal direction. The formation of vortices will twist the magnetic field lines in the plane. Then this process makes strong magnetic field and plasma fluctuations. Simulation also indicates transport of plasma into the magnetosphere due to magnetic reconnection in the KH vortices.

7.2 Summary and Open Problems

In summary, I have carried out two and three-dimensional investigations on the Kelvin-Helmholtz instability, magnetic reconnection, and their interaction at the magnetopause. In various research papers this has been viewed as a single often linear and two-dimensional mode in the presence of magnetic and velocity shear. The picture from my study is entirely different. In the presence of parallel magnetic and velocity shears (for configuration (1), see Chapter 1) in a two-dimensional

plane, there is either a tearing type solution (for small velocity shear) or a KH type solution (for small magnetic shear). Both modes show only minor modifications from the basic tearing or KH modes. Really new aspects are found in a three-dimensional geometry where both modes grow first independent of each other (for configuration (2), see Chapter 1). The structure in the nonlinear evolution is found to be entirely different from the single mode approach.

In the nonlinear evolution two cases can be distinguished, i.e., one in which the tearing mode reaches the nonlinear phase first and the other where the KH instability is faster. In the first case, the nonlinear tearing does not surpass the growth of the KH instability. However, the mutual interaction of both modes strongly changes the overall structure of the reconnection caused by the tearing mode and it generates magnetic flux with varying cross-section. In the second case, the KH vortices generate multiple current layer structure. The continuous thinning and actual interaction from neighboring layers generates random tearing modes with extremely fast growth and large nonlinear reconnection rates. The process should generate very effective plasma mixing and transport. It is this mechanism which provides a consistent explanation for an often observed magnetopause structure.

Finally the work provides the first quantitative confirmation that the KH instability operates at the flanks of the magnetotail. This is particularly intriguing because the particular case showed extreme magnetic field fluctuations although both the IMF and the geomagnetic field are strongly northward. The results indicate that, in addition to momentum and energy transport, the KH induced reconnection at the magnetospheric flux might be a source of magnetospheric plasma.

This work has demonstrated that the three-dimensional nonlinear interaction of

macro plasma instabilities, like the KH and tearing modes, generates entirely new plasma phenomena and structure. However, the dynamics depend strongly on the initial perturbation and plasma properties of the system. For the magnetopause, the comparison with observation appears to indicate that the KH instability, provided that it is not stabilized, grows very fast and competes with (and thus modifies) the tearing mode and magnetic reconnection. However, the regions of the magnetopause for which the KH instability is unstable are usually limited, such that the corresponding magnetopause structure depends on the onset conditions of the KH mode.

A central crucial question is the total transport mechanism of plasma and particularly magnetic flux. These are issues which require a large scale model of the magnetopause. On small scales of the order of the ion inertia length, the actual processes can be modified by a Hall term in Ohm's law. This implies that the magnetic field is actually frozen in the electron fluid rather than the bulk plasma which relaxes the constraints on the KH instability. This can be important for small scale KH modes and tearing modes although the Hall term can not generate a magnetic field-aligned electric field, such that it does not change the reconnection rate in a straight forward manner. Thus, in summary, it would be desirable to extend this investigation to include micro scale dynamical effect and to improve our understanding of the associated transport of plasma and magnetic flux on the global scale.

The other area of open and interesting topic refers to other potential application of my results. The vastly differing magnetospheric dimensions of the various planets are produced by the differences in the intrinsic strength of the plane-

tary magnetic fields. Mercury's magnetosphere is tiny compared to Earth's. The study can be carried out with proper length scale and magnetic field on its magnetopause. Jupiter's outer magnetosphere is time variable, and with turbulent boundary layer. Observations of the Jovian magnetopause at $40R_J$ show periodic current sheet crossings and may provide strong evidence of the KH instability with a much larger scale than for the case of the Earth's magnetopause.

As a process for the generation of turbulence and transport, it is particularly important at very large size (astrophysical) plasma boundaries. Here magnetic reconnection at a single thin magnetic boundary is probably a very inefficient plasma transport processes compared to astrophysical dimensions. However, reconnection at multiple current layers is generated by very large scale KH vortices will change this entirely. Potential areas for applications are the Heliopause, interstellar clouds of partially ionized material or even boundary of galactic magnetospheres.

My new results may also apply to the mechanism of the coronal heating on the Sun. It is widely believed that wave heating and magnetic field dissipation are candidates for this heating. Magnetic field dissipation in current sheets requires very thin current sheets. This problem is yet unresolved. In the corona region, a typical $\beta \leq 4$ gives a sound speed less than 200 km/s. The KH instability may generate thin current sheets if there is shear flow perpendicular to the magnetic field (Along the direction of the magnetic field, the KH instability is stabilized). Turbulence reconnection operating in the thin current sheets can produce very fast dissipation to generate the corona heating.

All of these topics provides highly interesting potential applications for the results and mechanisms studied in this thesis. The real relevance of the interaction

of the KH instability and magnetic reconnection to these areas, however, requires further study.

References

- Akasofu, S. -I., E. W. Hones Jr., S. J. Bame, J. R. Asbridge and A. T. Y. Lui, Magnetotail boundary layer plasmas at geocentric distance of $18 R_e$: Vela 5 and 6 observations, *J. Geophys. Res.*, *78*, 7257, 1973.
- Aubry, M. P., M. G. Kivelson, and C. T. Russell, Motion and structure of the magnetopause, *J. Geophys. Res.*, *76*, 1673, 1971.
- Axford, W. I., and C. O. Hines, A unifying theory of high-latitude geophysical phenomena and geomagnetic storms, *Can. J. Phys.*, *39*, 1433, 1961.
- Belmont, G., and G. Chanteur, Advances in magnetopause Kelvin-Helmholtz instability studies, *Phys. Scr.*, *40*, 124, 1989.
- Berchem, J., and C. T. Russell, The thickness of the magnetopause current layer: ISEE 1 and 2 observations, *J. Geophys. Res.*, *87*, 2108, 1982.
- Berchem, J., and C. T. Russell, Flux transfer events on the magnetopause: Spatial distribution and controlling factors, *J. Geophys. Res.* *89*, 6689, 1984.
- Birk, G. T., and A. Otto, The resistive tearing instability for generalized resistivity models: Applications, *Phys. Fluids B*, *3*(7), 1746, 1991.
- Brackbill, J. U., D. W. Forslund, K. B. Quest, and D. Winske, Nonlinear evolution of the lower-hybrid drift instability, *Phys. Fluids*, *27*, 2682, 1984.
- Chandrasekhar, S., *Hydrodynamic and Hydromagnetic Stability*, Oxford University Press, New York, 1961.
- Chen, X. L., and P. J. Morrison, Resistive tearing instability with equilibrium shear flow, *Phys. Fluids B*, *2*(3), 495, 1990.
- Chen, S. -H., M. G. Kivelson, J. T. Gosling, R. J. Walker, and A. J. Lazarus, Anomalous aspects of magnetosheath flow and of the shape and oscillations of the magnetopause during an interval of stringly northward interplanetary magnetic field, *J. Geophys. Res.*, *98*, 5727, 1993.
- Coppi, B., J. M. Greene, and J. L. Johnson, Resistive instabilities in a diffuse linear pinch, *Nucl. Fusion*, *6*, 101, 1966.

- Cowley, S. W. H., Comments on the merging of non-antiparallel fields, *J. Geophys. Res.*, *81*, 3455, 1976.
- Daly, P. W., and E. Keppler, Observation of a flux transfer event on the earthward side of the magnetopause, *Planet. Space Sci.*, *30*, 331, 1982.
- Dungey, J. W., Interplanetary magnetic field and the auroral zones, *Phys. Rev. Lett.*, *6*, 47, 1961.
- Eastman, T. E., E. W. Hones, Jr., S. J. Bame, and J. R. Asbridge, The magnetospheric boundary layer: Site of plasma momentum and energy transfer from the magnetosheath into the magnetosphere, *Geophys. Res. Lett.*, *3*, 685, 1976.
- Einaudi, G., and F. Rubini, Resistive instabilities in a flowing plasma, I, Inviscid case, *Phys. Fluids*, *29*(8), 2563, 1986.
- Fairfield, D. H., Global aspects of the earth's magnetopause, in *Proceedings of Magnetosphere Boundary Layers Conference*, ESA Scientific and Technical Publications Branch, Noordwijk, The Netherlands, 1979.
- Fairfield, D. H., and R. P. Lepping, Geotail observations of the Kelvin-Helmholtz instability at the magnetotail boundary for parallel Northward fields, paper presented at 1996 Fall Meeting, AGU, San Francisco, 1996.
- Fu, S. Y., Z. Y. Pu, and Z. X. Liu, Vortex induced magnetic reconnection and single X line reconnection at the magnetopause, *J. Geophys. Res.*, *100*, 5657, 1995.
- Fu, Z. F., and L. C. Lee, Multiple X line reconnection, 2. The dynamics, *J. Geophys. Res.*, *91*, 13373, 1986.
- Fu, Z. F., L. C. Lee, and Y. Shi, A three-dimensional simulation of the multiple X line reconnection process, in *Physics of Magnetic Flux Ropes*, *Geophys. Monogr. Ser.*, *58*, ed. by C. T. Russell, E. R. Priest, and L. C. Lee, P. 515, AGU, Washington, D. C., 1990.
- Furth, H. P., J. Killeen, and M. N. Rosenbluth, Finite-resistivity instabilities of a sheet pinch, *Phys. Fluids*, *6*, 459, 1963.
- Galeev, A. A., M. M. Kuznetsova, and L. M. Zelenyi, Magnetopause stability threshold for patchy reconnection, *Space Sci. Rev.*, *44*, 1, 1986.
- Goertz, C. K., E. Neilsen, A. Korth, K.-H. Glassmeier, C. Haldoupis, P. Hoeg, and D. Hayward, Observations of a possible ground signature of flux transfer events, *J. Geophys. Res.*, *90*, 4069, 1985.
- Gosling, J. T., M. F. Thomsen, S. J. Bame, and C. T. Russell, Plasma flow reversals at the dayside magnetopause and the origin of asymmetric polar cap convection, *J. Geophys. Res.*, *95*, 8073, 1990.
- Gosling, J. T., M. F. Thomsen, S. J. Bame, and C. T. Russell, Accelerated plasma flows at the near-tail magnetopause, *J. Geophys. Res.*, *91*, 3029, 1986.

- Heikkila, W. J., and J. D. Winningham, Penetration of magnetosheath plasma to low altitudes through the dayside magnetospheric cusps, *J. Geophys. Res.*, *76*, 883, 1971.
- Hesse, M., J. Birn, and K. Schindler, Flux transfer events: Reconnection without separators? in *Reconnection in Space Plasma*, ed. by T. D. Guyenne and J. J. Hunt, p. 263, ESA SP-285, Vol. II, Netherland, 1989.
- Hu, Y. D., and Z. X. Liu, Response and reconnection of magnetic field caused by fluid vortex at the boundary region of magnetopause, paper presented at International Symposium on Space Physics, Chin. Soc. of Space Res., Beijing, 1986.
- Huba, J. D., J. F. Drake, and N. T. Gladd, Lower hybrid drift instability in field reserved plasma, *Phys. Fluids*, *23*, 552, 1980.
- Huba, J. D., Hall dynamics of the Kelvin-Helmholtz instability, *Phys. Rev. Lett.*, *72*, 2033, 1994.
- Kan, J. R., A theory of patchy and intermittent reconnections for magnetospheric flux transfer events, *J. Geophys. Res.*, *93*, 5613, 1988.
- Kennel, C. F., L. J. Lanzerotti, E. N. Parker, *Solar System Plasma Physics*, Vol. II, North-Holland Publishing Company, Amsterdam - New York - Oxford, 1979.
- Killeen, J., and A. I. Shestakov, Effect of equilibrium flow on the resistive tearing mode, *Phys. Fluids*, *21*(10), 1746, 1978.
- La Belle-Hamer, A. L., Z. F. Fu, and L. C. Lee, A mechanism for patchy reconnection at the dayside magnetopause, *Geophys. Res. Lett.*, *15*, 152, 1988.
- La Belle-Hamer, A. L., Magnetic reconnection in the presence of sheared flow, *Ph. D. Thesis*, p. 93, University of Alaska Fairbanks, 1994.
- La Belle-Hamer, A. L., A. Otto, and L. C. Lee, Magnetic reconnection in the presence of sheared flow and density asymmetry: Applications to the Earth's magnetopause, *J. Geophys. Res.*, *100*, 11,875, 1995.
- Lee, L. C., R. K. Albano, and J. R. Kan, Kelvin-Helmholtz instability in the magnetopause boundary layer region, *J. Geophys. Res.*, *86*, 54, 1981.
- Lee, L. C., and Z. F. Fu, A theory of magnetic flux transfer at the Earth's magnetopause, *Geophys. Res. Lett.*, *12*, 105, 1985.
- Lepping, R. P., and L. F. Burlaga, Geomagnetopause surface fluctuations observed by Voyager 1, *J. Geophys. Res.*, *84*, 7099, 1979.
- Ma, Z. W., L. C. Lee, A. Otto, and Y. Shi, B_y enhancements in magnetospheric current sheets and magnetic flux tubes, in *Physics of Space Plasma (1992)*, SPI Conference Proceeding Reprint Series, ed. by T. Chang and J. R. Jasperse, Vol. 12, p. 575, Scientific Publishers, Inc., Cambridge, Mass., 1993.
- Matthaeus, W. H., and S. L. Lammkin, Turbulent magnetic reconnection, *Phys. Fluid*, *29*, 2513, 1986.

- McHenry, M. A., and C. R. Clauer, Modeled ground signatures of flux transfer events, *J. Geophys. Res.*, *92*, 11231, 1987.
- Mitchell, D. G., F. Kutchko, D. J. Williams, T. E. Eastman, L. A. Frank, and C. T. Russell, An extended study of the low-latitude boundary layer on the dawn and dusk flanks of the magnetosphere, *J. Geophys. Res.*, *92*, 7394, 1987.
- Miura, A., and P. L. Pritchett, Nonlocal stability analysis of the MHD Kelvin-Helmholtz instability in a compressible plasma, *J. Geophys. Res.*, *87*, 7431, 1982.
- Miura, A., Anomalous transport by magnetohydrodynamic Kelvin Helmholtz instabilities in the solar wind magnetosphere interaction, *J. Geophys. Res.*, *89*, 801, 1984.
- Miura, A., Kelvin Helmholtz instability at the magnetospheric boundary, *Geophys. Res. Lett.*, *12*, 635, 1985.
- Miura, A., Simulation of Kelvin Helmholtz instability at the magnetospheric boundary, *J. Geophys. Res.*, *92*, 3195, 1987.
- Miura, A., Kelvin Helmholtz instability for supersonic shear flow at the magnetospheric boundary, *Geophys. Res. Lett.*, *17*, 749, 1990.
- Miura, A., Kelvin Helmholtz instability at the magnetospheric boundary: Dependence on the magnetosheath sonic Mach number, *J. Geophys. Res.*, *97*, 10665, 1992.
- Miura, A., Kelvin Helmholtz instability at the magnetopause: Computer simulations, in *Physics of the Magnetopause*, *Geophys. Monogr. Ser.*, *90*, ed. by P. Song, B. U. Ö. Sonnerup, and M. F. Thomsen, p. 285, AGU, Washington, D. C., 1995.
- Nishida, A., Can random reconnection on the magnetopause produce the low latitude boundary layer, *Geophys. Res. Lett.*, *16*, 227, 1989.
- Ofman, L., X. L. Chen, P. J. Morrison, and R. S. Steinolfson, Resistive tearing mode instability with shear flow and viscosity, *Phys. Fluids B*, *3*(6), 1364, 1991.
- Ofman, L., P. J. Morrison, and R. S. Steinolfson, Nonlinear evolution of resistive tearing mode instability with shear flow and viscosity, *Phys. Fluids B*, *5*(2), 376, 1993.
- Ong, R. S. B., and N. Roderick, On the Kelvin-Helmholtz instability of the Earth's magnetopause, *planet. Space Sci.*, *20*, 1, 1972.
- Otto, A., The resistive tearing instability for generalized resistivity models: Theory, *Phys. Fluids B*, *3*(7), 1739, 1991.
- Otto, A., and G. T. Birk, Resistive instability of periodic current sheet, *Phys. Fluids B*, *4*(11), 3811, 1992.
- Otto, A., 3-D resistive MHD computation of magnetospheric physics, *Comput. Phys. Commun.*, *59*, 1985, 1990.
- Otto, A., Three-dimensional magnetohydrodynamic simulations of processes at the Earth's magnetopause, *Geophys. Astrophys. Fluid Dyn.*, *62*, 69, 1991.

- Otto, A., K. Schindler, and J. Birn, Quantitative study of the nonlinear formation and acceleration of plasmoids in the Earth's magnetotail, *J. Geophys. Res.*, *95*, 15,023, 1990.
- Otto, A., L. C. Lee, and Z. W. Ma, Magnetic field and plasma properties associated with pressure pulses and magnetic reconnection at the dayside magnetopause, *J. Geophys. Res.*, *100*, 14,895, 1995.
- Otto, A., Forced three-dimensional magnetic reconnection due to linkage of magnetic flux tubes, *J. Geophys. Res.*, *100*, 11,863, 1995.
- Papadopoulos, K., The role of microturbulence on collisionless reconnection, in *Dynamics of the Magnetosphere*, edited by S.-I. Akasofu, pp. 289, D. Reidel, Dorwell, Mass., 1980.
- Papamastorakis, I., G. Paschmann, W. Baumjohann, B. U. O. Sonnerup, and H. Luhr, Orientation, motion, and other properties of flux transfer events structures on september 4, 1984, *J. Geophys. Res.*, *94*, 8852, 1989.
- Paschmann, G., G. Haerendel, I. Papamastorakis, N. Skopke, G. Haerendel, S. J. Bame, J. R. Asbridge, J. T. Gosling, C. T. Russell, and R. C. Elphic, Plasma acceleration at the Earth's magnetopause: Evidence for reconnection, *Nature*, *282*, 243, 1979.
- Paschmann, G., G. Haerendel, I. Papamastorakis, N. Skopke, G. Haerendel, S. J. Bame, J. T. Gosling, and C. T. Russell, Plasma and magnetic characteristics of magnetic flux transfer events, *J. Geophys. Res.*, *87*, 2159, 1982.
- Paschmann, G., I. Papamastorakis, W. Baumjohann, N. Sckopke, C. W. Carlson, B. U. O. Sonnerup, and H. Luhr, The magnetopause for larger magnetic shear: AMPTE/IRM observations, *J. Geophys. Res.*, *91*, 11099, 1986.
- Phan, T. D., and G. Paschmann, Low-latitude dayside magnetopause and boundary layer for high magnetic shear, *J. Geophys. Res.*, *101*, 7801, 1996.
- Potter, D. E., *Computational Physics*, John Wiley, New York, 1973.
- Pu, Z. Y., M. Yan, and Z. X. Liu, Generation of vortex-induced tearing mode instability at the magnetopause, *J. Geophys. Res.*, *95*, 10,559, 1990a.
- Pu, Z. Y., P. T. Huo, and Z. X. Liu, Vortex induced-tearing mode instability as a source of flux transfer events, *J. Geophys. Res.*, *95*, 18,861, 1990b.
- Pu, Z. Y., and M. G. Kivelson, Kelvin-Helmholtz instability at the magnetopause: Solutions for compressible plasma, *J. Geophys. Res.*, *88*, 841, 1983.
- Rijnbeek, R. P., and S. W. H. Cowley, Magnetopause flux erosion events are flux transfer events, *nature*, *309*, 135, 1984.
- Rosenbauer, H., G. Grunwaldt, M. D. Montgomery, G. Paschmann, and N. Sckopke, Heos 2 plasma observations in the distant polar magnetosphere: the plasma mantle, *J. Geophys. Res.*, *80*, 2723, 1975.
- Rosenhead, L., The formation of vortices from a surface of discontinuity, *Pro. Roy. Soc.*

A 134, 96, 1931.

- Russell, C. T., and R. C. Elphic, Initial ISEE magnetometer results: Magnetopause observations, *Space Sci. Rev.*, 22, 681, 1978.
- Russell, C. T., and R. C. Elphic, ISEE observations of flux transfer events at the dayside magnetopause, *Geophys. Res. Lett.*, 6, 33, 1979.
- Saunders, M. A., Recent ISEE observations of the magnetopause and low latitude layer: A review, *J. Geophys. Res.*, 52, 190, 1983.
- Scholer, M., Magnetic flux transfer at the magnetopause based on single X line bursty reconnection, *Geophys. Res. Lett.*, 15, 291, 1988.
- Scholer, M., Magnetic reconnection, coalescence, and turbulence in current sheets, in *Physics of Magnetic flux Rope*, *Geophys. Monogr. Ser.*, 58, ed. by C. T. Russell, E. R. Priest and L. C. Lee, p. 85, AGU, Washington, D. C., 1990.
- Sckopke, N., G. Paschmann, G. Haerendel, B. U. O. Sonnerup, S. J. Bame, T. G. Forbes, E. W. Hones, Jr., and C. T. Russell, Structure of the low-latitude boundary layer, *J. Geophys. Res.*, 86, 2099, 1981.
- Sckopke, N., G. Haerendel, G. Paschmann, H. Rosenbauer, and P. C. Hedgecock, Mapping of the magnetospheric entry layer, paper presented at the Second Magnetospheric Cleft Symposium, St. Jovite, Quebec, 1976.
- Sibeck, D. G., A model for the transient Magnetospheric Response to Sudden Solar Wind Dynamic Pressure Variations, *J. Geophys. Res.*, 95, 3755, 1990.
- Siscoe, G. L., Solar system magnetohydrodynamics, in *Solar-Terrestrial Physics, Principles and Theoretical Foundations*, ed. by Carovillano and J. M. Forbes, p. 11, D. Reidel Publishing Company, 1983.
- Song, P., R. C. Elphic, and C. T. Russell, Multi-spacecraft observations of magnetopause surface waves: ISEE 1 and 2 determinations of amplitude, wavelength, and period, *Adv. Space Res.*, 8(9), 245, 1988.
- Song, Y., and R. L. Lysak, Evaluation of twist helicity of flux transfer event flux tubes, *J. Geophys. Res.*, 94, 5273, 1989.
- Sonnerup, B. U. O., Magnetic field reconnection at the magnetopause: An overview, in *magnetic Reconnection in Space and Laboratory Plasmas*, *Geophys. Monogr. Ser.*, 30, ed. by E. W. Hones, Jr., p. 92, AGU, Washington, D. C., 1984.
- Sonnerup, B. U. O., Magnetic field reconnection in cosmic plasmas, in *Unstable Current Systems and Plasma Instabilities in Astrophysics*, ed. by M. R. Kundu and G. D. Holman, D. Reidel Publ. Co., Dordrecht, Holland, 1985.
- Sonnerup, B. U. O., G. Paschmann, I. Papamastorakis, N. Sckopke, G. Haerendel, S. J. Bame, J. R. Asbridge, J. T. Gosling, and C. T. Russell, Evidence for magnetic field reconnection at the Earth's magnetopause, *J. Geophys. Res.*, 86, 10049, 1981.

- Sonnerup, B. U. O., I. Papamastorakis, G. Paschmann, and H. Luhr, Magnetopause properties from AMPTE/IRM observations of the convection electric field: Method development, *J. Geophys. Res.*, *92*, 12,137, 1987.
- Sonnerup, B. U. O., Magnetopause and boundary layer, in *Physics of Solar-Planetary Environments*, ed. by D. J. Williams, AGU, Washington, D. C., 1976.
- Sonnerup, B. U. O., and L. J. Cahill, Magnetopause structure and attitude from Explorer 12 observations, *J. Geophys. Res.*, *72*, 171, 1967.
- Southwood, D. J., The hydromagnetic stability of the magnetospheric boundary, *planet. space Sci.*, *16*, 587, 1968.
- Southwood, D. J., C. J. Farrugia, and M. A. Saunders, what are flux transfer events? *Planet. Space Sci.*, *36*, 503, 1988.
- Steinolfson, R. S., and G. Van Hoven, The growth of the tearing mode: Boundary and scaling effects, *Phys. Fluids*, *26*(1), 117, 1983.
- Terasawa, T., Hall current effect of tearing mode instability, *Geophys. Res. Lett.*, *10*, 6, 475, 1983.
- Terasawa, T., M. Fujimoto, H. Karimabadi, and N. Omid, Anomalous ion mixing within a Kelvin-Helmholtz vortex in a collisionless plasma, *Phys., Res. Lett.*, *68*, 2778, 1992.
- Thomas, V. A., and D. Winske, Kinetic simulation of the Kelvin-Helmholtz instability at the venus ionosphere, *Geophys. Res. Lett.*, *18*, 1943, 1991.
- Thomas, V. A., and D. Winske, Kinetic simulation of the Kelvin-Helmholtz instability at the magnetopause, *J. Geophys. Res.*, *98*, 11,425, 1993.
- Traver, D. P., D. G. Mitchell, D. J. Williams, L. A. Frank, and C. Y. Huang, Two encounters with the flank low-latitude boundary layer: further evidence for closed field topology and investigation of the internal structure, *J. Geophys. Res.*, *96*, 21,025, 1991.
- Tsurutani, B. T., and R. G. Stone, *Collisionless Shocks in Heliosphere: Reviews of Current Research*, ed. by B. T. Tsurutani and R. G. Stone, AGU, Washington, D. C., 1985.
- Tsurutani, B. T., A. L. Brinca, E. J. Smith, R. T. Okida, R. R. Anderson and T. E. Eastman, Aststistical study of ELF-VLF plasma waves at the magnetopause, *J. Geophys. Res.* *94*, 1270, 1989.
- Walén, C., On the theory of sunspots, *Ark. Mat. Astron. Fys.*, *30A*, (15), 1-87, 1944.
- Wang, Y. -M., and J. A. Robertson, A numerical investigation of the Kelvin-Helmholtz instability in the context of accreting neutron stars, *Astron. Astrophys.*, *139*, 93, 1984.
- Wei, C. Q., and L. C. Lee, Ground magnetic signatures of moving elongated plasma clouds, *J. Geophys. Res.*, *95*, 2045, 1990.
- Willis, D. M., The microstructure of the magnetopause, *Geophys. J. Roy. Astr. Soc.*, *41*, 355, 1975.

Wu, C. C., Kelvin-Helmholtz instability at the magnetopause boundary, *J. Geophys. Res.*, *91*, 3042, 1986.

Yan, M., A. Otto, D. Muzzell, and L. C. Lee, Tearing mode instability in a multiple current sheet system, *J. Geophys. Res.* *99*, 8657, 1994.